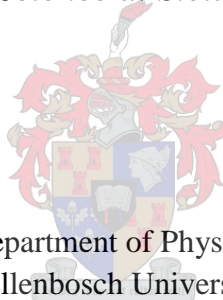


# Surface Enhanced Raman spectroscopy (SERS) of amino acids

by

Ngaatendwe Buhle Cathrine Pfukwa

*Thesis presented in partial fulfilment of the requirements for  
the degree of Masters of Science in Laser Physics in the  
Faculty of Nature Science at Stellenbosch University*



Department of Physics,  
Stellenbosch University,  
Private Bag X1, Matieland 7602, South Africa.

Supervisor: Dr. P.H. Neethling  
Co-supervisors: Prof. E.G. Rohwer and Prof. H. P. H. Schwoerer

March 2016

## **Declaration**

By submitting this thesis electronically, I declare that the entirety of the work contained therein is my own, original work, that I am the sole author thereof (save to the extent explicitly otherwise stated), that reproduction and publication thereof by Stellenbosch University will not infringe any third party rights and that I have not previously in its entirety or in part submitted it for obtaining any qualification.

# Abstract

## Surface Enhanced Raman spectroscopy (SERS) of biomolecules

N. B. C. Pfukwa

*Department of Physics*

*Stellenbosch University*

*Private Bag XI, Matieland 7602, South Africa*

Thesis: MSc (Physics)

March 2016

Raman spectroscopy (RS) is an invaluable technique for sample identification. This method requires little sample preparation and is not completely non-invasive. The intensity of Raman scattered light can be enormously increased or boosted when a sample molecule is adsorbed on a metallic surface, a technique known as Surface Enhanced Raman spectroscopy (SERS). Since the development of this technique a lot of studies have been done on molecules adsorbed on various types of metallic structures due to the sole purpose of the increase in Raman signal which occurs under such conditions. This has led to the applications of SERS in industry and in basic research.

In this study, silver and gold nanospheres of average size 20 nm were successfully synthesised and characterised using UV-Vis (Ultraviolet-visible) spectroscopy and Transmission Electron Microscopy (TEM). Two RS setups were available, a double stage Raman spectrometer using 514.5 nm Ar<sup>+</sup> laser as excitation source and a single stage Raman spectrometer using 532 nm frequency doubled Nd:YAG laser as excitation source. The synthesised silver nanospheres were employed in SERS studies on biomolecules (amino acids) using the single stage Raman setup with the aim of advancing SERS as a bio-analytical tool using our in-house developed RS setup. Qualitative analysis was done on amino acid spectra by band profiling and quantitative analysis was performed by carrying out concentration studies so as to determine the detection limit of the measuring instrument. Results are explained based on the setup used and by comparing with what is expected from literature.

It was found that amino acids mostly adsorb on a metallic surface via the common carboxylate, amine and R-groups. This is due to the availability of free electron pairs on the oxygen and nitrogen atoms which take part in charge transfer mechanisms and promote chemical enhancement. It was also observed that some amino acids have functional groups which either have strong affinity for metals or have an electronic structure that contribute to chemical enhancement, thus boosting the Raman signal. A low detection limit of  $1 \times 10^{-4}$  M from amino acid L-Lysine was obtained. Ultimately, these results are new and provide a set of measurements done on four groups of amino acids using gold and two types of silver nanoparticles. These results form a foundation for future studies on larger biological organisations using the setup available in our labs.

# Uittreksel

## Oppervlak versterkte Raman spektroskopie van bio-molekules

N. B. C. Pfukwa

*Department of Physics*

*Stellenbosch University*

*Private Bag XI, Matieland 7602, South Africa*

Tesis: MSc (Physics)

Maart 2016

Raman spektroskopie (RS) is 'n waardevolle tegniek om onbekende molekules mee uit te ken. Die metode verg baie min voorbereiding van die monster en is meestal nie-indringend. Die intensiteit van die Raman verstrooide lig kan noemenswaardig vergroot of versterk word wanneer die molekule wat ondersoek word geadsorbeer is op 'n metaal oppervlak, 'n tegniek wat Oppervlak Versterkte Raman Spektroskopie (SERS) genoem word. Sedert die ontwikkeling van die tegniek, is daar al talle studies gedoen op molekules wat op 'n groot aantal verskillende metaal strukture geadsorbeer is, met die doel om die Raman sein wat onder die toestande ontstaan te vergroot. Dit het gelei tot toepassings van SERS in industrie en basiese navorsing.

In hierdie studie is silwer en goud nano-sfere van gemiddeld 20 nm in deursnee suksesvol gesintetiseer en gekarakteriseer deur middel van UV-Vis (ultraviolet – sigbare) spektroskopie en Transmissie Elektron Mikroskopie (TEM). Twee RS opstellings was beskikbaar; 'n dubbele rooster Raman spektrometer met 'n 514.5 nm Ar<sup>+</sup> laser as bron en 'n enkel rooster Raman spektrometer met 'n 532 nm frekwensie verdubbelde Nd:YAG laser as bron. Die gesintetiseerde silwer nano-sfere was gebruik in SERS meetings op bio-molekules (aminosure) met die enkel rooster Raman opstelling met die doel om SERS te bevorder as 'n bio-analitiese tegniek deur gebruik te maak van ons tuisgeboude Raman opstelling. Kwalitatiewe analises was op die spektra van die aminosure gedoen deur na die profiele van die Raman bande te kyk, terwyl kwantitatiewe analises gedoen is deur middel van konsentrasie studies om die deteksie limiet van die aminosure op die instrument te bepaal. Die resultate word beskryf in die konteks van die opstelling wat gebruik is en deur hulle te vergelyk met die literatuur.

Dit was gevind dat aminosure hoofsaaklik via die karboksilaat, amien, en R-groepe op die metaal oppervlakte adsorbeer. Dit is weens die beskikbaarheid van vrye elektronpare op die suurstof en stikstof atome wat deel neem aan ladingsuitruil meganismes en sodoende chemiese versterking bevorder. Dit was ook gevind dat van die aminosure funksionele groepe bevat wat of 'n sterk affiniteit vir metale het, of 'n elektron struktuur het wat bydrae tot chemiese versterking, en sodoende die Raman sein vergroot. 'n Lae deteksie limiet van  $1 \times 10^{-4}$  M was gevind vir L-Lysine. Op die ou end is die resultate nuut en verskaf dit 'n stel meetings gedoen op vier verskillende groepe aminosure deur gebruik te maak van goue en twee tipes silwer nanopartikels. Hierdie resultate vorm die grondslag vir toekomstige studies op groter biologiese strukture met die bestaande toerusting in ons laboratorium.

# Acknowledgements

First and foremost I would like to thank God for the gift of life and for strength to be able to complete this project.

My utmost gratitude goes to my supervisor **Dr. P.H. Neethling** for his care and support. I would never have been able to finish this project without his excellent guidance. I thank him for patiently correcting my thesis and for teaching me skills as well as helping me to improve my background in laser physics. I would like to thank **Prof. E.G. Rohwer** and **Prof. H. P. H. Schwoerer** for allowing me to join the Laser research Institute (LRI) and for creating a great environment to undergo research as well as for funding the majority of my project. Their financial support is sincerely appreciated. Thank you to the **ALC** for the remainder of my funding.

I would like to thank **Prof. T. Parker** for his input, for patiently correcting my thesis and for teaching me experimental skills which are beyond the textbooks.

I also thank and appreciate my mother, **Mrs D.G. Pfukwa** for her prayers and for always supporting me. I am forever grateful. I thank my brothers, **Mr. M. Pfukwa**, **Dr. R. Pfukwa**, **Mr. A. Pfukwa** and **Mr. M. Pfukwa** for never giving up on me and for their encouragement and support. I am grateful for Mwashonga and Rueben Pfukwa for always being there for me, for protecting me and for providing for all my needs, without them I would have not been able to accomplish my dreams. I also thank my sisters, **Mrs L. Pfukwa**, **Dr. H. Pfukwa** and **Mrs A. Matimbira** for their support in my academic and social life and for strength.

My sincere gratitude also goes to:

The **LRI team** at Stellenbosch University, for their input and ideas during the weekly meetings.

**Ms C. J. Ruperti**, for patiently editing my thesis and last but not least, **Shane Smith**, for assisting with me with coding.

# Contents

<b>Declaration .....</b>	<b>ii</b>
<b>Abstract .....</b>	<b>iii</b>
<b>Uittreksel .....</b>	<b>iv</b>
<b>Acknowledgements.....</b>	<b>v</b>
<b>Contents.....</b>	<b>vi</b>
<b>1 Introduction .....</b>	<b>1</b>
<b>2 Raman spectroscopy.....</b>	<b>3</b>
2.1 Principles of vibrational spectroscopy .....	5
2.1.1 Polarisability and selection rules .....	5
2.1.2 Raman cross section .....	8
2.2 Surface Enhanced Raman spectroscopy (SERS) .....	9
2.2.1 Principles of SERS .....	9
<b>3 Metallic colloids as SERS substrates .....</b>	<b>11</b>
3.1 Localised Surface Plasmon Resonance (LSPR) .....	14
3.2 Enhancement and enhancement factors .....	15
3.3 LSPR dependence on nanoparticle distance separation and morphology .....	16
<b>4 Biological molecules.....</b>	<b>19</b>
4.1 Amino acids .....	19
4.1.1 Polar but uncharged amino acids.....	20
4.1.2 Hydrophobic amino acid(s).....	22
4.1.3 Basic amino acid(s) .....	22
4.1.4 Acidic amino acids .....	23
4.2 Proteins .....	24
<b>5 Materials and methods.....</b>	<b>25</b>
5.1 Instrumentation .....	25
5.1.1 The Double monochromator .....	25
5.1.2 The Single stage monochromator.....	27

5.1.3	Calibration of spectrometers .....	29
5.2	Materials .....	33
5.2.1	Data processing .....	34
5.2.2	Preparation of nanoparticles .....	34
<b>6</b>	<b>Results and discussion.....</b>	<b>37</b>
6.1	Characterisation of nanoparticles: UV-Vis and TEM.....	37
6.1.1	Aggregation of citrate reduced nanoparticles with Hydrochloric acid.....	39
6.2	Qualitative and quantitative analysis .....	39
6.2.1	L-cysteine .....	43
6.2.2	L-serine.....	46
6.2.3	L-tyrosine .....	48
6.2.4	Glycine .....	50
6.2.5	L-lysine .....	52
6.2.6	L-aspartic acid.....	54
6.2.7	L-glutamic acid .....	56
6.3	SERS with aggregated nanoparticles .....	58
6.4	SERS with gold nanoparticles .....	59
6.5	Enhancement factors and detection limit.....	61
6.6	Application of RS and SERS .....	63
<b>7</b>	<b>Conclusion.....</b>	<b>67</b>
7.1	Standard protocols of measurement on biomolecules (amino acids).....	67
7.2	Summary .....	68
7.3	Future work and general comments.....	70

## Appendices

<b>A. Modified Polyfit Method for background subtraction written in Matlab .....</b>	<b>67</b>
<b>B. Polar but uncharged amino acids showing carboxylate and amine groups .....</b>	<b>69</b>
<b>C. Acidic amino acids showing carboxylate and amine groups .....</b>	<b>70</b>
<b>D. Basic amino acid(s) showing carboxylate and amine groups .....</b>	<b>71</b>
<b>E. Hydrophobic amino acid(s) showing carboxylate and amine groups.....</b>	<b>72</b>

## List of Tables

<b>Table 4-1:</b> Summary of amino acids examined in this study and their characteristics...	23
<b>Table 5-1:</b> Comparison of the two Raman setups used in this study, the double stage and the single stage Raman spectrometers [78], [79].....	29
<b>Table 6-1:</b> Information table for the amino acids used in this study showing their molecular formulae and their solubility values in water. ....	42
<b>Table 6-2:</b> Experimental Raman shifts and Raman band assignments for Cys [27], [81], [88], [94], [95]. ....	44
<b>Table 6-3:</b> Experimental Raman shifts and Raman band assignments for Ser [27], [88], [97], [98].....	47
<b>Table 6-4:</b> Experimental Raman shifts and Raman band assignments for Tyr [27], [88], [99], [100].....	49
<b>Table 6-5:</b> Experimental Raman shifts and Raman band assignments for Gly [27],[102].	51
<b>Table 6-6:</b> Experimental Raman shifts and Raman band assignments for Lys [27], [97], [103]–[105].....	53
<b>Table 6-7:</b> Experimental Raman shifts and Raman band assignments for Asp [88], [90]. ....	55
<b>Table 6-8:</b> Experimental Raman shifts and Raman band assignments for Glu [27], [88].	57
<b>Table 7-1:</b> Enhancement factors for SERS of amino acids with AgHANP and with AgCNP. ....	62
<b>Table 6-9:</b> Experimental Raman shifts and Raman band assignments for chicken egg white and yolk [30], [106]–[109]. ....	64

## List of Figures

<b>Figure 1:</b> Schematic of energy levels for Rayleigh Scattering (elastic) and Stokes and Anti-Stokes scattering (inelastic) [19].	4
<b>Figure 2:</b> The changes in the polarisability ellipsoid during vibrations for CO <sub>2</sub> molecule (left) and the Raman spectrum of CCl <sub>4</sub> (right) at 488.0 nm excitation [13].	7
<b>Figure 3:</b> Schematic of LSPR showing free conduction band electrons in the metal nanoparticle oscillate due to coupling with incident light [51].	14
<b>Figure 4:</b> A schematic representation of electromagnetic and chemical enhancement. Electromagnetic enhancement shows, $\vec{E}_0$ , which is the incoming field. The outgoing field, $\vec{E}_R$ , represents a resultant electromagnetic field which the molecule experiences. $\vec{E}_R$ is the sum of the incident field, $\vec{E}_0$ , and the field produced by the oscillating dipole, $\vec{E}_{dip}$ . In chemical enhancement below the processes (i) and (ii) show the charge transfer which happen between the metal and the molecule and the double arrow indicates the resonant Raman processes which happen in the molecule's electronic states [30], [57].	15
<b>Figure 5:</b> General structure of an amino acid showing the four groups (amino group (left), carboxylate group (right), hydrogen atom (top), R-group (bottom)) surrounding the central $\alpha$ C atom.	19
<b>Figure 6:</b> Chemical structure of L-tyrosine (left), L-cystein (middle) and L-serine (right) [67].	20
<b>Figure 7:</b> Chemical structure of Glycine [67].	22
<b>Figure 8:</b> Chemical structure of L-lysine [67].	22
<b>Figure 9:</b> Chemical structure of L-aspartic acid (left) and L-glutamic acid (right) [67].	23
<b>Figure 10:</b> Molecular structure of primary (left), secondary (middle) and tertiary amides (right) [73].	24
<b>Figure 11:</b> Image (A) is the double spectrometer (this was the double monochromator modified into a double spectrometer) used in this study and (B) is a schematic of the SPEX model 1403/4 double monochromator [13].	25
<b>Figure 12:</b> Image (A) is the top view of our in built single stage Raman spectrometer showing the laser excitation source, the sample environment, the spectrometer and other optical instruments. Image (B) is a schematic of the single stage monochromator [78].	28
<b>Figure 13:</b> Two close peaks from spectra of toluene used for scaling so as to have pixel separation in wavelength scale.	30
<b>Figure 14:</b> Ten toluene spectra acquired using the double Raman spectrometer, used for calibrating the instrument.	31
<b>Figure 15:</b> Calibration curve for double Raman spectrometer	31
<b>Figure 16:</b> Toluene spectrum measured using the single stage Raman spectrometer (A) and a calibration curve for the single stage Raman spectrometer (B).	32

- Figure 17:** Images showing colours of the synthesised citrate reduced gold nanoparticles (A), citrate reduced silver nanoparticles (B) and hydroxylamine hydrochloride reduced silver nanoparticles (C).....36
- Figure 18:** UV-Vis spectra for hydroxylamine hydrochloride and citrate reduced AgNP (A).....37
- Figure 19:** TEM images for hydroxylamine hydrochloride (C) and citrate (D) reduced AgNP and citrate reduced (E) AuNP.....37
- Figure 20:** UV-Vis spectra for unaggregated and aggregated citrate reduced AgNP. The aggregating agent used was 1M HCl.....39
- Figure 21:** Comparison of Cys spectra measured using a double Raman spectrometer with 514.5 nm laser excitation source and a single stage Raman spectrometer with 532 nm laser excitation source. The spectra have been vertically offset for clarity.....42
- Figure 22:** RS spectra of Cys solid and 1M solution are shown in A. B and D are SERS spectra of Cys with AgHANP and AgCNP respectively. C and E are graphs showing the change in Cys concentration against peak height for AgHANP and AgCNP respectively. The horizontal line in figs. C and E show the background counts. ....44
- Figure 23:** RS spectra of Ser solid and 0.5 M solution are shown in A. Images B and D are SERS spectra of Ser with AgHANP and AgCNP respectively. C and E are graphs showing the change in Ser concentration against peak height for AgHANP and AgCNP respectively. The horizontal line in figs. C and E show the background counts.....46
- Figure 24:** RS spectra of Tyr solid and 0.6 M solution are shown in A. B and D are SERS spectra of Tyr with AgHANP and AgCNP respectively. C and E are graphs showing the change in Tyr concentration against peak height for AgHANP and AgCNP respectively. The horizontal line in figs. C and E show the background counts.....48
- Figure 25:** RS spectra of Gly solid and 1M solution are shown in A. B and D are SERS spectra of Gly with AgHANP and AgCNP respectively. C and E are graphs showing the change in Gly concentration against peak height for AgHANP and AgCNP respectively. The horizontal line in figs. C and E show the background counts. ....50
- Figure 26:** RS spectra of Lys solid and 0.1 M solution are shown in A. B and D are SERS spectra of Lys with AgHANP and AgCNP respectively. C and E are graphs showing the change in Lys concentration against peak height for AgHANP and AgCNP respectively. The horizontal line in figs. C and E show the background counts.....52
- Figure 27:** RS spectra of Asp solid and 0.4 M solution (with HCl as solvent) are shown in A. B is SERS spectra of Asp with AgHANP. C is a graph showing the change in Asp concentration against peak height for AgHANP. The horizontal line in fig. C shows the background counts. ....54
- Figure 28:** RS spectra of Glu solid and 0.7 M solution (with HCl as solvent) are shown in A. B and D are SERS spectra of Glu with AgHANP and AgCNP respectively. C and E are graphs showing the change in Glut concentration against peak height for AgHANP and AgCNP respectively. The horizontal line in figs. C and E show the background counts.....56
- Figure 29:** Spectra of Asp dissolved in HCl with AgCNP and Asp dissolved in water with AgCNP aggregated with HCl. ....58

<b>Figure 30:</b> SERS spectra for amino acids with citrate reduced AgNP and AuNP. Spectrum A is 1M Cys, B is 0.5 M Ser, C is 0.6 M Tyr (with HCl as solvent), D is 1 M Gly, E is 0.4 M Asp (with HCl as solvent), F is 0.7 M Glu (with HCl as solvent), G is 0.1 M Lys.....	60
<b>Figure 31:</b> RS and SERS of egg white. ....	63
<b>Figure 32:</b> RS and SERS of egg yolk. ....	63
<b>Figure 33:</b> Example of graph, before and after background subtraction. ....	72
<b>Figure 34:</b> SERS spectra of polar but uncharged amino acids with AuNP. The samples have different concentrations and the spectra were only for showing the carboxylate, amine and R-groups in the amino acids. ....	73
<b>Figure 35:</b> SERS spectra of polar but uncharged amino acids with AgHANP. The concentration is the same for all three samples, the carboxylate, amine and R-groups have been labelled. ....	73
<b>Figure 36:</b> SERS spectra of polar but uncharged amino acids with AgCNP. The concentration is the same for all three samples, the carboxylate, amine and R-groups have been labelled. ....	74
<b>Figure 37:</b> SERS spectra of acidic amino acids with AuNP. The carboxylate and amine groups have been labelled.....	74
<b>Figure 38:</b> SERS spectra of acidic amino acids with AgHANP. The carboxylate and amine groups have been labelled. The samples are of the same concentration.....	75
<b>Figure 39:</b> SERS spectra of a basic amino acid with AgHANP, AgCNP and AuNP. All three spectra have been presented on one plot only to show the carboxylate, and amine groups which appear in the spectra. ....	75
<b>Figure 40:</b> SERS spectra of a hydrophobic amino acid with AgHANP, AgCNP and AuNP. All three spectra have been presented on one plot only to show the carboxylate and amine groups which appear in the spectra. ....	76

## List of abbreviations

EPS	: Extra-cellular polymeric substance
SERS	: Surface enhanced Raman spectroscopy
LSPR	: Localised surface plasmon resonance
HOMO	: Highest occupied molecular orbital
LUMO	: Lowest unoccupied molecular orbital
KCl	: Potassium chloride
MgSO <sub>4</sub>	: Magnesium sulphate
NaCl	: Sodium chloride
NaBr	: Sodium bromide
NaNO <sub>3</sub>	: Sodium nitrate
AgNO <sub>3</sub>	: Silver nitrate
HCl	: Hydrochloric acid
HNO <sub>3</sub>	: Nitric acid
M <sub>w</sub>	: Molecular weight
$\lambda$	: Wavelength
Asp	: L-aspartic acid
Glu	: L-glutamic acid
Lys	: L-lysine
Gly	: Glycine
Tyr	: L-tyrosine
Cys	: L-cystein
Ser	: L-serine
Phe	: Phenylalanine
Trp	: Tryptophan
Ag	: Silver
Au	: Gold

AgHANP : Hydroxylamine reduced silver nanoparticles  
AgCNP : Citrate reduced silver nanoparticles  
AuNP : Citrate reduced gold nanoparticles

# 1 Introduction

For over 100 years microorganisms<sup>1</sup> have been scientifically studied and documented. One early discovery about microorganisms namely biofilms was in 1933 when Henrici, A. T. discovered that water bacteria were not always floating freely in water, but would grow on submerged surfaces [1].

Biofilms represent a type of microorganisms attached to either biotic or abiotic surfaces. By definition, biofilms are communities of microorganisms implanted in a matrix of extracellular polymeric substances (EPS) [2], [3]. On earth, 99% of microorganism life is represented as biofilms [2]. Under nutrient-sufficient environmental conditions bacteria initiates the development of biofilms from attachment of microorganisms, growth of cells, development of biofilm up to the termination of biofilms [1]. Basically, depending on what type of biofilm it is, biofilms can consist of up to 90% EPS which helps maintain the outer structure of biofilms. EPS is essential for biofilm life. It mainly consists of proteins, polysaccharides, lipids, nucleic substances and natural organic materials [2], [3]. EPS also prevents biofilm dehydration, mediates communication amongst cells and protects cells from environmental hazards [2], [4]. What EPS is made up of and its conformation is greatly influenced by its age, the nutrients available, cells present and their metabolic activities as well as its physical environment [2], [5]. EPS is divided into two types which are soluble EPS and bound EPS. Soluble EPS includes colloids, slimes and soluble macro-molecules whereas bound EPS constitutes of loosely bound polymers, sheaths, capsular polymers, condensed gel and attached organic material. Bound EPS are closely bound to cells while soluble EPS are loosely attached to cells, often dissolved in solution. Studies on these classes of EPS are explained in detail in [6] and [7].

Biofilms are found in a range of environments that includes the inside walls of water pipes, oil pipes, catheter tubes in hospital facilities, on teeth and on rocks in water bodies. The impact of biofilms on the healthcare equipment includes catheter related infections on urinary and intravascular catheters as well as on orthopaedic implants [8]. Shower inner pipes also create ideal environments for biofilm formation in the home. Biofilms can then be released as aerosols and can cause severe effects on the lungs if inhaled. Drinking water can also contain biofilms stemming from soiling of the inside walls of plumbing materials or wells [9]. In industry, biofilms develop into slime and accumulate inside pipelines, leading to the blockage of filters and corrosion [10].

Thus, in-order to have a better understanding of the biofilms, several analytical techniques have been employed so as to eventually be able to detect, control and prevent biofilm life. For biological and technical processes it is important to know and understand the chemical composition of biofilms. If this particular information is known it then helps in knowing how to carry out processes such as waste water treatment and to know which antibiotics are best suited for eradication and treatment of the biofilms.

One nano-scale imaging technique is fluorescence-induced confocal laser scanning microscopy (CLSM). With this technique studies have been done on activated sludge in

---

<sup>1</sup> Other microorganisms also include yeasts, protozoa and bacteria

order to understand its structure and 3D volume of multispecies biofilms using different staining substances [11]. In that study a foundation for understanding and controlling biofilms was illustrated. Raman tweezers have also been used in trapping individual cells so as to carry out Raman micro-spectroscopy to obtain vibrational spectra that can be directly correlated with the chemical make-up of the trapped cells studied [12]. Surface Enhanced Raman Spectroscopy (SERS) has been employed as well for *in-situ*, label free imaging on biofilms in order to show the applicability of the technique in characterising the EPS matrix [2]. In the report by Ivleva *et al* on label free *in-situ* imaging of biofilms, emphasis is also made on the choice of SERS instead of normal Raman Spectroscopy (RS) due to the restricted sensitivity of RS and long acquisition times, even when using a laser with high power. Infrared (IR) absorption is another technique used in providing vibrational information on sample molecules.

RS is an invaluable non-destructive tool for identifying compounds. The technique requires no sample preparation, and the spectra is unaffected by water since water is a poor Raman scatterer. This then becomes a great advantage when analysing biological samples however due to the small cross section of RS for various samples, RS is often overcome by competing signals such as fluorescence. Fluorescence diminishes the quality of Raman spectra and there are several ways used to address the problem such as the use of SERS technique. SERS shall be explained in detail in section 2.2

### **Aim**

This study aims to advance SERS as a bio-analytical tool. The study shall be based on SERS measurements done using a new in-house built RS setup constructed in our labs. For understanding microbial life it is important to investigate on the chemical make-up of its constituent components, such as amino acids as a starting point. This is being done so as to pioneer future studies of larger biological organisations and microorganisms. Compared to other techniques SERS which stems from RS was chosen because of its high sensitivity for analyses of biological molecules [2]. These techniques shall be explained in detail. In this report the setup and calibration of a new in-house built RS setup is reported and evaluation of our results is done based on the performance of that setup. We compare and contrast the technical performance with recent reports found in the literature. Concentration studies were done on this new setup using two types of nanoparticles (NPs) in-order to determine the detection limit of the setup.

### Aim:

To advance SERS as a bio-analytical tool.

### Objectives:

- Setup and calibrate RS system
- Synthesis and characterisation of metallic nanoparticles
- Qualitative and quantitative analysis of amino acids by RS and SERS

### Application

Identify amino acids in egg white

## 2 Raman spectroscopy

Raman and infrared spectroscopy are techniques used to observe the vibrational transitions which take place in a molecule. In IR spectroscopy the absorbed infrared light is measured as a function of frequency [13]. During IR spectroscopy, a molecule absorbs incident radiation and the molecule is promoted to higher vibrational states. The energy lost due to this absorbed radiation is then detected [13], [14]. RS is different and its background and mechanism shall be explained below.

In 1928 RS was discovered by K. S. Krishna and C. V. Raman in India. In that time Sir Raman used sunlight as the source together with a telescope as a collector and his eyes as the detector [2], [15]. The discovery of such an outstanding phenomenon was and is well documented and the technique has led to great amounts of research to date. From the beginning Raman spectroscopy had been used in understanding molecular structure of substances as well as understanding the scattering processes. However, over time the technique evolved as it became applicable in the fields of analytical chemistry, biology, forensic science, biochemistry, archaeology and art, electronics and other related disciplines due to the short analysis times, minimum sample preparation required and the vast amounts of technology available. Improvements have been done in terms of the instrumentation used, from the use of photomultiplier tubes in 1940s and 1950s to the introduction of charged coupled device detectors (CCDs) in 1987 for detection [16]. CCDs are presently used and in this study they were employed. Instrument improvements have also been in the lasers used, the spectrometers and other holographic optical components with applications ranging from single channel to multichannel systems to filtration units for signal purification [17]. This has indeed showed the diversity of the instrumental configurations employed in this technique [17]. RS is a sensitive, versatile tool for material analysis and its applications have evolved from technical developments ranging from use of fast fourier transform (FFT) to applications of fibre optics in RS. This has stimulated high interests in RS in the academic sector and in industry. Fibre optics have been utilised in RS remote sensing applications and research in diagnostics since fibre optics are fairly easy to align. Presently, many variations of RS techniques are present, such as Resonance Raman spectroscopy (RRS) [18], and surface techniques such as SERS.

When light from a monochromatic light source is incident on a material several optical processes can occur such as absorption, transmission, emission and scattering [15]. RS is one technique based on the scattering of light by a material and over the years it has been greatly employed in studies of biological materials.

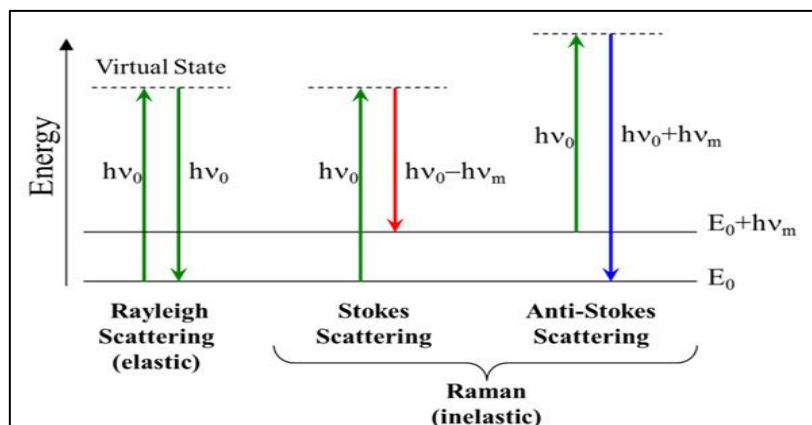


**Figure 1:** Schematic of energy levels for Rayleigh Scattering (elastic) and Stokes and Anti-Stokes scattering (inelastic) [19].

In principle, a molecule in its ground vibrational state has electrons in their lowest energy states. When electromagnetic radiation of energy  $h\nu_o$  is incident on a sample molecule, distortion (polarisation) of the electron cloud can happen which leads to generation of an unreal state known as a *virtual state*. The molecule is excited into this virtual state and upon de-excitation of the molecule, a photon is scattered with its energy,  $h\nu_o$ , either shifted up or down depending on the type of scattering process which took place. This energy shift,  $h\nu_m$ , is termed *Raman shift* and it is a shift from the incident energy  $h\nu_o$ .

There are two types of scattering processes, elastic and inelastic scattering. During elastic scattering, there is no energy transfer between the incident photon and the molecule. The scattered photon will have the same energy as the incident photon and this is known as *Rayleigh* scattering [15]. In contrast, during inelastic scattering, there is an energy exchange between the photon and the molecule. Either the incident photon gives part of its energy to the molecule which leads to creation of a vibrational hot state and the photon is emitted with energy less than its initial energy,  $h\nu_o - h\nu_m$ . This is a process known as Stokes Raman scattering and the Raman photon created is shifted to the red of the incoming photon. Or the molecule will already be in an excited vibrational state and during inelastic scattering, the molecule makes a transition to the ground vibrational state giving its energy to the photon which is then emitted with higher energy,  $h\nu_o + h\nu_m$ , thus, the photon is blue shifted. This process is called anti-Stokes Raman scattering. During anti-Stokes Raman scattering, for molecules to already be in an excited vibrational state it can be due to thermal excitation [13]. This implies that at equilibrium the anti-Stokes scattering depends on temperature, through the Boltzmann distribution law. As a result the anti-Stokes signal is much weaker compared to the Stokes signal in a Raman spectrum with the peaks becoming exponentially weaker with increasing vibrational energy [13], [15]. These three processes are illustrated in fig. 1.

Raman scattering is very weak and only a small fraction of approximately 1 in 10 million photons of the incident light beam are Raman scattered. Raman shifts are usually expressed in units of wavenumbers ( $\text{cm}^{-1}$ ). A representation of this Raman shift for a specific vibrational mode with its corresponding intensity is known as a Raman spectrum. Peaks in the Raman spectrum are vibrational modes of the molecule with their corresponding energies shown as Raman shifts. The Raman spectrum is a unique

fingerprint of a molecule and in a spectrum, not all Raman vibrational bands have the same intensity. This is governed by selection rules which shall be explained further in section 2.1.1.

## 2.1 Principles of vibrational spectroscopy

Vibrational motions inside a molecule are described by normal modes. Each atom in a molecule has 3 independent normal modes of vibration known as degrees of freedom in 3D space [13]. Consider a molecule fixed at its centre of mass with  $N$  number of atoms such that in total it will have  $3N$  degrees of freedom of motion for the atoms in it, namely translational, rotational and vibrational. Three coordinates describe the translational motion around the centre of symmetry, three and two coordinates describe the rotational motion in non-linear and linear molecules respectively, the vibrational motion is then described by  $3N-6$  internal degrees of freedom for a non-linear molecule and  $3N-5$  internal degrees of freedom for a linear molecule [13], [15], [20]

### 2.1.1 Polarisability and selection rules

Here we explain the foundation of the use of vibrational spectroscopy for molecular identification and characterisation. This is illustrated using a property of molecules which is affected by the inter-nuclear distance and is defined by the charge distribution at the equilibrium geometry of the electronic state known as molecular polarisability,  $\alpha$ . This section is explained with reference to; [13], [20]–[22]

Selection rules are applied in determining whether a vibration is IR or Raman active. For an IR active mode, the dipole moment must change during a vibration and for a Raman active mode the polarisability must change during a vibration. A molecule experiencing an external electric field will have its electron cloud distorted. Negative charges migrate towards the positive pole while positive charges move towards the negative pole, thus inducing a dipole with a dipole moment. The ability of the molecule's electron cloud to be distorted is known as polarisability. Polarisability is a tensor representing the shape and volume of the molecule's electron cloud and the molecule's response towards the external electric field is non-uniform in all directions. The tensor transforms in the  $x$ ,  $y$  and  $z$  directions. In the polarisability tensor,  $\alpha_{ij}$ , the indices  $i$  and  $j$  represent the  $x$ ,  $y$  and  $z$  directions to make up the tensor components. The subscript  $i$  shows the direction of the induced dipole moment by the oscillating external electric field component which will be in the  $j$  direction. The tensor can be expressed in matrix form as:

$$\alpha_{ij} = \begin{pmatrix} \alpha_{xx} & \alpha_{xy} & \alpha_{xz} \\ \alpha_{yx} & \alpha_{yy} & \alpha_{yz} \\ \alpha_{zx} & \alpha_{zy} & \alpha_{zz} \end{pmatrix} \quad (1)$$

For spectroscopic applications the tensor is considered to be symmetric;  $\alpha_{xy} = \alpha_{yx}$ ,  $\alpha_{xz} = \alpha_{zx}$  and  $\alpha_{yz} = \alpha_{zy}$  and this reduces the number of unknowns to only six. Each polarisability tensor component can be written as a series expansion about the equilibrium geometry as:

$$\alpha_{ij} = \alpha_0 + \left( \frac{\partial \alpha_{ij}}{\partial q} \right)_0 q + \frac{1}{2} \left( \frac{\partial^2 \alpha_{ij}}{\partial q^2} \right)_0 q^2 + \dots \quad (2)$$

with  $\alpha_0$  representing the equilibrium value of the Raman polarisability tensor and  $q$  the deviation from equilibrium. The first derivative, which is the second term, is responsible for observing the vibrational fundamentals in the Raman spectrum. Polarisability is defined as the molecule's response to the external electric field hence, the polarisability and its derivatives are second rank tensors. The polarisability derivative tensor is expressed as:

$$\alpha'_{ij} = \begin{pmatrix} \alpha'_{xx} & \alpha'_{xy} & \alpha'_{xz} \\ \alpha'_{yx} & \alpha'_{yy} & \alpha'_{yz} \\ \alpha'_{zx} & \alpha'_{zy} & \alpha'_{zz} \end{pmatrix} \quad (3)$$

with  $\alpha'_{ij}$  representing the first partial derivative of the derivative tensor element. Some of the properties of the tensor are that it is symmetric and trace invariant. For a symmetric tensor each vibration has six chances of appearing in the Raman spectrum. This further implies that at least one of the six tensor components must be non-zero in order for that vibrational transition to be allowed in the Raman spectrum. From this we then explain that RS is as a result of the molecule interacting with electric vector of the external electromagnetic field. During the interaction an electric dipole moment is induced and it is given by:

$$p_i = \alpha_{ij} E_j \quad (4)$$

where  $\mathbf{p}$ , the dipole moment and  $\mathbf{E}$ , the electric field are vectors with components in the  $x$ ,  $y$  and  $z$  directions and  $\alpha_{ij}$  taking the form of eqn. (1) and again as mentioned before, the subscript  $i$  shows the direction of the induced dipole moment by the oscillating external electric field component which will be in the  $j$  direction. The equation can also be written as

$$\begin{aligned} p_x &= \alpha_{xx} E_x + \alpha_{xy} E_y + \alpha_{xz} E_z \\ p_y &= \alpha_{yx} E_x + \alpha_{yy} E_y + \alpha_{yz} E_z \\ p_z &= \alpha_{zx} E_x + \alpha_{zy} E_y + \alpha_{zz} E_z \end{aligned} \quad (5)$$

By expressing the equation as a series expansion for each component:

$$p_i = \alpha_0 E_j + \left( \frac{\partial \alpha_{ij}}{\partial q} \right)_0 q E_j + \frac{1}{2} \left( \frac{\partial^2 \alpha_{ij}}{\partial q^2} \right)_0 q^2 E_j + \dots \quad (6)$$

however, since  $E = E_0 \cos(\omega t)$  which is the time dependant electric field strength and  $q$  describes an oscillation at the natural frequency  $\omega_0$  so that  $q = q_0 \cos(\omega_0 t)$  and ignoring the second and higher derivatives we have:

$$p_i = \alpha_0 E_0 \cos(\omega t) + \left( \frac{\partial \alpha_{ij}}{\partial q} \right)_0 q_0 \cos(\omega_0 t) E_0 \cos(\omega t) \quad (7)$$

and using the trigonometric identity:

$$\cos(x) \cos(y) = \frac{1}{2} [\cos(x + y) + \cos(x - y)] \quad (8)$$

eq. (7) becomes:

$$p_i = \alpha_0 E_0 \cos(\omega t) + \left( \frac{\partial \alpha_{ij}}{\partial q} \right)_0 q_0 E_0 \cos(\omega_0 - \omega) t + \left( \frac{\partial \alpha_{ij}}{\partial q} \right)_0 q_0 E_0 \cos(\omega_0 + \omega) t \quad (9)$$

Where, according to classical theory, the first term represents Rayleigh scattering, the second term is for Stokes Raman scattering and the third term is for anti-Stokes Raman scattering.

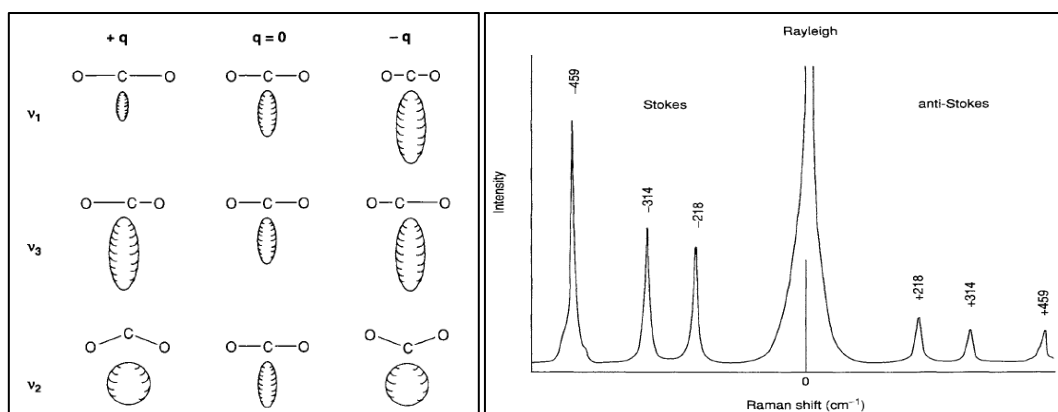


**Figure 2:** The changes in the polarisability ellipsoid during vibrations for CO<sub>2</sub> molecule (left) and the Raman spectrum of CCl<sub>4</sub> (right) at 488.0 nm excitation [13].

For linear molecules such as CO<sub>2</sub>, polarisability,  $\alpha$ , is observed along the chemical bond. A plot of  $\frac{1}{\sqrt{\alpha_i}}$ , with  $\alpha$  in the  $i$  direction, would give the polarisability ellipsoid and this is shown in fig. 2 (left). A vibration mode would then be considered as Raman active if the size, shape or orientation of the ellipsoid changes during a normal vibration. This is the case for v<sub>1</sub> in fig. 2 (left), polarisability is changing in all directions and  $(\partial \alpha / \partial q_n)_0 \neq 0$ . Vibrations v<sub>2</sub> and v<sub>3</sub> have their polarisability changing symmetrically with respect to  $q$ , thus  $(\partial \alpha / \partial q_n)_0 = 0$  rendering the vibration not Raman active.

For RS and SERS studies, it is possible that some modes of vibration which do not appear in the normal RS will appear in the SERS while others may disappear or appear much stronger. This cannot be given any straightforward explanation. However, the intensity of Raman modes as shown above in eq. 5 depends on the polarisability of the

bond, which in turn is determined by symmetry of the molecule and associated selection rules [23]. When a molecule is in contact with the surface of a metal, distortion occurs to the molecular structure bringing about geometric differences and a modification of the molecule's symmetry compared to its native solution phase structure [23].

For molecules which have a centre of symmetry, when they are in close proximity to a metallic surface there is a change of symmetry which occurs which consequentially changes intensities and the transition probabilities. The rule of mutual exclusion illustrates that Raman bands which are present in RS are absent in IR spectroscopy and vice versa. This rule only applies to those molecules with a centre of symmetry, however, when this feature is lost, the rule of mutual exclusion no-longer applies and similar bands can be found in both the Raman spectrum and the IR spectrum.

Inspection of the normal mode provides information on whether a vibration mode is infrared or Raman active, but this simple notion is inapplicable to larger molecules. Modes are altered depending on the orientation of the molecule as it lies on the metal surface, i.e. whether the molecule is parallel or perpendicular to the surface. However, polarisability must change during a particular Raman vibration while the dipole moment remains the same, the reverse of an infrared absorption driven transition.

For molecular systems observation of a vibrational transition is highly dependent upon the polarisability of the molecule. In RS not all vibrational transition are allowed, some are forbidden according to the selection rules which are applied to each normal vibration. Thus, peaks which appear in a normal Raman spectrum show the Raman active modes of vibration providing the molecular fingerprint. Fig. 2 above shows the Raman spectra of  $\text{CCl}_4$ . In that spectra the anti-stokes lines appear weaker than Stokes lines. However, both Anti-stokes and Stokes lines are symmetric about the excitation laser line. Due to the strength of the Stokes lines, they are considered in this study.

### 2.1.2 Raman cross section

The function 'cross section' connects theory and experiments for inelastic scattering. The overall Stokes-scattered light averaged over all random molecular orientations is proportional to the incoming photon flux [20]. This is mathematically expressed as:

$$I_{RS} = \sigma_{RS} I_0 \quad (10)$$

where  $I_{RS}$  is the intensity of Raman scattered light,  $I_0$  the initial intensity of the light beam and the constant of proportionality,  $\sigma_{RS}$ , known as the Raman cross section. This Raman cross section is dependent upon the excitation frequency. Cross section is explained as the target area presented by the molecule for absorption or scattering purposes [20].

In this study, for analysis of biomolecules, RS was chosen mainly because when working with biological samples, the technique shows a weak Raman spectrum for water. Water is a poor Raman scatterer and for measurement of aqueous samples there would be little interference from the solvent. Though RS is similar to infra-red (IR) spectroscopy in the sense that they both provide vibrational information of samples, each one has advantages over the other. With IR spectroscopy there is strong absorption

of water which limits the technique for measurements of aqueous biological samples. Thus, the technique RS is employed instead. With RS, small sample quantities can also be measured, ranging from gases, liquids, powders and fibres [14]. However, the technique also comes with disadvantages. Firstly, the technique requires careful operation by use of computer software to drive the equipment and setting of measuring conditions. In this study it was of utmost importance for the measuring conditions to be followed per equipment through the measurement. This was important as it would contribute greatly to setting of the standard measuring protocols of biomolecules. Fluorescence is also another aspect which affects Raman signals especially when dealing with biological samples. It affects the quality of Raman spectra and in some cases it may completely camouflage the weak RS peaks. One such method which tries to address this problem, amongst many, is SERS which shall be further explained below.

## 2.2 Surface Enhanced Raman spectroscopy (SERS)

SERS is a form of RS technique whereby high Raman cross section is achieved due to the sample molecules being in close proximity to the metallic surface. It is an analytical method for characterising biological molecules and with SERS as a technique, the Raman signal is increased significantly relative to the fluorescence. SERS relies on the enhancement of the Raman signal by several orders of magnitude through the interaction of the sample molecule and a metallic surface, usually silver (Ag) or gold (Au). This results in shorter acquisition times during measurements and a marked improvement in signal to noise ratio. Since its establishment the technique has received great appreciation and considerable interest in the analysis of fluorescence prone biomolecules.

From this technique, it is possible to extract information on orientation of the sample molecule on the metallic surface. The first observation of SERS was reported by Fleischman *et al.* when studies were done on pyridine<sup>2</sup> and a large enhancement was observed using a silver electrode surface [24]. Verification on pyridine and further studies on amines were then carried out by Jeanmaire and Van Duyne, and Albrecht and Creighton, and the adsorbed samples gave enhancements in the order of  $10^5$ - $10^6$  [25] [26]. These and other early findings prompted and forged ahead studies of molecules adsorbed on metallic structures due to the reason that a molecule in close proximity to a metallic surface gave increased intensity as compared to an isolated molecule. This then led to use of metallic structures in RS, now called SERS, in studying solids, liquids, gases, powders and fibres to date [13].

### 2.2.1 Principles of SERS

Ultraviolet to infrared laser excitation sources are utilised for SERS studies. Along with the laser wavelength used it is also important to choose the most effective type of metal to bring about the SERS effect. Several types of metallic surfaces have been used including electrochemical surfaces [27] and the use of metallic structures in colloidal

---

<sup>2</sup> Pyridine is a basic heterocyclic organic compound which has a structure similar to that of benzene, but with one methane group replaced with a nitrogen atom.

solution [21], [28]. The results of which revealed that the substrate nature has great influence on the enhancement of Raman signals.

For a molecule adsorbed on a metallic surface, for there to be a Raman signal enhancement there must be an enhancement in molecular polarisability. Enhancement is brought about due to mechanisms involved between a molecule and a metallic surface which include chemical and electromagnetic enhancement. By employing either roughened or fine metallic surfaces, under the influence of an external optical field and according to the two enhancement mechanisms (chemical and electromagnetic enhancement), there is the generation of surface plasmons on the metal surfaces [29] which further promote the increase of the Raman signal. This shall be illustrated in sections below.

Metallic colloids can be made from different metals such as silver (Ag), gold (Au), aluminium (Al) and copper (Cu) [30] with Ag and Au being preferred [31]. Each material has characteristic surface plasmons which are size dependant [30] and in this study Ag and Au were employed for SERS on biomolecules. Though SERS has greater sensitivity compared to RS, several challenges are also encountered while in the process of obtaining amplified Raman signals. Some of the challenges being photo-dissociation<sup>3</sup> of adsorbed molecules which will leave its own fingerprints on SERS spectra as well as the presence of impurities which further complicates analyses of SERS spectra [20].

---

<sup>3</sup> This is the breaking down of a chemical compound when it interacts with one or more photons. Also, known as photolysis or photo-decomposition.

### 3 Metallic colloids as SERS substrates

In this section we explain mechanisms which bring about signal enhancement due to sample molecules being in close proximity to metallic surfaces and connect this to SERS.

Signal enhancement crucially depends on the SERS substrate. Since the independent discoveries by Creighton *et al* and Jeanmaire *et al* in 1977 that the enhancement of Raman scattering was attributed to an intrinsic surface enhancement effect, significant attention has been given to the successful fabrication of SERS substrates due to the fact that applications greatly rely on the activity and reproducibility of the substrate [25], [26]. The mostly used SERS substrates are metallic colloidal particles. Colloids are a state of matter in between a solution and a suspension. They are not a solid since they do not have a rigid structure and they cannot be classified as a solution since the solute will not be completely dissolved in the solvent. When considering SERS colloids, they are an artificially made substance comprising of particles dispersed in a fluid medium, either air, liquid or gel. The colloidal particles generally tend to have large relative molecular masses, have diameter sizes in the order of nano-meters (1-100 nm), thus, they are also known as nanoparticles [31]. Nanoparticles can be made into any shape, for example nanospheres, nanotriangles or nanorods [29], [32], [33] and many other shapes. Compared to their bulk material, colloidal nanoparticles offer great Raman signal enhancement which is the foundation of SERS. Unlike solid or bulk SERS substrates, colloidal nano-structures allow the use of high laser power as there is minimal burning of samples. Nanoparticles also have the ability to scatter visible light when they are dispersed in a solvent, this is known as the *Tyndall effect*. Thus, the technique UV-Vis absorption spectroscopy can be used to characterise the size and morphology of nanoparticles since it is based on how electromagnetic radiation interacts with matter [34], [35].

There are several methods of making metal colloids which include photo-induced reduction, laser ablation and chemical reduction in aqueous and non-aqueous media [36], [37]. By applying these and other types of nanoparticle preparation methods, the nanoparticles can be used for several purposes which include use as chemical catalysts [38], [39], biosensors [33], [40], used in bio-imaging [41], used as anti-bacterials [42] and in SERS applications [25], [30], [31], [34], [35], [43]. The most widely used method of preparation is preparation by chemical reduction and this tends to form different sized particles suspended in a liquid (colloids). Chemical reduction is mainly used because it is easily achieved, it produces stable suspended nanoparticles, there is rapid preparation of colloidal particles and there is production of stabilising counter-ions during the reaction, preventing large multi-particle units [31]. The particle size and distribution are affected by how the method is carried out. Furthermore, the method of colloid synthesis highly affects the nature, morphology and environment of the colloids and this is important to consider for SERS applications [34], [35]. The main chemical reaction for preparation of nanoparticles is reduction of a metallic assay by different types of reducing agents in solution. Typical reducing agents include hydroxylamine hydrochloride [34], [35], sodium borohydride and trisodium citrate [34]. By controlling the reducing agent, reaction temperature, pH of reactants and reaction time, nanoparticles of varying shapes and sizes can be synthesized.

Several metals have been utilised before in making metallic colloids. Those favourable for modern optical techniques such as SERS being Ag and Au [31]. Silver is the one widely used due to its high stability, broad plasmon resonance and easy preparation [34]. Silver and gold nanoparticles are commonly utilised as SERS protein substrates due to their optical properties as they can generate strong surface plasmon resonances [43], [44]. However, silver nanoparticles tend to offer better resonance peaks which are sharper than those of gold. Hence, silver usually provides better sensitivity in techniques such as SERS.

In the past decade research has been done on effects of metallic nanoparticles towards biological substances. Nanoparticles are one of the most promising substances being looked at for their applications in chemistry, industrial applications in manufacturing nanoparticle-related products which include clothes, cosmetics, toys and devices and in medical applications such as antimicrobial coatings, cancer detection and wound dressing [45], [46]. Thus, due to these and many other applications nanoparticles of different metals, sizes, made using various methods and having different surface charges have been investigated as these factors affect the performance of nanoparticles. This ultimately implies then that for engineered nanoparticles, by altering any one of those factors, the performance or characteristics and interaction of nanoparticles with molecules is consequently affected.

Interaction of nanoparticles and proteins is explained according to the surface chemistry between the nanoparticles and proteins (amino acids). The surface chemistry is according to selective adsorption of proteins caused by electrostatic interactions [47]. The selective adsorption of the amino acids is according to the amino acid functional groups and their affinity for positively charged metals. Some of the known functional groups include the carboxyl, amine, hydroxyl and thiol (also known as the sulphur (S) group) groups. The bonds formed include the anchoring bonds, where the lone pairs of electrons of oxygen, sulphur or nitrogen are transferred to the metal, and the non-conventional hydrogen bonds where the lone electron pairs of the metal are transferred to the anti-bonding orbital of O-H and N-H bonds [47]. The sulphur group is usually found on the peripheral of large proteins and anchors very well to metals such as Ag and Au. For SERS purposes, the strong bonds formed between a functional group and a metal promotes charge transfer between the two and charge transfer in turn greatly enhances the Raman signal via chemical enhancement. For a greater SERS effect it is also vital to tune/ choose a laser wavelength which matches the wavelength that the nanoparticles absorb according to their size, thus promoting near-resonance excitation which increases the Raman signal.

For nanoscience and nanotechnologies it is vital to consider the toxic effects of nanoparticle interaction with biomolecules. Studies have been done on toxic effects of nanoparticles on cell walls of the *E.coli*<sup>4</sup> bacteria. The production of silver ions from nanoparticles in aqueous state results in the produced ions binding with the sulphur group of the inner cell structures of proteins, thus prohibiting them from carrying out their task [46]. Studies done on stem cells [48] have shown that nanoparticles can have negative influences on living organisms depending on the nanoparticle concentration, size and how they were prepared.

---

<sup>4</sup> *E.coli* is a rod-shaped bacterium found in the lower intestine of warm blooded organisms.

Compared to silver nanoparticles (AgNP), gold nanoparticles (AuNP) tend to quench fluorescence to a certain degree. When performing SERS measurements it is essential to consider the nature of samples to be analysed. Samples which fluoresce, such as biomolecules, have fluorophores which emit at wavelengths above 500 nm. This means the light photons absorbed have a wavelength which is below that of 500 nm. Ultimately, this then implies the importance of having nanoparticles of a size which makes them absorb light in the range above 500 nm and at the same time choosing a laser wavelength which matches the wavelength absorbed by those nanoparticles to ensure near-resonance excitation. In this study, a 532 nm laser was utilised, hence the average size of synthesised nanoparticles was 20 nm for both AuNP and AgNP. For AuNP, the 20 nm sized nanoparticles absorb light in the range 500 – 550 nm (blue – green colour) [32], [49] and hence they tend to quench fluorescence. Energy transitions favourable for fluorescence to take place are not supported. On the other hand, 20 nm sized AgNP absorb wavelengths below 500 nm and fluorescence quenching is minimised however, the SERS enhancement factor for Ag is 10 to 100 times more than that of Au [34]. Other desirable properties for Au surfaces are that the oxidation potential of Au is higher than that of Ag such that there is prevention of oxidant formation and also biological molecules bound to Au surface retain their conformation [50].

As a result, great care was taken in synthesising the nanoparticles in order to ensure the right physical properties (size and shape) which would lead to a greater SERS effect. Applications and uses of nanoparticles in industry include the use of nanoparticles made from transition metals such as platinum for catalysing and speeding up chemical reactions and by using smaller sized nanoparticles, large surface areas can be achieved using small volumes of the colloid [32]. In biology and medicine, detection of trace substances is achieved by utilising nanoparticles as they are environmentally sensitive, making it possible and easier to track and detect contaminants [32]. Technological applications include the use of nanoparticles in making memory elements, due to their small size, information can be saved and stored on a small area which requires not much space [49]. Other applications are in photonics and antimicrobial applications.

### 3.1 Localised Surface Plasmon Resonance (LSPR)

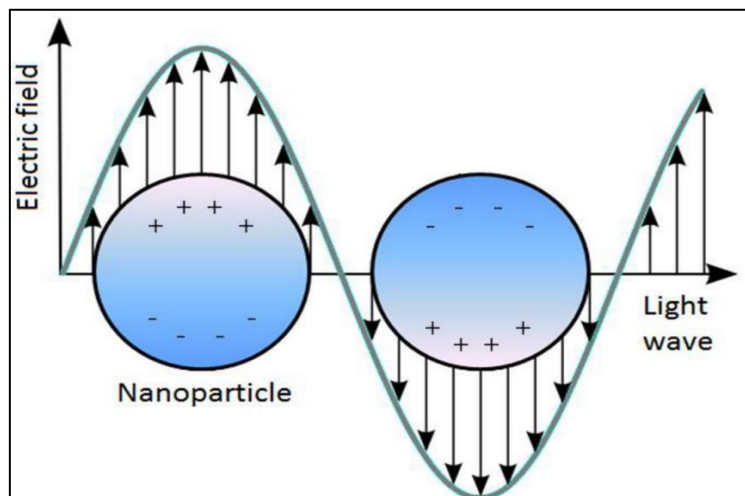


**Figure 3:** Schematic of LSPR showing free conduction band electrons in the metal nanoparticle oscillate due to coupling with incident light [51].

In bio-sensing and detection the optical properties of nanoparticles are exploited. Metallic nanoparticles of sizes smaller than the wavelength have free electrons in the conduction band, which when excited by light in the visible and near-infrared region display unique and strong optical resonances [52]. Upon excitation of the conduction electrons by incident photons, the electrons coherently oscillate as shown in fig. 3. This collective oscillation is known as surface plasmon resonance and its frequency depends on the shape, size composition and distance separation of nanoparticles [33], [53]. The oscillating surface electrons produce an oscillating dipole which oscillates with its own characteristic frequency, thus producing localised electromagnetic radiation [30]. The increased electromagnetic field enhances Raman signals for molecules close to the metal nanostructures. Localised Surface Plasmon Resonance (LSPR) differs from surface plasmon resonance (SPR) in the sense that the former has the resonance electrons oscillating on the nanostructure and not on a metal dielectric interface [51]. Thus, the electromagnetic field exponentially decays on the order of 200 nm for SPR while for LSPR it decays on the order of 6 nm [54]. This reduced exponential decay in LSPR provides increased sensitivity to refractive index changes on the metal surface and this forms the basis for LSPR applications in bio-sensing [54]. There are two known explanations of enhancement, namely chemical and electromagnetic enhancement [35].

## 3.2 Enhancement and enhancement factors

The mechanisms of electromagnetic and chemical enhancement are explained below with reference to [20], [30], [55], [56] and [57].

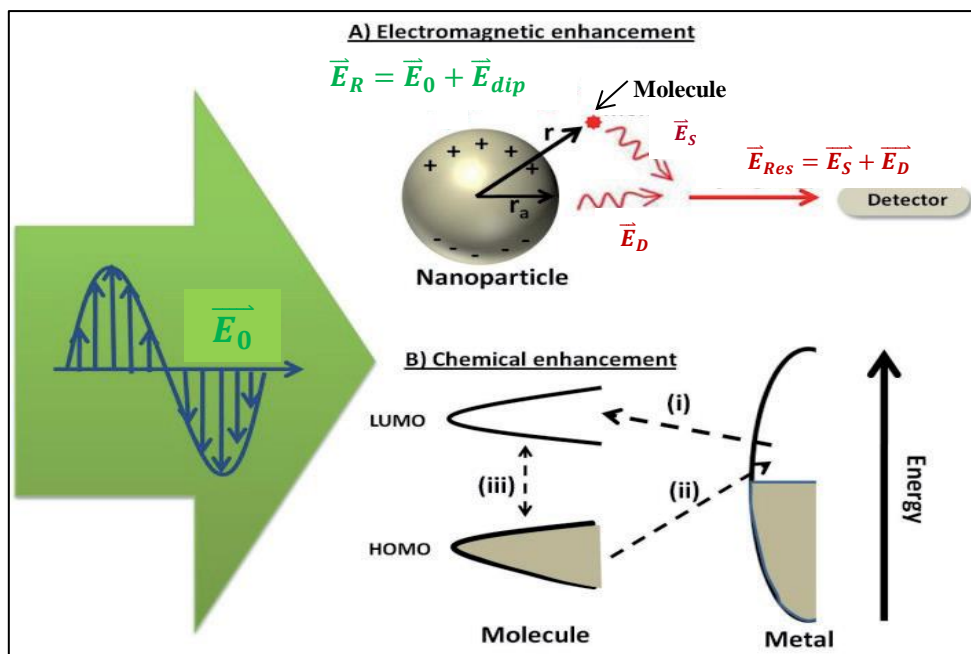


**Figure 4:** A schematic representation of electromagnetic and chemical enhancement. Electromagnetic enhancement shows,  $\vec{E}_0$ , which is the incoming field. The outgoing field,  $\vec{E}_R$ , represents a resultant electromagnetic field which the molecule experiences.  $\vec{E}_R$  is the sum of the incident field,  $\vec{E}_0$ , and the field produced by the oscillating dipole,  $\vec{E}_{dip}$ . In chemical enhancement below the processes (i) and (ii) show the charge transfer which happen between the metal and the molecule and the double arrow indicates the resonant Raman processes which happen in the molecule's electronic states [30], [57].

### Electromagnetic enhancement

A metal atom comprises of a nucleus surrounded by a cloud of electrons. The attraction between the nucleus and the electrons keeps the electrons in their respective orbitals. For nanoparticles made from noble metals which are utilised for SERS applications, each type of metal has its own characteristic plasmon (collective oscillation of electrons) associated with it. This characteristic plasmon is also size dependant. When the plasmon electrons are excited by an external electric field, they oscillate leading to the induction of an oscillating dipole which has its own characteristic frequency. The oscillating induced dipole generates a localised electromagnetic field, thus any molecule in close proximity to the nanoparticle experiences a field equal to the sum of the external electric field,  $\vec{E}_0$ , and the field generated by the induced dipole,  $\vec{E}_{dip}$ . As a result, a resultant incoming electromagnetic field experienced by the molecule will be,  $\vec{E}_R = \vec{E}_0 + \vec{E}_{dip}$ . After the resultant incoming field interacts with the molecule,  $\vec{E}_S$ , then represents the red shifted dipole radiation in the case of Stokes scattering and  $\vec{E}_D$  stands

for additional elastically scattered light. Thus, the resultant outgoing field detected after Stokes RS will be  $\vec{E}_{Res} = \vec{E}_S + \vec{E}_D$ . This is as depicted in fig. 4. Electromagnetic enhancement plays a key role in SERS. A molecule in close proximity to the metal surface will have a strong Raman signal due to the increased electromagnetic field which it experiences resulting in SERS.

### Chemical enhancement

During chemical enhancement, the sample molecule has to be in direct contact with the metal nanostructure since bonding has to occur. Electronic coupling between metal and molecule leads to charge transfer which in turn increases the Raman cross section [30], [33]. Charge transfer between the electronic levels (the highest occupied molecular orbitals (HOMO) to the lowest unoccupied molecular orbitals (LUMO)) of the adsorbate<sup>5</sup> and the metal orbitals leads to the observed broadening and shifting of bands in the Raman spectra as well as the appearance of new bands. In fig. 4 the processes (i) and (ii) show the charge transfer which happens between the metal and the molecule. The double arrow indicates the resonant Raman processes which happen in the molecule's electronic states. These mechanisms are well illustrated by [57] and [30].

### Enhancement Factors (EF)

Enhancement factor is considered to be the magnitude by which the signal increases from a normal Raman signal,  $I_{RS}$ , to a surface enhanced Raman signal,  $I_{SERS}$ . The two signals are compared when measurements were taken under the same conditions of laser power, laser wavelength, angle of incidence of the laser and use of the same spectrometer [58]. Thus, the enhancement factor is a value used to characterise the strength of the SERS effect. There are several types of enhancement factors such as Single Molecule EF (SMEF), Orientation-Averaged Single Molecule Enhancement Factor (OASMEF) and average enhancement Factor (AEF) [59]. Enhancement factors are distinguished based on their sensitivity to experimental conditions, the SERS probe in use and the SERS substrate [58]. In this study, a simple procedure of finding the ratio between  $I_{SERS}$  and  $I_{RS}$  was calculated in order to find the enhancement factor. These calculations and values are in the section 6.1 in this report. Depending on the excitation wavelength enhancement factors are known to range from a factor of  $10^4$  to  $10^{11}$  [60].

## 3.3 LSPR dependence on nanoparticle distance separation and morphology

From theory it has been shown that two or more aggregated nanoparticles can result in a stronger Raman signal enhancement as compared to the signal from individual particles [33]. Aggregation is one way in which the LSPR effect can be controlled. This is due to the coherent interference of the coupled electromagnetic fields of the nanoparticles. Nanoparticles on their own enhance the Raman signal but aggregated nanoparticles, with distance separation smaller than the wavelength of light, can create a much stronger enhancement [33], [55]. The spectral wavelength for clustered nanoparticles

---

<sup>5</sup> An adsorbate is a substance adsorbed. In this case it will be the sample molecules adsorbed onto the metal surface.

tends to red shift or even approach the near infra-red region, thus, enabling the colloids to be used in analysis of biological tissue with minimum absorption [61]. Aggregation of nanoparticles is usually achieved by using surfactants, organic amines, mineral acids or the use of inorganic salts such as KCl, MgSO<sub>4</sub>, NaCl, NaBr, NaNO<sub>3</sub> or the target molecule itself. However, most chemicals are not well-suited for biomolecule aggregation [31], [43]. Upon addition of anions, nanoparticles form clusters/agglomerates such that a molecule can be located in-between the clusters. Direct contact between molecule and nanoparticle is essential in order for electronic coupling to happen which in turn increases the Raman cross section as charge transfer occurs resulting in a much greater enhancement [55]. This region in which the molecule will be trapped in is called a “hot spot” and enhancement factors under such a situation can be as high as 10<sup>12</sup> [60]. Studies have shown that aggregation of AgNP with negative ions such as citrate or halide ions (chlorine, bromide, iodide ions) greatly amplifies the Raman scattered light with enhancement as much as 10<sup>11</sup>-10<sup>12</sup> [55].

Three major reasons for the Raman signal enhancement reported were due to increased electromagnetic field brought about by aggregated nanoparticles. The first reason, as explained by Wang and co-workers reported on how concentrations as low as 10<sup>-12</sup> M of a sample molecule can be detected upon aggregation of AgNP with chloride ions because of increased electromagnetic enhancement by nanoparticle clusters as well as reorientation of the molecule on the nanoparticle surface [62]. The second reason leading to signal enhancement by nano-clustering was by charge transfer mechanism between the molecule and nanoparticles. Studies have shown that halide ions create surface active sites on colloidal surfaces [63]. The third reason is in relation to findings by Grochala *et al.* where they illustrate that the signal enhancement not only resulted from the generation of “hot spots” or charge transfer mechanism from unstable roughened metal surfaces, but instead it should also be attributed to anion-induced reorientations of the molecule in question [64]. Results based on aggregation of nanoparticles with organic molecules have been shown in the case when a substance avidin<sup>6</sup> was used to induce aggregation of silver nanoparticles for detection of another molecule. The clustering was due electrostatic interactions brought about by avidin resulting in strong SERS bands and detection of the complex ligand [43].

The properties of nanoparticles are also determined by their shape and size as nanoparticle shape directly affects polarisation. Regarding this aspect, reference is made to [33]. Nanoparticles can be produced in various shapes such as triangles, spheres, rods, stars, bipyramids, cubes and prisms. Nanoparticles which have sharp edges have more charge separation as compared to those which are spherical. LSPR is affected by nanoparticle shape and for more symmetrical nanoparticles there is increased LSPR. Non-spherical nanoparticles have LSPR peaks which are more red-shifted and they exhibit multipoles given that they can be polarised in more than one direction [32], [33]. For spherical nanoparticles the LSPR peak dominates more in the visible region and in this study, it was important for the type of nanoparticles chosen to have a LSPR peak in that region as it was close to the wavelength of the excitation source, of 532 nm. Nanoparticles with a resonance peak located close to the wavelength of the excitation

---

<sup>6</sup> Avidin is a glycoprotein found in egg white of birds, reptiles and amphibians. It has four similar subunits.

source allow for near resonance excitation which is of great advantage in performing SERS studies as it relies on signal enhancement. The choice of size for the nanoparticles greatly influences the magnitude of the scattering cross section. For very small colloids of size less than 20 nm the dominant process will be absorption, but with increasing size, light scattering becomes more favoured [65].

## 4 Biological molecules

### 4.1 Amino acids

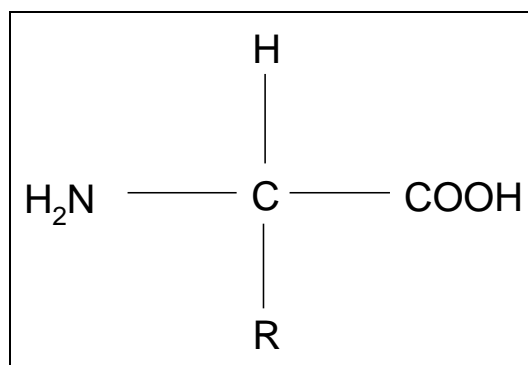
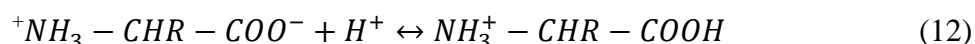


**Figure 5:** General structure of an amino acid showing the four groups (amino group (left), carboxylate group (right), hydrogen atom (top), R-group (bottom)) surrounding the central  $\alpha$  C atom.

Amino acids are the basic building blocks of proteins. They participate in several reaction mechanisms such as energy transfer, muscle activities and chemical reactions [66]. In living organism amino acids are classified as either essential<sup>7</sup> or non-essential<sup>8</sup>. Those that are essential include isoleucine, leucine, histidine, lysine, methionine, phenylalanine, threonine, valine and tryptophan and the non-essential are asparagine, cysteine, alanine, glutamine, proline, glycine, serine and tyrosine [66]. Of the several types of amino acids, those found in living organisms include alpha amino acids which mainly consist of a central alpha carbon (C) atom surrounded by a carboxyl (-COOH), an amine (-NH<sub>2</sub>) functional group and a side chain (R-group) which is characteristic of the type of amino acid. Amino acids are tetrahedral in structure and exist as zwitterions. Zwitterions are formed when there is internal movement of a proton from the carboxylic acid to the amino group. Amino acids are also amphoteric implying that in water the zwitterion can either act as an acid, proton donor:



or base, proton acceptor:



<sup>7</sup> Those which have to be consumed in a diet.

<sup>8</sup> Those which the body can produce on its own.

Amino acids can polymerise to form a peptide bond when two amino acid residues<sup>9</sup> combine via covalent linkage. Due to their varying side chains, amino acids have different structures, electric charges and size, thus, ultimately resulting in them having different solubilities in water. Below are the amino acids used in this study, classified according to the properties of their R-groups.

#### 4.1.1 Polar but uncharged amino acids

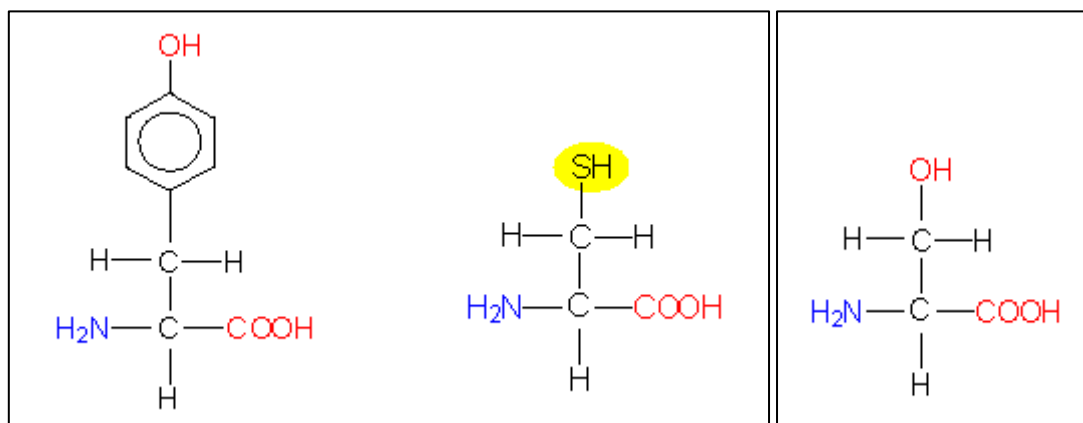
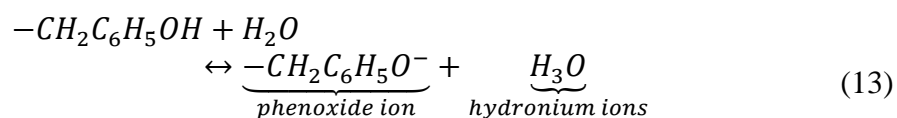


**Figure 6:** Chemical structure of L-tyrosine (left), L-cystein (middle) and L-serine (right) [67].

- *Aromatic: L-tyrosine*

L-tyrosine is a neutral or uncharged polar amino acid and it is a phenol. It has an aromatic ring which is hydrophobic and only reacts under extreme conditions. In water, it has very limited solubility. The reason for its insolubility is due to the phenyl ring structure which has limited association with water, thus non-polar, giving the whole amino acid little solubility in water [68]. One way to make the substance more soluble in water is by increasing the acid strength of the solvent. Thus, an acid can be added in a tyrosine/water solution followed by a bit of heating leading to it dissolving. Or the whole amino acid can be dissolved in an acid. In HCl it has a solubility of 0.1g/ml with added heating. Phenol is a weak acid [69] and so in water the side chain can be deprotonated to form a phenoxide ion and a hydronium ion:



This leaves lone pairs of electrons on the oxygen atom of the phenoxide ion. The lone electron pairs which will then overlap with the electrons of the benzene ring. This overlap means electrons are well spread out and charge transfer takes place, thus stabilising the structure. However, oxygen has high electronegativity so it will tend to draw those electrons back to itself, thus destabilising the structure again [68]. Upon

<sup>9</sup> Residue refers to something which remains after a portion has been removed. In this case water is removed and the remaining parts form a peptide bond.

addition of an acid such as HCl, the chlorine group will interact with the para and ortho positions of the ring structure, reducing the negative charge on the phenoxide ion, thus making the structure stable [68]. Other negative groups which also stabilise the ring are (bromide)  $-\text{Br}$  ions [68]. This hydroxyl group of tyrosine is also more acidic compared to other amino acids with hydroxyl groups on their side chains, e.g. serine [70]. When the hydroxyl group is ionised, the phenyl ring stabilises the anionic phenolate form [70]. However, the delocalised electrons in the ring structure can be readily polarised. A Raman spectra for L-tyrosine would show a peak close to  $830\text{ cm}^{-1}$  which is a marker for the presence of a ring structure [27].

- *Sulphur: L-cysteine*

The sulfhydryl ( $-\text{SH}$ ) functional group in L-cysteine is also known as the thiol group. The whole R-group of L-cysteine is slightly polar and the thiol group can ionise at slightly alkaline pH. L-cysteine is a sulphur analogue of alcohol. Compared to alcohols, thiols have covalent bonding and less association with hydrogen bonding. This gives them a lower solubility in water compared to alcohols, thus, L-cysteine has a lower solubility than that of L-serine [69]. The  $-\text{SH}$  bond is non-polar due to the low electronegative difference between the sulphur (S) and the hydrogen (H) groups ( $2.58 - 2.2 = 0.38$ ) [69]. Thus, L-cysteine is slightly polar and hydrophilic. When L-cysteine is exposed to air two L-cysteine molecules can combine to form cystine which has a hydrophobic, non-polar disulphide bond, S-S, under oxidation reaction [71]. The same S-S can be reduced again to form  $-\text{SH}$  using a variety of reducing agents. The sulphur in L-cysteine anchors the amino acid to the metal.

- *Alcohol: L-serine*

L-serine is also a neutral or polar uncharged amino acid. Its polarity is attributed to the hydroxyl group which also qualifies it as a proton donor and an acceptor during hydrogen bond formation. Alcohols tend to be less acidic compared to phenols and as aqueous solutions alcohols have pH the same as that of water [69].

## 4.1.2 Hydrophobic amino acid(s)

### *Glycine*

Glycine is the smallest of all the known 20 amino acids generally found in proteins and it is non-polar. This is the simplest amino acids as it has H as its side chain. All amino acids are chiral except for glycine [71]. The carboxyl and the amide group neutralise in the zwitterion state and the hydrogen side chain is non-polar.

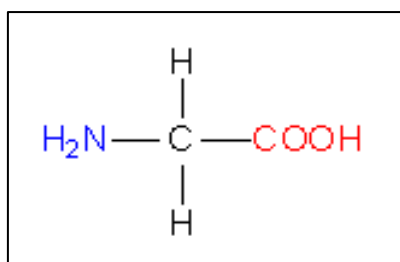


**Figure 7:** Chemical structure of Glycine [67].

## 4.1.3 Basic amino acid(s)

### *L-lysine*

This is a basic, polar (positive charge at the end of its side chain due to the amine group) amino acid. It has one carboxyl group and two amide groups, giving a net basic effect. L-lysine has four alkyl groups attached to the second amide group to make the side chain. L-lysine has a strong positive charge at neutral pH and it has a high solubility [71].

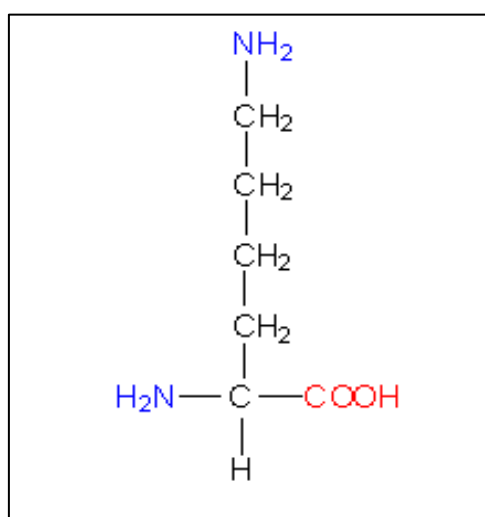


**Figure 8:** Chemical structure of L-lysine [67]

#### 4.1.4 Acidic amino acids

*L-aspartic acid,*

*L-glutamic acid*

These amino acids are polar (negative charge at the end of its side chain due to the carboxylate group) when in solution and have acidic side chains at neutral pH [72]. Thus, they can readily form hydrogen bonds by acting as a donor or acceptor. L-aspartic acid and L-glutamic acid both have one amide group and two carboxyl groups giving them a net negative charge. In addition to the second carboxyl group side chain, these acidic amino acids differ in the methylene groups in their side chains. L-aspartic acid has one methylene group while glutamic acid has two. Alkyl groups affect polarity and the more alkyl groups there are, the less polar the amino acid will be. Thus, L-aspartic acid is more polar than L-glutamic acid.

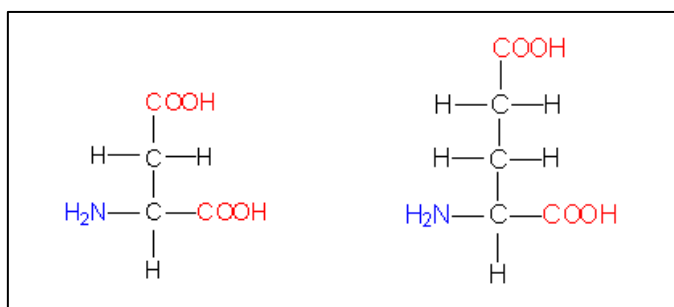


**Figure 9:** Chemical structure of L-aspartic acid (left) and L-glutamic acid (right) [67].

Amino acid name	3-letter & 1-letter code of amino acids	R-group side chain	Molecular weight [g/mol]	Group	Characteristics
L-cysteine	Cys, C	-CH <sub>2</sub> SH	121	Sulphur	Polar but uncharged
L-serine	Ser, S	-CH <sub>2</sub> OH	105	Alcohol	
L-tyrosine	Tyr, Y	-CH <sub>2</sub> C <sub>6</sub> H <sub>5</sub> OH	181	Aromatic	
Glycine	Gly, G	-H	75	Hydrophobic	non-polar
L-lysine	Lys, K	-(CH <sub>2</sub> ) <sub>4</sub> NH <sub>3</sub>	146	Basic	Polar and charged
L-aspartic acid	Asp, D	-CH <sub>2</sub> COOH	133	Acidic	Polar and charged
L-glutamic acid	Glu, E	-CH <sub>2</sub> CH <sub>2</sub> COOH	147	Acidic	

**Table 4-1:** Summary of amino acids examined in this study and their characteristics.

## 4.2 Proteins

Proteins are made up of amino acids. Proteins are found in a large number of varieties in cells. The smaller monomer amino acids make up proteins which are constructed from a set of 20 amino acids which are covalently linked in a linear sequence. The sequence of amino acids gives the protein unique properties, leading to it forming a particular structure and permitting it to perform a specific cellular function and makes it distinguishable from other proteins. RS is one technique which has the ability to provide information on protein structure. It can also be used in studying and understanding protein interactions. From the Raman spectra of biomolecules, bands can be assigned and in SERS the position and intensity of these bands is influenced by the molecule's environment, pH, salt concentration, orientation of molecule on a metallic surface and distance of the molecule from the metallic nanostructure. From the Raman or SERS spectra several bands can be observed attributed to the protein's amino acid side chains which include aromatic rings, sulphurs, acidic and basic groups, alkenes, alkanes and amides [71].

The amide functional group is composed of a carboxyl and amine group. There are three types of amides; primary (nitrogen atom attached to a single carbon atom), secondary (nitrogen atom attached to two carbon atoms) and tertiary (nitrogen atom attached to three carbon atoms) amides. This is shown in the image below.

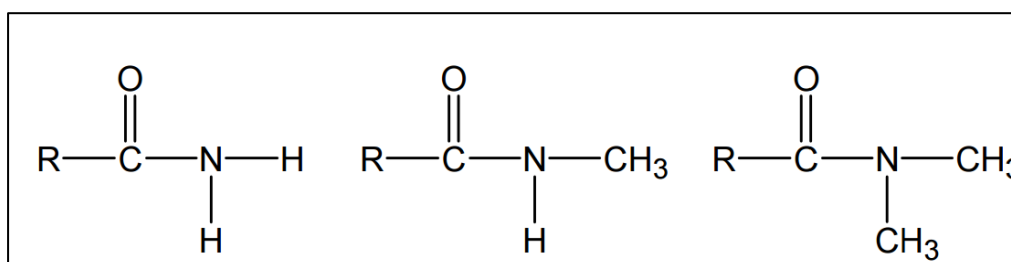


**Figure 10:** Molecular structure of primary (left), secondary (middle) and tertiary amides [73].

Using the technique RS, band allocation can be done for amide bands in proteins. The amide I bands in regions  $1660-1665\text{ cm}^{-1}$ ,  $1665-1680\text{ cm}^{-1}$  and  $1640-1658\text{ cm}^{-1}$  are for the different conformation which are random coil, beta pleated sheet and the alpha-helix respectively [30], [74]. This band also consists of out-of-plane CN stretching vibration, CCN deformation and C=O stretching vibrations with some contribution from N-H bending. The amide II, located in the region around  $1550\text{ cm}^{-1}$  comprises of the NH in plane bending and the CN stretching vibration [30], [74]. There are also contributions from the CO in-plane bending and the CC stretching vibration [75]. The amide III band is in the region from  $1200-1400\text{ cm}^{-1}$  and it comprises of the NH bending and the CN stretching vibration with additional contributions from in plane CO bending and the CC stretching vibration [74]. There are other aromatic side chains found in proteins such as tryptophan (Trp), tyrosine (Tyr), and phenylalanine (Phe) [30]. In this study generic proteins were chosen for SERS studies and the amino acids chosen were representative of different types of amino acids.

## 5 Materials and methods

A Raman spectrometer is a combination of major components which are:

- Excitation source, usually a continuous wave (CW) laser
- Sample environment with collection geometry
- Sample holder
- Monochromator / Spectrometer
- Detection system

### 5.1 Instrumentation

#### 5.1.1 The Double monochromator

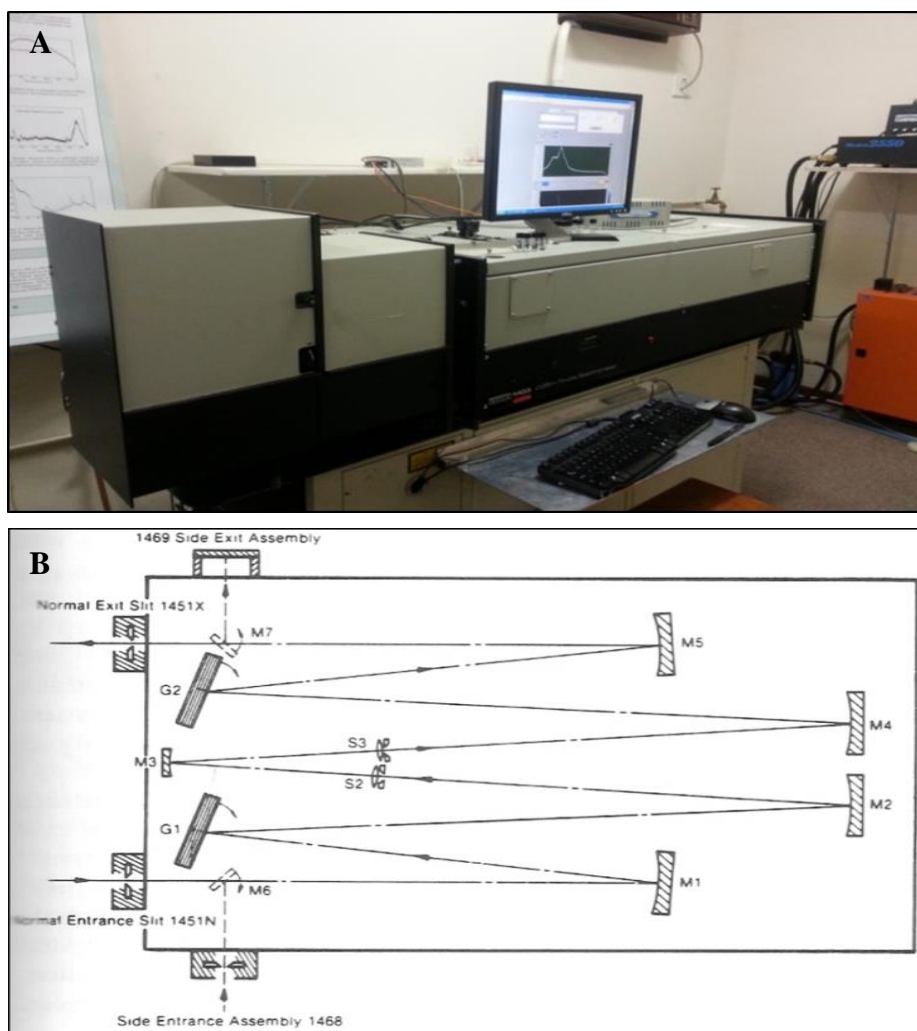


**Figure 11:** Image (A) is the double spectrometer (this was the double monochromator modified into a double spectrometer) used in this study and (B) is a schematic of the SPEX model 1403/4 double monochromator [13].

In this study two RS setups were available. In order for standard protocols of measurement to be set, it was important to understand and highlight the differences of the two setups used for measurements. The first system was a double spectrometer with a two stage monochromator, SPEX model 1403/4. This two stage monochromator was modified into a double spectrograph by removing the exit slit and fitting an Intensified Charged Coupled Device (ICCD) detector.

Initially, light from the laser excitation source is directed towards the sample by reflecting mirrors employing the  $90^\circ$  geometry. The sample then Raman scatters the light in all directions. However, the collected Raman scattered light will be at  $90^\circ$  to the laser beam path. The focusing mirror concentrates the scattered light and focuses it on the entrance slit of the monochromator. Inside the monochromator the gratings disperse the light, mirrors direct the light which is then focused and collimated at a focal distance of 0.85 m. On the side of the monochromator was a wavelength counter. This was a small window of a 5-digit counter which displayed the position of the spectrometer to the nearest  $0.1 \text{ cm}^{-1}$ . The monochromator was a dispersive double monochromator with Czerny Turner mounting. When light is inside the monochromator, some of it scatters from the monochromator walls or the face of the grating. This stray light then overlaps with the Raman scattered light. By having a two stage monochromator the Raman scattered light can be purified by filtering out the stray light [13]. For further reading on this instrument the 1403/1404 monochromator instructions manual may be consulted. However, summarised description of the spectrometer elements with reference to the schematic above are illustrated below. It may be noted that some of the instrument settings used for the study were not according to those in the manual. The settings were chosen as desired.

### *1. Excitation source*

The excitation source was a 514.5 nm argon ion laser manufactured by Spectra-Physics Lasers Inc, Model 2551WR which used high purity argon gas as the medium. Advantages of this laser are that it is reliable, predictable and it has excellent beam quality.

### *2. Sample, sample holder and scattering geometry*

Since Raman scattering is inherently weak, proper focusing of the laser beam and collection of scattered light is required. In-order to achieve this, the  $90^\circ$  geometry (right angle) was employed. This configuration was used as it was ideal for clear samples and it minimised Rayleigh scattering reaching the detector. Also the incident light beam path was different from the scattered light path. A collecting mirror was there for collecting and directing light towards the entrance slit.

### *3. Double monochromator*

- Entrance aperture

This was a slit/ opening through which the Raman scattered light entered the monochromator.

- Dispersing elements

The light dispersing elements were gratings. Holographic gratings were utilised because they bring about less stray light as compared to ruled gratings. This is an ideal characteristic when using a double monochromator, especially when the holographic grating has a higher groove density.

- Collimating elements

These were the mirrors M1, M2, M4 and M5. Mirror M2 received wavelength separated light and focused it into slit S2. These slit widths were to only allow Raman scattered laser light to pass through while filtering Rayleigh light from proceeding to the next half of the double spectrometer. If a sensitive detector had been placed at focal plane S2 it would have been possible to detect photons and record the counts against position but, a second monochromator is aligned immediately after the first. Thus, for the second mirror M3 is for imaging S2 onto S3. Then the instruments M4, G2 and M5 do the same task as M1, G1 and M2 respectively, which have been discussed previously.

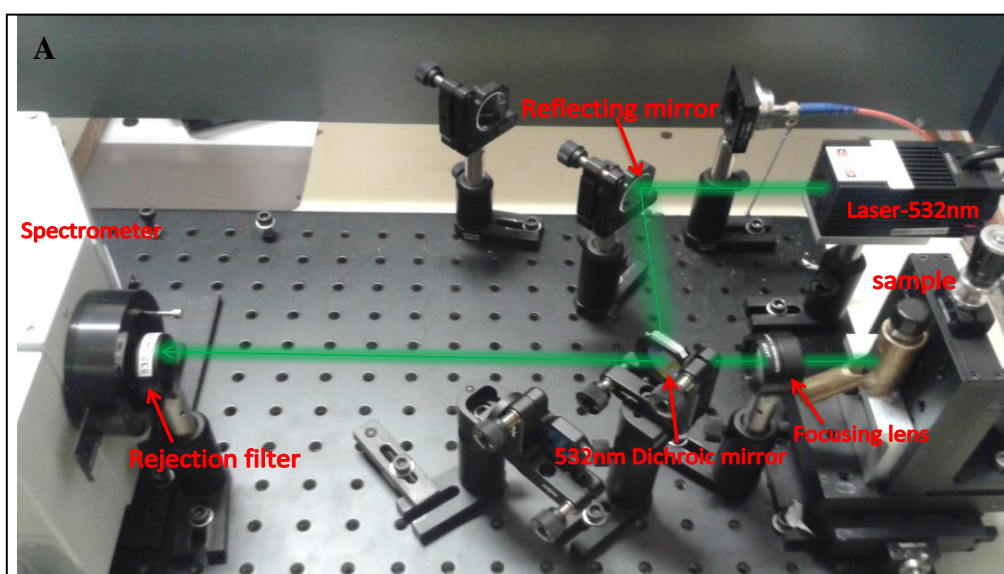
- Exit aperture/ The detection System

The exit aperture of the two stage monochromator was replaced by an ICCD detector, model 354308 supplied by Horiba Jobin Yvon Inc. It was chosen because of its good characteristics such as low noise and high sensitivity, thermoelectric cooling of the detector at  $-70^{\circ}$  and signal linearity [76], [77].

#### 4. Computer software for controlling the Double monochromator

The computer software employed was LabVIEW. It was a package designed in such a way that commands were fed into the system software in order to control the instruments for data acquisition during RS or SERS.

### 5.1.2 The Single stage monochromator



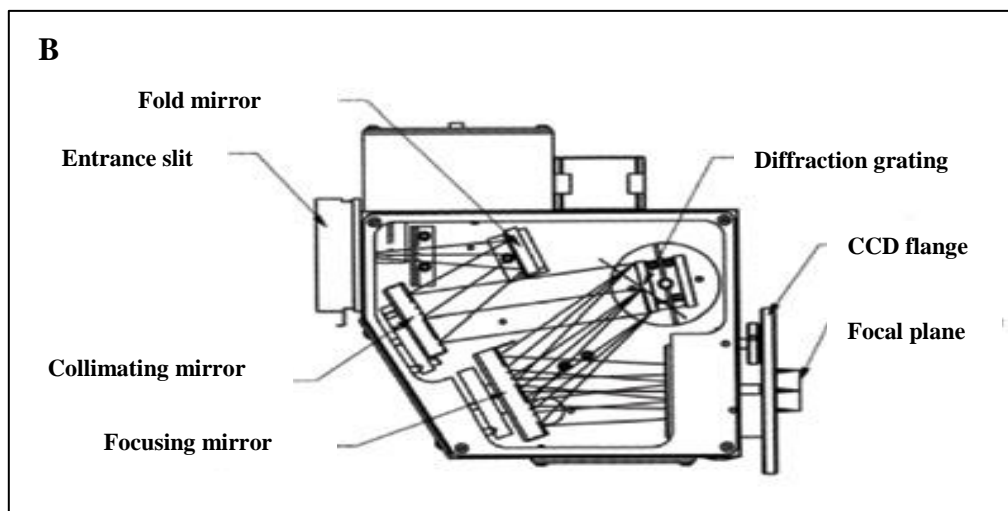


**Figure 12:** Image (A) is the top view of our in built single stage Raman spectrometer showing the laser excitation source, the sample environment, the spectrometer and other optical instruments. Image (B) is a schematic of the single stage monochromator [78].

### 1. *Excitation source*

The excitation source model V-H532 10031699 was a frequency doubled solid state 532 nm Nd:YAG (neodymium-doped yttrium aluminium garnet;  $\text{Nd:Y}_3\text{Al}_5\text{O}_{12}$ ) continuous wave laser which used a crystal as its lasing medium.

### 2. *Optical parameters and Sample environment.*

When the light beam exits from the lasing medium it is directed towards the reflecting mirror at  $45^\circ$  incidence. This mirror then reflects the beam to the 532 nm dichroic mirror, also known as a beam splitter at  $45^\circ$  incidence. The dichroic mirror guides the light beam onto the sample via the focusing lens which has a 5 cm focal length. This is common especially for single stage setups. The light from the sample is backscattered, focused and collimated by the lens and transmitted by the dichroic mirror again. In this case the dichroic mirror reflects the Rayleigh light while at the same time transmitting the Raman scattered light towards the 532 nm long pass rejection filter. This filter blocks the stray light. From the rejection filter light then enters the spectrometer and is dispersed onto a two dimensional Synapse ICCD detector. For this single stage setup,  $180^\circ$  / backscattering geometry was employed because it is a viable configuration for all sample types [78]. However, important alignment was necessary so as to properly guide the excitation light beam towards the sample without obstructing the scattered light.

### 3. *Spectrometer*

This was a spectrometer model MicroHR Horiba Jobin Yvon. Its layout was a one stage Czerny turner mount which minimised stray light while optimising its performance. Scattered light enters the spectrometer via the entrance slit. The light is incident on a fold mirror which reflects towards the collimating mirror. The collimated light beam is directed to the diffraction grating where light is spatially separated and directed to the focusing mirror. The mirror then directs the light towards the detector.

### Comparison of double and single stage Raman spectrometers

Double stage Raman spectrometer	Single stage Raman spectrometer
LASER	
Is water cooled thus, expensive to maintain	Is air cooled thus, less costly to utilise and maintain
RAMAN COLLECTION GEOMETRY	
90° configuration for collection of Raman scattered light	180° /backscattering configuration for collection of Raman scattered light
Ideal geometry for transparent sample	Ideal geometry for all sample types
MONOCHROMATORS	
2 stray light rejection stages	1 stray light rejection stage
Lower light throughput	Higher light throughput
Higher resolution	Lower resolution
Big in size and takes up lots of space	Small lightweight setup which saves space and allows it to be incorporated into other systems
Czerny turner mount	Czerny turner mount

**Table 5-1:** Comparison of the two Raman setups used in this study, the double stage and the single stage Raman spectrometers [78], [79].

### 5.1.3 Calibration of spectrometers

Calibration check for the Raman measuring system was done to ensure the system's accuracy. Measurements are done to check calibration using a standard sample toluene. Spectra acquired from the instrument would be compared to those from literature to see whether our instrument was able to produce expected results.

#### Double Monochromator

- Scaling

This is done so as to have pixel separation in wavelength scale. In order to do this, two peaks from a known standard sample can be utilised. Raman spectra are generated showing peak intensity against Raman shift. For an observed peak with Raman shift  $\Delta\tilde{\nu}$  (in  $\text{cm}^{-1}$ ), from the reference laser line,  $\lambda_1$  (in nm), the equation for the corresponding wavelength,  $\lambda_2$  (in nm), due to that shift is given by:

$$\lambda_2 = \frac{1}{\frac{1}{\lambda_1} - \Delta\tilde{\nu} \times 10^{-7}} \quad (14)$$

Using eq. (14) the wavelengths of the two chosen peaks can be calculated and that together with the number of pixels which separates the maximum points of the peaks can be used to find the wavelength measured per pixel.

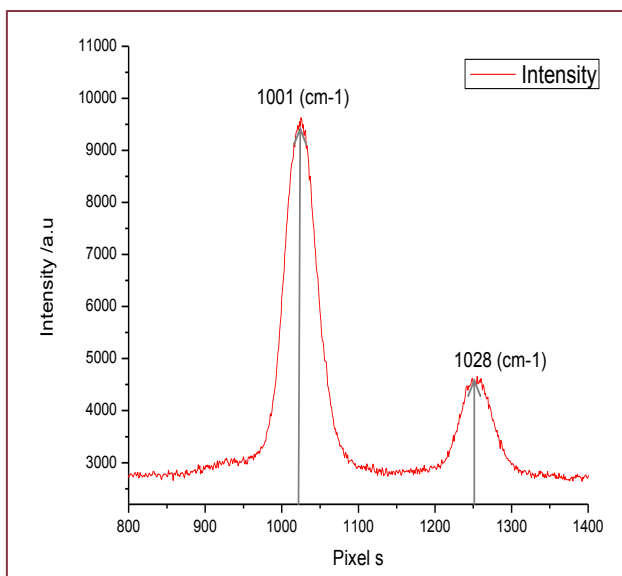


**Figure 13:** Two close peaks from spectra of toluene used for scaling so as to have pixel separation in wavelength scale.

- From eq. (14):

$$1001 \text{ cm}^{-1} \sim 542.4 \text{ nm}$$

$$1028 \text{ cm}^{-1} \sim 543.2 \text{ nm}$$

- Wavelength difference between the two peaks is 0.8 nm and the maximum of the two peaks is separated by 230 pixels.

- Ratio of wavelength difference, 0.8 nm, to peak separation, 230 pixels, gives a pixel separation in wavelength scale = **0.003 nm/pixel**

- Doing the same procedure with other standard samples such as Ethanol and Acetonitrile gave the same result.

- Calibration

Calibration was done so as to ensure that the instrument recorded correct wavelength positions. To determine this, spectra were generated from toluene and the measured peak positions are compared to literature values.

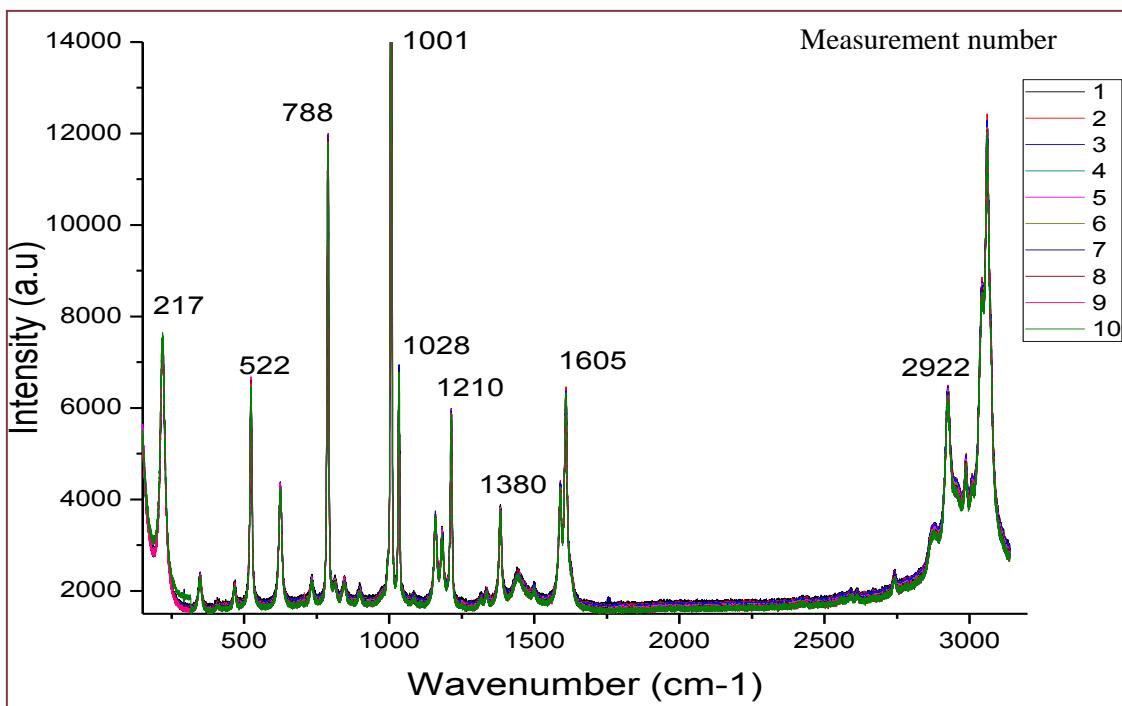


**Figure 14:** Ten toluene spectra acquired using the double Raman spectrometer, used for calibrating the instrument.

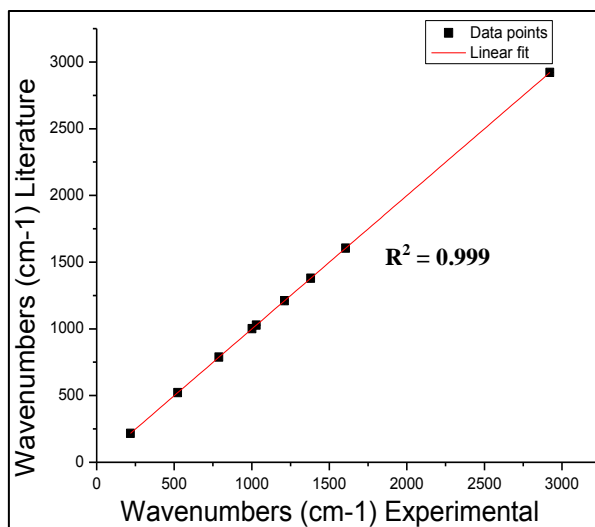


**Figure 15:** Calibration curve for double Raman spectrometer

- Experimental data points of Toluene peaks can be plotted together with known data points of Toluene peaks from literature.

- With the plot, we were able to evaluate the offset of our calibration.

- Offset =  $-0.9 \text{ cm}^{-1}$

-  $R^2$  coefficient of the linear fit was 0.999 which is  $\sim 1$ .

- Repeatability

This is the ability of the instrument to reproduce results under the same conditions, method, measured with the same instrument and repeated in a short time period [80]. Toluene was utilised and deductions were made based on the 10 sets of measurements taken in the range  $400.0 \text{ cm}^{-1}$  to  $3000.0 \text{ cm}^{-1}$  as shown above. Nine marked Raman

shifts in that range were all reproduced with uncertainty in the range  $0.0 \text{ cm}^{-1}$  to  $0.3 \text{ cm}^{-1}$ . Evaluation was done using Guide to Uncertainty and Measurement (GUM) [80].

### Single stage Spectrometer

- Calibration

This was done by generating ten spectra of Toluene and averaging them. Known strong peaks were identified according to their positions. These peak positions (Raman shifts) were then plotted against their respective wavenumber values known from literature to generate a second order polynomial fit. The closer the  $R^2$  value from the polynomial fit was to 1, the best the fit. Thus, using the generated second order polynomial equation  $y = Ax^2 + Bx + C$ , where  $x$  was the wavelengths from the raw data, those wavelength values could be converted to wavenumbers,  $y$ . These wavenumbers would then be used together with intensity values to plot the Raman spectrum. For all measurements done with this system, this calibration procedure would be done so as to calculate the wavenumber values to be used together with intensity values (counts) for plotting sample spectra. Below is a spectrum from ten averaged toluene spectra (fig. 16 A) and the calibration curve (fig. 16 B) of the Raman shifts (shown in fig. 16 A) in nm (x- axis) plotted against the Raman shifts from literature in  $\text{cm}^{-1}$  (y- axis).

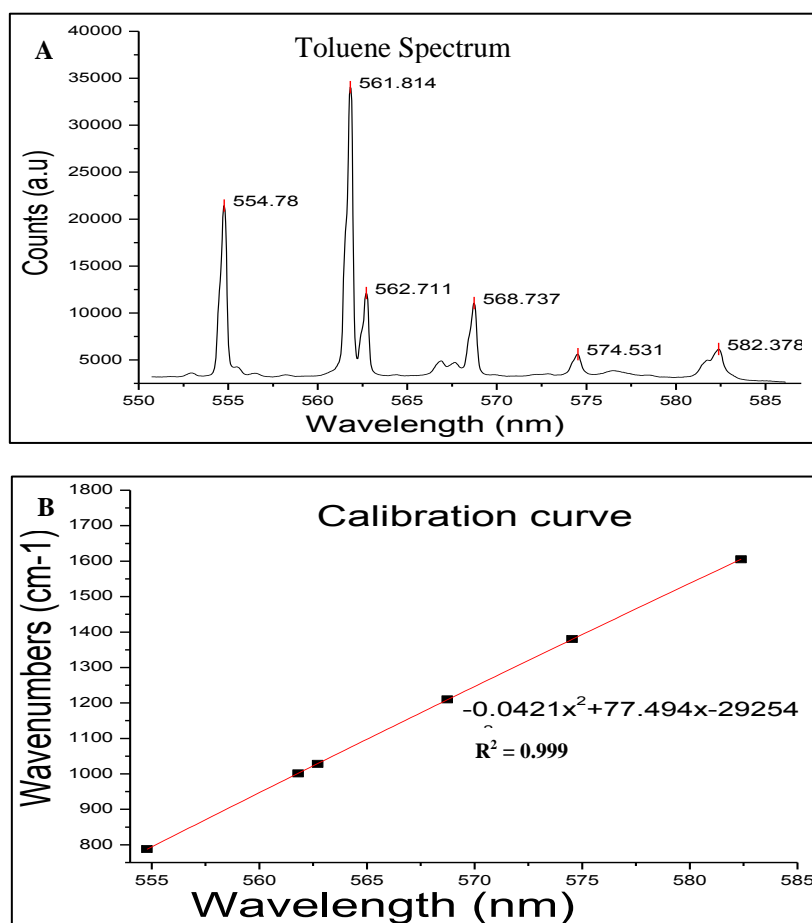


**Figure 16:** Toluene spectrum measured using the single stage Raman spectrometer (A) and a calibration curve for the single stage Raman spectrometer (B).

## 5.2 Materials

Silver nitrate,  $\text{AgNO}_3$  0.01 M (Sigma-Aldrich Co), hydroxylamine hydrochloride (Sigma-Aldrich Co), trisodium citrate dehydrate (Sigma Aldrich), amino acid samples (L-cystein, L-serine, L-tyrosine, glycine, L-lysine, L-aspartic acid, L-glutamic acid) (Sigma Aldrich) were of analytical grade purity and were utilised without any further purification. Sodium hydroxide (NaOH) and chloroauric acid ( $\text{HAuCl}_4$ ) were from existing stock and a chicken egg was sourced locally. Deionised water was used as a solvent for sample preparations. Prepared stock solutions of silver nitrate ( $\text{AgNO}_3$ ), hydroxylamine hydrochloride and trisodium citrate were kept in a refrigerator. It was also important to store colloidal solutions in a cool dry place away from sunlight to avoid photo-induced oxidation.

UV-visible spectra were recorded using a UV-Vis-NIR spectrometer Cintra 101 and scanning was in the range 200-800 nm. Sample images for silver and gold nanoparticles were acquired using a transmission electron microscope. The RS and SERS spectra were acquired using Raman spectrometers SPEX model 1403/4 double spectrometer equipped with a 514.5 nm argon ion laser and a single stage spectrometer equipped with a frequency doubled solid state 532 nm Nd:YAG laser. All samples to be measured were contained in 4 ml glass vials. Acquisition times used on the double spectrometer depended on the range being scanned and the type of sample being looked at. For the single stage spectrometer the acquisition times were 100 s (ten 10 s scans) thus, the spectra would be an average of ten 10s scans.

To have knowledge on nanoparticle size and morphology, UV-Vis spectroscopy and Transmission Electron Microscopy (TEM) were employed. The UV-Vis spectra were taken after diluting the as-prepared silver nanoparticles with deionised water in a ratio of 1:5 respectively, to avoid detector saturation. It was also important to measure the Raman spectra for the nanoparticles (blank spectra) so as to ensure that there were no anomalous bands in the spectra and to further account for any which may be present. Diameter sizes for the nanoparticles were measured using the computer software used to analyse the TEM images. RS measurements were done using fresh samples at all times. For SERS measurements, 500  $\mu\text{l}$  of sample would be added first into a 4ml vial followed rapid addition of the 500  $\mu\text{l}$  of nanoparticles. Measurements were done without delay. For the amino acid solution spectra (with no nanoparticles) 500  $\mu\text{l}$  of sample + 500  $\mu\text{l}$  of water were measured, with water being added to maintain volume and concentration. For the spectrum of solid amino acid, a small amount of sample were placed in a vial and measured. In case of aggregating the nanoparticles, the aggregating agent would be added last, to ensure that the sample molecules would be trapped in the “junctions” in the process of clustering of nanoparticles. A volume of 100  $\mu\text{l}$  was used for aggregating the nanoparticles, an amount enough to not precipitate out the nanoparticles, but just to form clusters in solution. Use of too much aggregating agent precipitates out the nanoparticles leading to reduced SERS intensity or no SERS at all [55], [81].

## 5.2.1 Data processing

The use of RS in this study for analysis of biomolecules was chosen because the technique is non-destructive and highly sensitive to any molecular conformational or chemical changes. However, the technique comes with challenges when acquiring the data, such that it becomes necessary to treat the Raman spectra so as to extract useful information from it. There are several methods of treating the Raman spectra. Mathematical methods whereby software is used are preferred as they do not require any system modification. In this study, polynomial curve fitting was employed in accordance with Lieber and Mahadevan Jansen [82]. It is a method whereby a polynomial is fitted through the measured raw data to generate a baseline spectrum. This baseline spectrum will then be subtracted from the raw Raman spectrum, thus removing fluorescence and enabling the Raman peaks to be analysed. This method is known as the modified polyfit method (MPM). For the reduction of noise such as read-out noise, the Savitsky-Golay filter from OriginPro 8 was applied in order to smooth the data. It was necessary to treat the spectra as such since all Raman spectra experience such influences. A MPM code was written in MATLAB, adapted from Lieber and Mahadevan Jansen as shown in Appendix A. Band assignment was done in comparison with spectra found in the literature. Some bands which are not assigned are just indicated as well for completeness.

It was also important to have an idea of how efficiently the Raman scattered light was being collected using the optical instruments in our 532 nm RS setup. Ideally scattering takes place in all directions but of that scattered light there is a portion of it which enters the lens and is then transmitted towards the spectrometer via the dichroic mirror (refer to fig. 12(A) ). The focusing lens, LA1131 plano-convex lens from Thorlabs had a focal distance of 5cm with a diameter of 2.5 cm. Through this lens the Raman scattered light entered through a solid angle of 28.9°. From the lens the Raman scattered light then passed through the dichroic mirror, which had an average transmission >93%. From the dichroic mirror the scattered light then proceeded to the laser line rejection filter which had average transmission >93%. From the filter the scattered light then entered the monochromator and finally reached the detector.

## 5.2.2 Preparation of nanoparticles

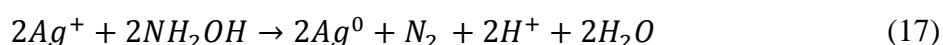
Preparation of nanoparticles was done by reduction of Ag or Au ions in aqueous solution. Reducing agents can either be polymers or surfactants which help to maintain stability of the colloids. In this study the reducing agents used were hydroxylamine hydrochloride and trisodium citrate with the synthesis methods from Leopold and Lendl [35] and Stiufiuc *et al* [34] in accordance with Lee and Meisel [28]. These methods were chosen because they are simple, fast, effective, and they yield stable colloids. The main reaction occurring in synthesis of AgNP was reduction of Ag<sup>+</sup> to Ag<sup>0</sup>. Gold nanoparticles were made following the procedure by Haiss *et al* in concordance with Grabar *et al*. [83], [84]. For AuNP synthesis there is reduction of Au<sup>3+</sup> to Au<sup>0</sup>, shown in the equations below.





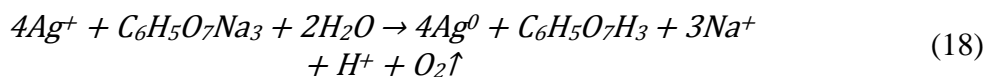
### 5.2.2.1 Hydroxylamine hydrochloride reduced silver nanoparticles (AgHANP)

The synthesis method by Leopold and Lendl in concordance with Lee and Meisel was employed but with slight variations in volume. Into a beaker, 90  $\mu\text{l}$  of NaOH were added together with 4.3 ml of 0.0015 M hydroxylamine hydrochloride. To this mixture 22.604 ml of  $\text{H}_2\text{O}$  were added. Under vigorous stirring on a magnetic stirrer, 3 ml of 0.001 M  $\text{AgNO}_3$  were added. Use of hydroxylamine hydrochloride as a reducing agent requires an alkaline pH to speed up the reaction, thus the use of NaOH. The reaction between the reducing agent and Ag ions is described below.



### 5.2.2.2 Citrate reduced silver nanoparticles (AgCNP)

The recipe by Stiuftuc *et. al.*, used in concordance with Lee and Meisel method, was employed in synthesis of citrate reduced nanoparticles. A volume of 100 ml of 0.001 M  $\text{AgNO}_3$  was heated to boiling point on a magnetic stirrer with a heating option. To it 2 ml of 1% trisodium citrate was added rapidly under vigorous stirring and the solution was boiled for a further 7 minutes. The reaction mechanism for citrate reduced silver nanoparticles is as shown below.



### 5.2.2.3 Citrate reduce gold nanoparticles (AuNP)

Firstly, all glassware and magnetic stir bars were thoroughly cleaned in aqua regia (3 parts of  $\text{HCl}$ +1part of  $\text{HNO}_3$ ), rinsed with distilled water and oven dried prior to use. This would help avoid introduction of foreign particles which would cause undesired nucleation during synthesis. Stock solutions made were of 25.4 mM  $\text{HAuCl}_4 \cdot 3\text{H}_2\text{O}$  and 40 mM sodium citrate. A glass spatula was used since  $\text{HAuCl}_4$  is corrosive to metal spatulas. In a 250 ml round bottomed flask attached to a condenser, 125 ml of 25.4 mM  $\text{HAuCl}_4$  was boiled under vigorous stirring in an oil bath at  $145^\circ\text{C}$ . 12.5 ml of 40 mM sodium citrate was added rapidly to the boiling mixture. The mixture gradually turned burgundy/maroon as boiling continued for 10 mins. The heating mantle was removed and stirring continued for 15 mins. Below are the images showing the colours of the synthesised nanoparticles.

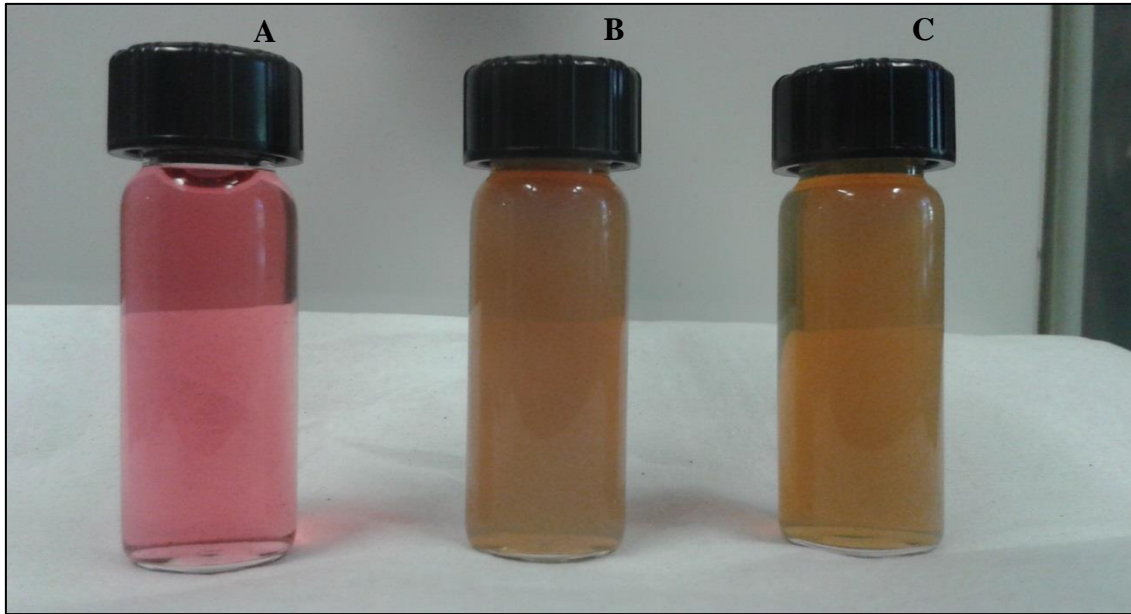


**Figure 17:** Images showing colours of the synthesised citrate reduced gold nanoparticles (A), citrate reduced silver nanoparticles (B) and hydroxylamine hydrochloride reduced silver nanoparticles (C).

## 6 Results and discussion

### 6.1 Characterisation of nanoparticles: UV-Vis and TEM

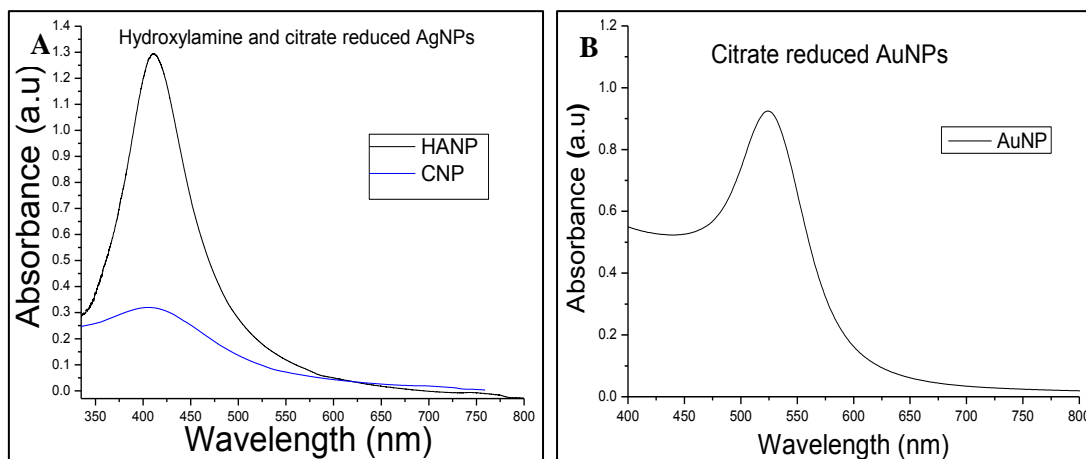


**Figure 18:** UV-Vis spectra for hydroxylamine hydrochloride and citrate reduced AgNP (A) and citrate reduced AuNP (B).

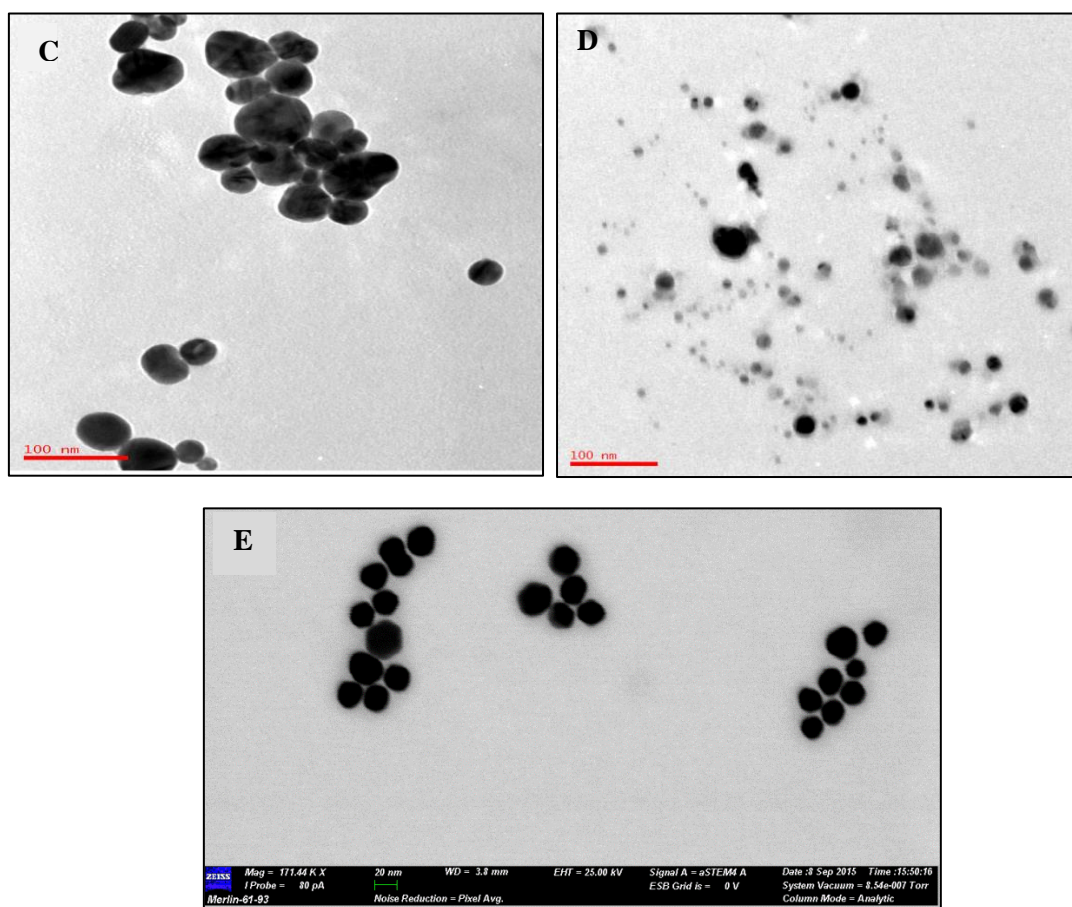


**Figure 19:** TEM images for hydroxylamine hydrochloride (C) and citrate (D) reduced AgNP and citrate reduced (E) AuNP.

All colloids were characterised using UV-Vis spectroscopy and TEM. The hydroxylamine hydrochloride reduced silver nanoparticles (AgHANP) have an absorption peak at 410 nm with an average diameter of ~23 nm measured from their TEM micrographs. The nanoparticles in solution had a pH of 7.9.

The citrate reduced silver nanoparticles (AgCNP) had an absorption peak at 405 nm. TEM micrographs gave an average diameter of ~20 nm. The measured pH for the nanoparticles in solution was 7.3. AgCNP tend to be negatively charged due to the citrate ions on their surfaces. This results in electrostatic repulsion amongst the nanoparticles in colloidal solution and thus, preventing them from clustering. Hence, the nanoparticles tend to be very stable [85, p. 289]. The presence of negatively charged capping ions is the major difference between the AgHANP and AgCNP giving them different colloid environments. These synthesised nanoparticles corresponded well with those from literature [35] [34].

Lastly, the citrate reduced gold nanoparticles (AuNP) had a well pronounced peak at 524 nm and were spherical in shape with an average diameter of ~20nm. AuNP also have a citrate coating around them which stabilises them by preventing aggregation through static repulsion [86]. Depending on their size and shape they will have an absorption band in the visible-infrared region of the electromagnetic spectrum.

From the TEM images and the absorption spectra of silver nanoparticles, it is evident that there is wide size distribution for AgCNP in comparison with the AgHANP. Ideally, the nanoparticle size distribution is affected by how the nanoparticles are synthesised. For synthesis via chemical reduction, the reducing agent and the silver assay are either mixed rapidly or drop-wise and this in-turn affects how the nanoparticles nucleate/form. Preparation of highly active SERS nanoparticles is significant but in this case, the observed size heterogeneity for AgCNP was large which in-turn would have an effect on the SERS intensity of amino acids spectra [20] and consequently result in varying enhancement factors [35].

### 6.1.1 Aggregation of citrate reduced nanoparticles with Hydrochloric acid

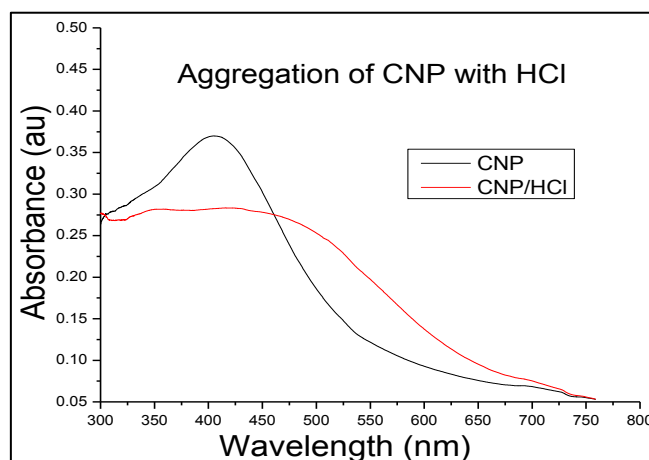


**Figure 20:** UV-Vis spectra for unaggregated and aggregated citrate reduced AgNP. The aggregating agent used was 1M HCl.

Not all samples analysed in this study gave enhanced Raman signals when SERS was performed on them. All absorption spectra of raw colloids had one absorption band, indicative of the dipole plasmon resonance. In this study the aggregating agent used was 1M HCl. After addition of HCl, the AgCNP absorption band was shifted towards longer wavelength and greatly broadened, characteristic of increasing particle size due to aggregation [55], [87]. Aggregated nanoparticles can lead to increased Raman signals due to formation of small assemblies of closely spaced nanoparticles which give strong plasmon resonances thus, generating “hot spots”. It is possible for acid addition to cause an acidic pH and this acidic pH will in-turn have an influence on the biomolecules to be measured in that same solution with the aggregated nanoparticles. Thus, it is important to measure pH before and after the addition of the acid in order to see if there is pH changes occurring. However, in this case the pH was not measured.

## 6.2 Qualitative and quantitative analysis

This section presents the results together with possible reasonable explanations. Spectra of the amino acids in their solid and in solution forms are first shown. The spectra of amino acids in their solid form were for performing qualitative analysis in terms of band profiling, that is, to know which bands were present in the specific amino acids, and to know the identifiers/ markers of that particular amino acid, as well as other vibrational bands. The spectra for the amino acids in solution form were for comparison with those of the solid form so as to see which bands remained present, disappeared or weakened as a result of solvent-amino acid interaction. Also knowing that Raman bands from the spectrum of solid do not present significant spectral shifts and hence the positions of the bands for amino acids in solution could be identified by correlating them with the bands from their corresponding spectrum of solid.

The results show that spectra for amino acids in solid form are always sharper and more pronounced than those of the amino acids in aqueous solution. According to Zhu *et al* [88] this is because when in solid form the amino acid has a lattice structure, each molecule vibrates about a fixed position and has other molecules neighbouring it in a 3D structure which also vibrate similarly. Whereas, in solution amino acid molecules form different types of bonds, such as hydrogen bonds which have different bond lengths and this then causes the solution to have different band frequencies. This random motion brings about a shift in frequency of the vibrational bands of amino acid molecules as well as broadening of Raman peaks. Intermolecular forces bring about a shift in the frequencies of intra-molecular vibrations and this causes broadening of Raman bands [88]. These differences between solid and aqueous spectra are consistent with what is expected from literature [88].

We explain enhancement using electromagnetic and chemical enhancement (charge transfer) mechanisms which are currently the accepted theories of explanation [28], [34], [35], [89], [90]. The possible geometry/orientation of molecules on the metallic surfaces is also proposed. Peak assignments are done based on comparisons from literature. Several literature sources which contained information on Raman band assignments of amino acids similar to the ones employed in this study were used. By comparing these sources with experimental data for this study, Raman peak positions for particular bands did not all appear on the exact same position, possibly due to different measuring conditions. However, depending on the type of amino acid, every band has a particular region where it is expected to appear and if the band was present in that region then it would be assigned accordingly.

Raman bands are shown for the region  $650 - 1700 \text{ cm}^{-1}$  because this is the fingerprint region containing useful information about amino acids. The spectra presented are of good quality and are reproducible when using our in-house developed RS instrument. It should also be emphasised that spectra measured in this study may, in some cases, seem different from those in literature due to different measuring conditions. These differences seem to suggest that there remains extensive work which needs to be done in terms of SERS spectra of such types of amino acids. The RS/ SERS results are obtained from the instrument setup in our labs because it was our main aim to show that this new setup is indeed able to produce reliable results when measuring biomolecules.

A quantitative analysis was done by carrying out a concentration study using the in-house developed Raman setup. The concentration study was for determining the detection limit of the Raman setup. The detection limit being defined as the lowest amino acid concentration which could be confidently measured using the RS setup for each type of amino acid. The two types of silver nanoparticles were employed namely the AgHANP and the AgCNP knowing that the two different reducing agents used for synthesising silver nanoparticles brought about a different environment for the individual nanoparticles.

### Determining peak height and calculation of error bars

In this study, each presented RS or SERS spectrum was an average from 10 measured spectra. This meant that each data point plotted in the spectra would be an average value with an associated standard deviation. For determining the detection limit a strong Raman band would be identified and its change in peak height for decreasing amino acid concentration would be plotted. For the peak height the highest point on the peak would be located and from it, the averaged background counts from both sides of the peak would be subtracted to give the peak height. The associated standard deviation (error bar) for the peak height was calculated as:

$$stdev = \pm \sqrt{\delta(\text{highest point})^2 + \delta(\text{background})^2} \quad (19)$$

Thus, each data point was plotted together with its standard deviation (error bar). Higher amino acid concentrations gave high peak heights and low concentrations gave low peak heights. Determining the detection limit meant finding the lowest amino acid concentration which gave a peak height which could be confidently identified and distinguished from the background. The background counts being the counts from the nanoparticles only, that is, when there is no amino acid present. These background counts are depicted by the horizontal line on the concentration study graphs fig. 22 – 28 C and E.

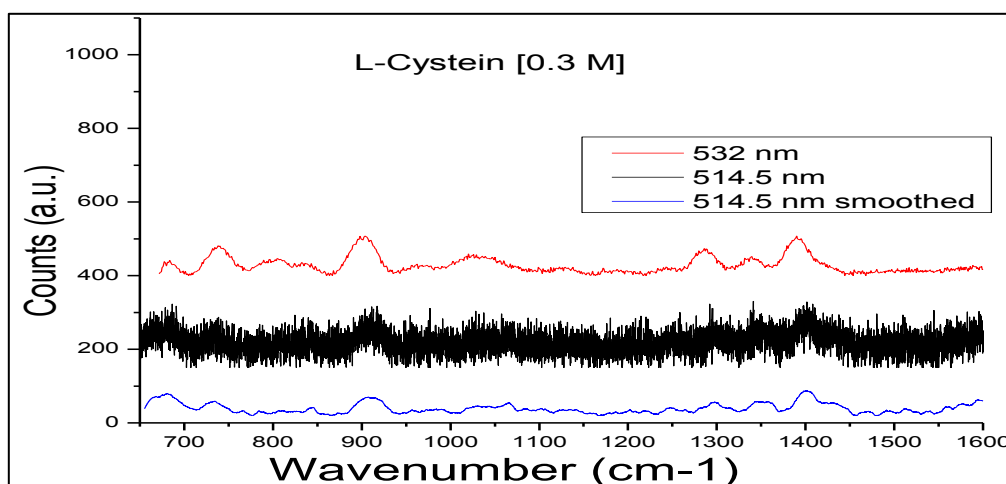
From this point onwards the notation ‘amino acid/nanoparticle’ will be used as short hand for the amino acid and nanoparticles used, e.g. Cys/AgHANP for amino acid L-cystein with AgHANP. There are different vibrational modes inside a molecule such as stretching mode, asymmetric stretching mode, symmetric stretching mode, deformation, wagging, scissoring, bending, twisting and rocking. These are abbreviated as str = stretch, asym = asymmetric, sym = symmetric, def = deformation, wag = wagging, sciss = scissors, bend = bending/bend, twist = twisting/twist, rock = rocking/rock. Laser power for the 514.5 nm argon ion laser and the 532 nm frequency doubled laser on the sample were on average 150 mW and 130 mW respectively. All presented spectra were vertically offset for clarity and as mentioned before, band assignments were done by comparing measured spectra with spectra from literature. References given in the table captions under section 6.2 were used for band assignments in our measured spectra. These are references with information on band assignments done on the particular amino acid. The explanations given for each amino acid explain the trends in the particular amino acid result obtained in this study. Bands were assigned for the highest concentrations measured with silver and gold nanoparticles for each amino acid.

Full name	Abbreviated Name	Molecular formula	Solubility in H <sub>2</sub> O [in mg/ml]
L-aspartic acid	Asp	C <sub>4</sub> H <sub>7</sub> NO <sub>4</sub>	5
L-glutamic acid	Glu	C <sub>5</sub> H <sub>9</sub> NO <sub>4</sub>	8.6 at 25°C
L-lysine	Lys	C <sub>6</sub> H <sub>14</sub> N <sub>2</sub> O <sub>2</sub>	100
Glycine	Gly	C <sub>2</sub> H <sub>5</sub> NO <sub>4</sub>	100 at 25°C
L-tyrosine	Tyr	C <sub>9</sub> H <sub>11</sub> NO <sub>3</sub>	0.45 at 25°C
L-cystein	Cys	C <sub>3</sub> H <sub>7</sub> NO <sub>2</sub> S	25
L-serine	Ser	C <sub>3</sub> H <sub>7</sub> NO <sub>3</sub>	250 at 20°C

**Table 6-1:** Information table for the amino acids used in this study showing their molecular formulae and their solubility values in water.

### Comparison of SERS results from a double and a single stage Raman spectroscopy setups

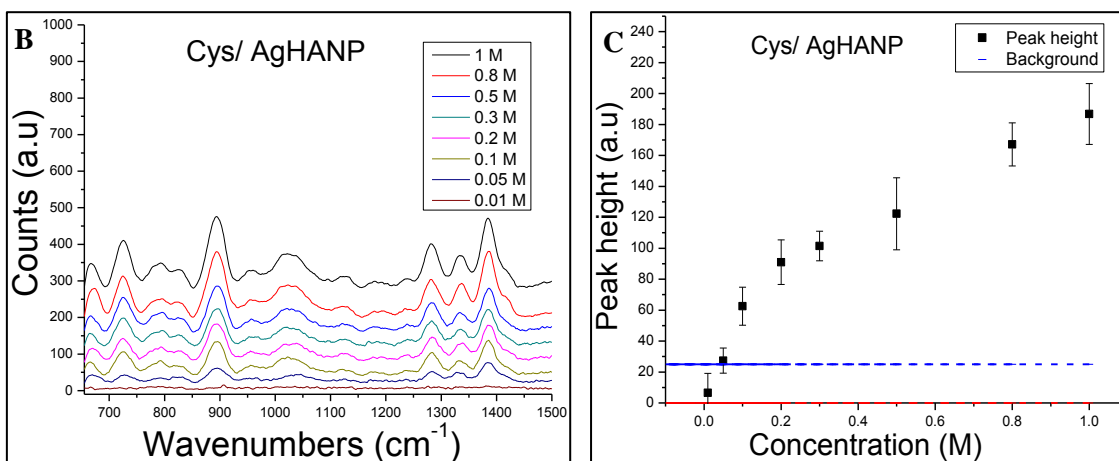
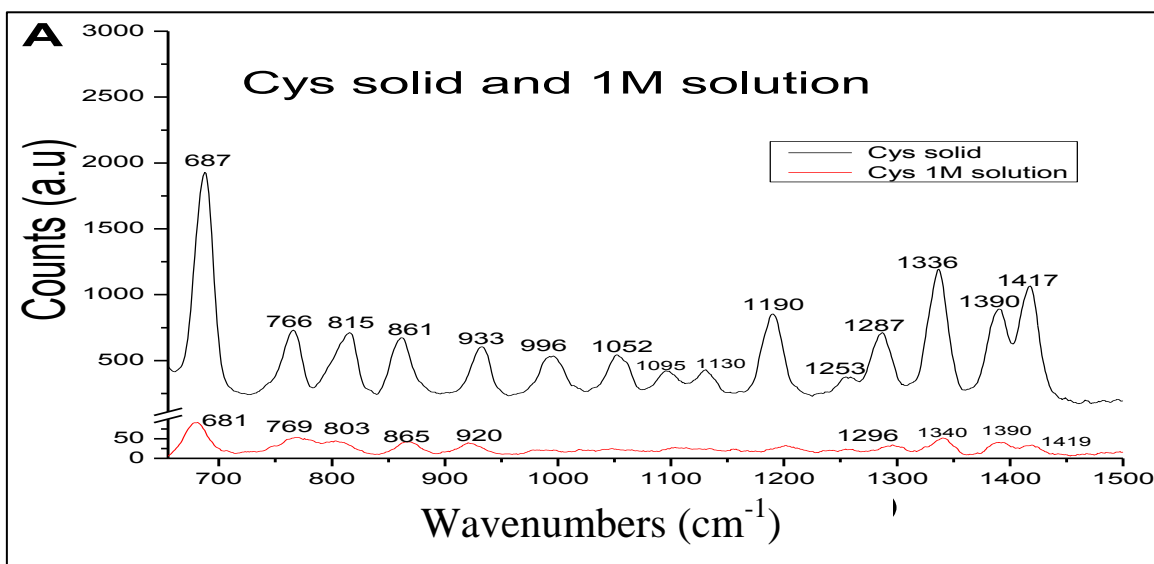
We present first the measurements done on L-cystein to show results obtained from the two RS setups used. Cys was chosen because, in terms SERS, the sample has been extensively studied and a lot of information is present in literature [49], [69], [86], [96 – 98].



**Figure 21:** Comparison of Cys spectra measured using a double Raman spectrometer with 514.5 nm laser excitation source and a single stage Raman spectrometer with 532 nm laser excitation source. The spectra have been vertically offset for clarity.

A comparison is made of results of 0.3 M Cys/AgHANP measured with different setups. For this study in order for concentration studies to be carried out it was important to use the setup which not only gave vibrational information about the sample but also high peak intensity. The double monochromator gave better stray light rejection which improved the resolution of the system. However, it had less light throughput which meant low band intensity, increased fluorescence affecting the spectra, low signal-to-noise ratio and longer acquisition times were required which would mean overexposure of the sample with laser light leading to sample burning. Also, the system was water cooled and thus expensive as measurements required long acquisition times. On the other hand the single stage spectrometer had less stray light rejection compared to the double spectrometer and it gave lower resolution. It gave more light throughput which meant bands had more intensity, it was also fast, air cooled and less costly to operate. The single stage Raman spectrometer, with 532 nm laser excitation source indeed gave good and reasonable results for the sample L-cysteine. Vibrational bands could be located in precise positions. Thus, the single stage Raman spectrometer was chosen for carrying out concentration studies.

### 6.2.1 L-cysteine



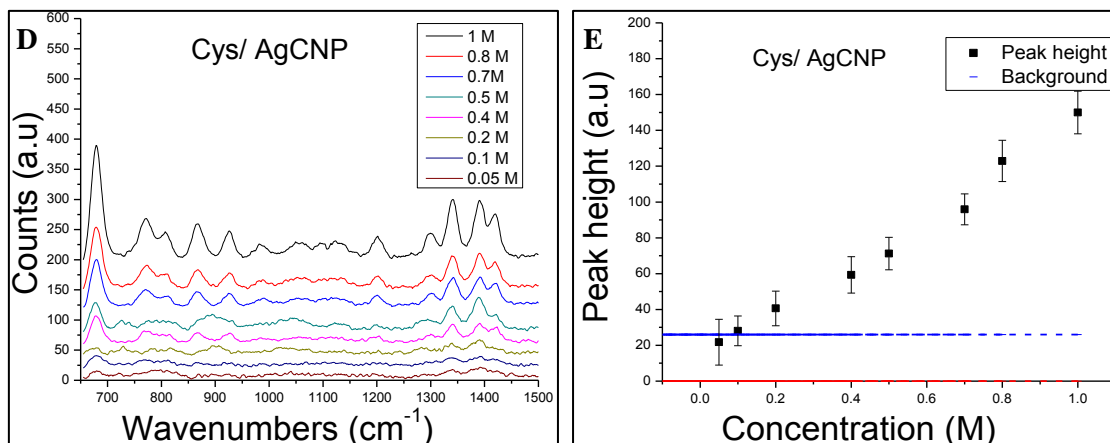


**Figure 22:** RS spectra of Cys solid and 1M solution are shown in A. B and D are SERS spectra of Cys with AgHANP and AgCNP respectively. C and E are graphs showing the change in Cys concentration against peak height for AgHANP and AgCNP respectively. The horizontal line in figs. C and E show the background counts.

RS bands [ $\text{cm}^{-1}$ ]		SERS bands for each type of nanoparticle [ $\text{cm}^{-1}$ ]				Band assignment
Spectrum of solid	Solution spectra	AgHANP <sub>514.5nm</sub>	AgHANP <sub>532nm</sub>	AgCNP	AuNP	
687	681	681	667	678	678	C-S str.; C-S asym.str.
766	769	733	724	770	768	COO <sup>-</sup> def.;
		783	792			
815	803		826	808	808	COO <sup>-</sup> wag.
861	865		893	867	869	C-C str.; CH <sub>2</sub> rock
933	920	912	955	926	919	C-COO <sup>-</sup> str.
996			1020	981	990	NCH bend + HCH bend
1052				1048	1046	C-N str., C-N sym.str.; HCH rock + NCH bend
1095		1066		1093		C-N str.;
1130		1140	1125	1123	1127	NH <sub>3</sub> <sup>+</sup> def.
1190	1200		1238	1200	1201	CO str. + HCN bend
1253	1296	1294	1281	1299	1303	CH <sub>2</sub> wag; CCH bend
1336	1340		1334	1340	1339	CH <sub>2</sub> wag; CH <sub>2</sub> twist + HNH bend
1390	1390	1402	1384	1390	1390	COO <sup>-</sup> sym.str.
1417	1419	1431		1419	1420	CH <sub>2</sub> sciss.; CH <sub>2</sub> def.

**Table 6-2:** Experimental Raman shifts and Raman band assignments for Cys [27], [81], [88], [94], [95].

The concentration of the Cys solution was 1M. Some Raman bands in the spectra for Cys/AgCNP in fig. 22 B are comparable to those in the spectra of Cys/AgHANP in fig. 22 D. The observed C-S band is very strong in all spectra suggesting strong bond formation between the sulphur and the metallic nanoparticle. The strength of the C-S bond formed is further supported by observation of the strong C-S band for decreasing concentrations of the amino acid. This result was in agreement with previous results done on Cys [27], [95]. However the C-S band is slightly shifted to lower wavenumbers in the spectra of Cys/AgHANP. This shift in the C-S band is also reported by Watanabe and Maeda in [95]. So this implies that Cys has been deprotonated probably due to the change in pH being brought about by the solution in which the nanoparticles are in. By deprotonation the amino acid has acted as an acid. Theoretically the S-H band is expected in the region 2550-2600  $\text{cm}^{-1}$ , however, for Cys RS/ SERS spectra we do not know if the band was present or not since only the fingerprint region was looked at in this study. According to some literature sources the S-H band appears in normal RS spectra but in SERS, the S-H disappears and is not observed due to ionisation of the sulfhydryl group on the metallic surface [27], [94], [95]. Also, sulphur has low electronegativity<sup>10</sup> and so it does not easily form new H-bonds [96].

In the spectra for Cys/ AgHANP the  $\text{COO}^-$  symmetric stretch band in the range 1370 – 1410  $\text{cm}^{-1}$  is very strong. This suggests a chemical enhancement, with the  $\pi$  electron rich  $\text{COO}^-$  having electrons which are taking part in charge transfer with the silver metal. This metal-carboxylate group interaction is also reported by C. Jing and Y. Fang [94] and S. Stewart and P. M. Fredericks [27]. Due to this metal-carboxylate band interaction, the two  $\text{CH}_2$  bands from 1250 to 1350  $\text{cm}^{-1}$  benefit as well and also have a fair enhancement.

From the information above, due to the significant enhancement of the C-C band and the carboxylate group, we propose the orientation to be that these bands are directly on the metal surface and experiencing chemical enhancement, while the amino group is away from the metal. In general for sulphur-containing compounds, C-S is a strong diagnostic band in Raman spectra. This is observed when using both types of nanoparticles, AgHANP and AgCNP. Concentration study is determined with respect to the Raman band between 850 and 940  $\text{cm}^{-1}$  for Cys/AgHANP and between 650 and 700  $\text{cm}^{-1}$  for Cys/AgCNP. The detection limit for Cys AgHANP was 0.01 M and that for Cys/AgCNP was 0.05M.

---

<sup>10</sup> Electronegativity is the ability to attract electrons so as to form new bonds.

## 6.2.2 L-serine

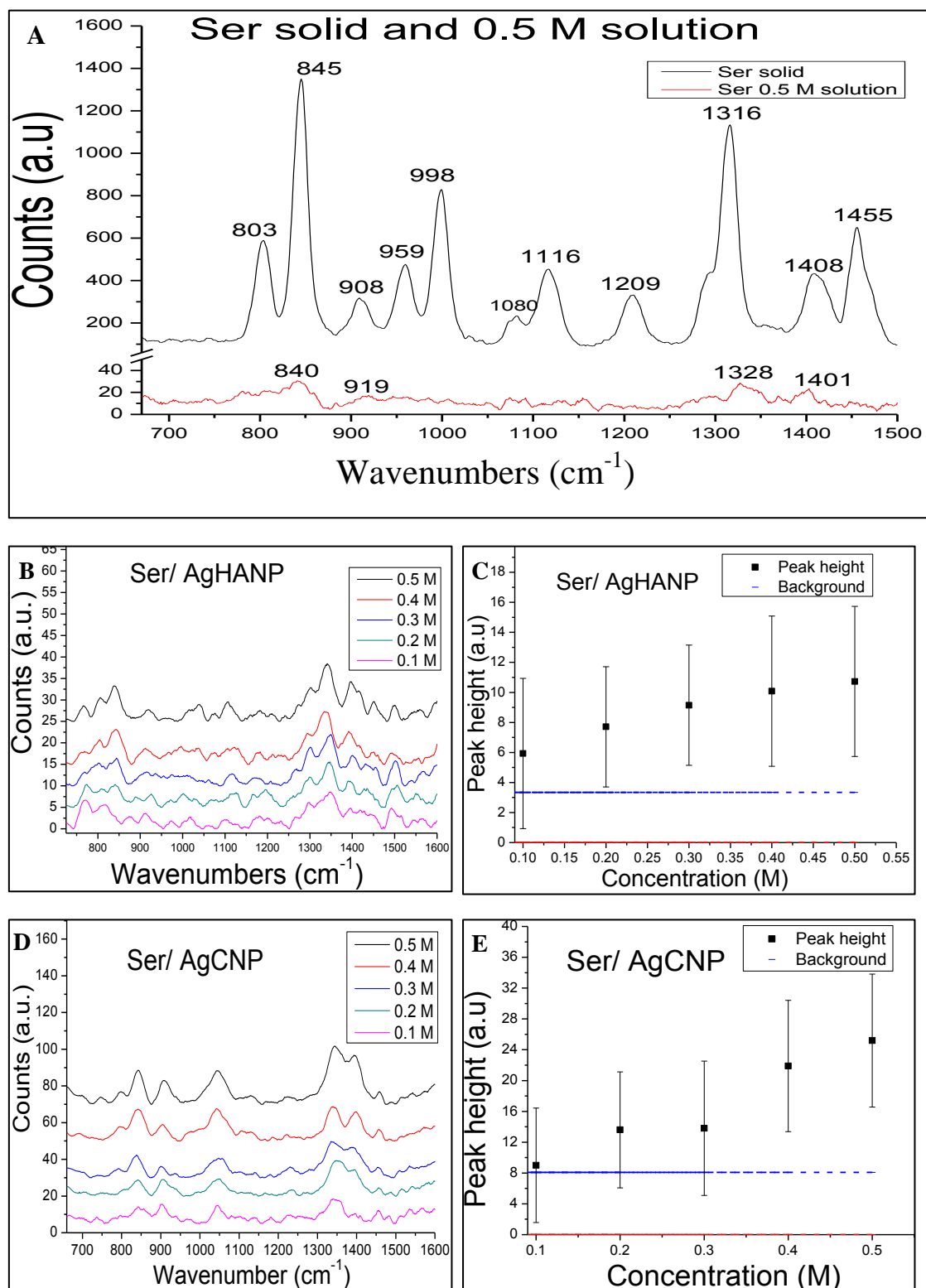


**Figure 23:** RS spectra of Ser solid and 0.5 M solution are shown in A. Images B and D are SERS spectra of Ser with AgHANP and AgCNP respectively. C and E are graphs showing the change in Ser concentration against peak height for AgHANP and AgCNP respectively. The horizontal line in figs. C and E show the background counts.

RS bands [ $\text{cm}^{-1}$ ]		SERS bands for each type of nanoparticle [ $\text{cm}^{-1}$ ]			Band assignment
Spectrum of solid	Solution spectra	AgHANP	AgCNP	AuNP	
		768	746	770	$\text{COO}^-$ def.
803		804	799	807	C-C-O sym. Str. of primary alcohol groups
845	840	838	841	847	C-C-N symmetric stretching
908	919	918	906	915	C- $\text{COO}^-$ str.
959				969	
998		1038	1044	1042	C-O-H deformation of alcoholic hydroxyl; C-C str
1080		1075		1077	
1116		1107	1128	1121	$\text{NH}_3^+$ def.;
1209		1181			
1316	1328	1340	1343	1339	
1408	1401	1396	1394	1402	$\text{COO}^-$ sym.str.
1455		1451	1458	1459	$\text{CH}_2$ sciss.

**Table 6-3:** Experimental Raman shifts and Raman band assignments for Ser [27], [88], [97], [98].

A concentration of 0.5 M Ser solution was prepared. The band at  $998 \text{ cm}^{-1}$  in the spectrum of solid in fig. 24 A is likely from C-O-H frequency of alcoholic hydroxyls which is the position for the deformation frequency for alcohols [88]. This C-O-H deformation band appears in spectra taken with all nanoparticles. In general alcohols show a weak Raman effect due to the easily polarisable OH group. This makes them outstanding solvents for other substances for use in RS [99]. SERS spectra could not be measured for lower than 0.1 M concentrations. The carboxylate band in all spectra is strong due to adsorption of the band on the metallic nanostructure. This is also in accordance to findings in ref. [27]. We propose that the C-C-N and the  $\text{COO}^-$  bands in Ser/AgHANP and Ser/AgCNP are close to the metal structure while the R-group is further away. Concentration study is done with respect to the Raman band between  $1320$  and  $1360 \text{ cm}^{-1}$ . For this amino acid, we do not state the detection limit for Ser with AgHANP and with AgCNP because unfortunately, concentrations lower than 0.1 M could not be measured and thus, it is possible that the detection limit could be less than 0.1 M.

## 6.2.3 L-tyrosine

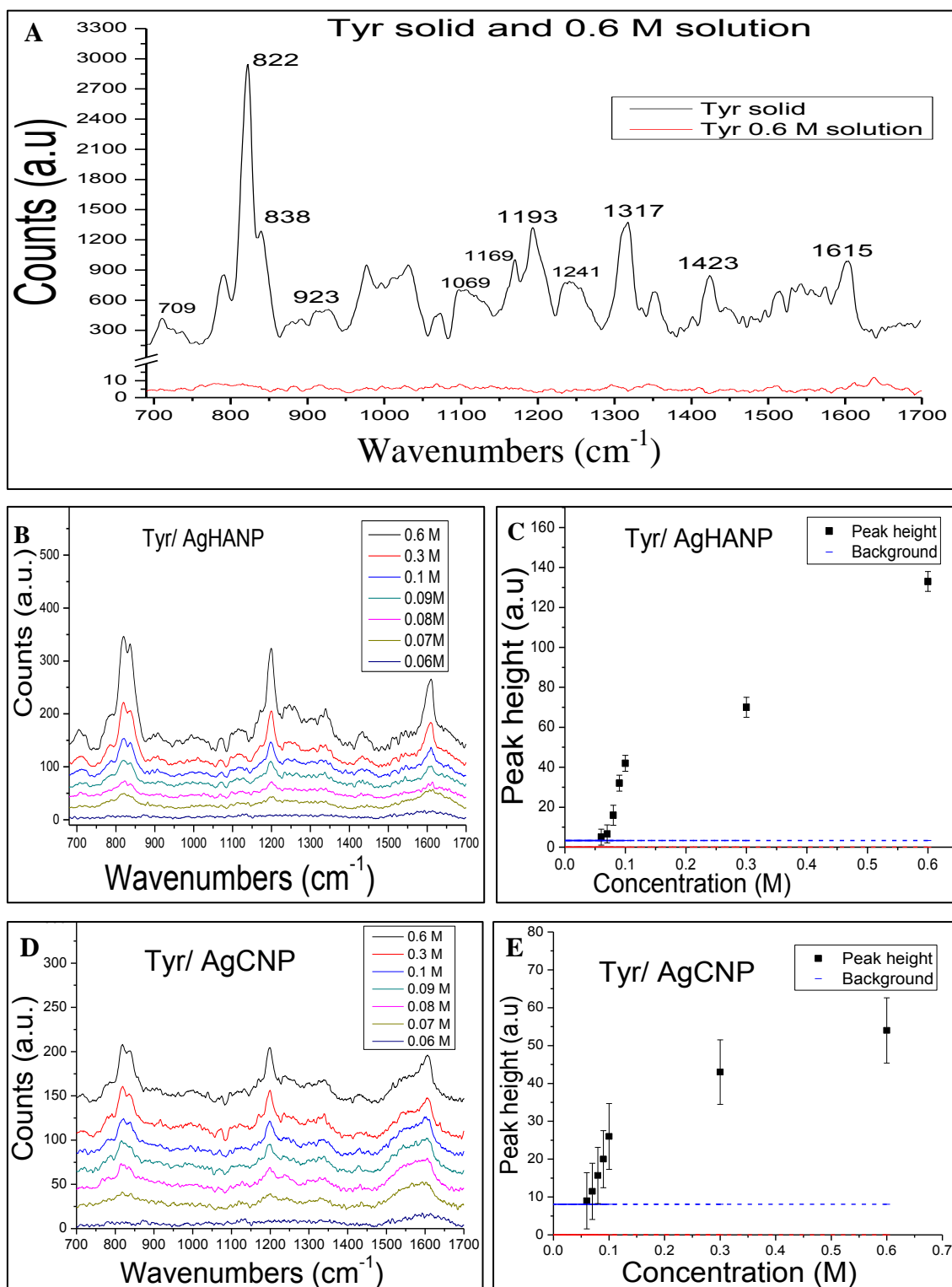


**Figure 24:** RS spectra of Tyr solid and 0.6 M solution are shown in A. B and D are SERS spectra of Tyr with AgHANP and AgCNP respectively. C and E are graphs showing the change in Tyr concentration against peak height for AgHANP and AgCNP respectively. The horizontal line in figs. C and E show the background counts.

RS bands [cm <sup>-1</sup> ]	SERS bands for each type of nanoparticle [cm <sup>-1</sup> ]			Band assignment
Spectrum of solid	AgHANP	AgCNP	AuNP	
709	703	717	709	COO <sup>-</sup> def.
796	786	785	787	C-C-O sym. str. of primary alcohol groups
822	820	819	819	Fermi resonance between out-of-plane deformation and ring breathing vibration ( <i>marker of tyrosine</i> )
838	837	839	837	
923	907		906	C-COO <sup>-</sup> str.
1069		1074	1070	
1169	1171		1170	Ring CH bend
1193	1198	1197	1198	sym. str. of para-substituted benzene; C <sub>β</sub> -C <sub>γ</sub> str.
1241			1249	
1317	1338	1337	1338	CH def.
1423	1432	1425	1430	COO <sup>-</sup> sym.str.
1615	1609	1606	1607	In-phase C <sub>2</sub> -C <sub>3</sub> and C <sub>5</sub> -C <sub>6</sub> str.

**Table 6-4:** Experimental Raman shifts and Raman band assignments for Tyr [27], [88], [99], [100].

A concentration of 0.1 g/ml of Tyr was dissolved using 1M HCl as a solvent with added heating. This gave 0.6 M of solution. The bands close to 1600 cm<sup>-1</sup> in the spectrum of solid in fig 24 A are assigned to the C-C partial double bonds of the aromatic ring in the side chain [99]. This band is also seen in Tyr/AgHANP (fig. 24 B) and Tyr/AgCNP (fig. 24 D) spectra. In the spectrum of solid are also the characteristic doublet peaks of tyrosine at 822 and 838 cm<sup>-1</sup>. These are as a result of the Fermi resonance between the out-of-plane deformation and the ring breathing vibration [27], [66], [88], [98], [101]. The bands may vary depending on their chemical environment when in solution. These two peaks are well pronounced for Tyr/AgHANP spectra in fig. 25 B and are shifted slightly to positions 820 and 837 cm<sup>-1</sup> due to sample-metal interaction. With both types of nanoparticles the two band markers of Tyr in the region 800-850 cm<sup>-1</sup>, the band due to the para-substituted benzene ring and the in-phase C<sub>2</sub>-C<sub>3</sub> and C<sub>5</sub>-C<sub>6</sub> bonds were likely oriented close to the nanoparticle surface. The ring side chain took part in chemical enhancement with the metals. Concentration study was done with respect to the Raman band between 1150 and 1250 cm<sup>-1</sup>. The detection limit for both Tyr/AgHANP and Tyr/AgCNP was 0.06 M.

## 6.2.4 Glycine

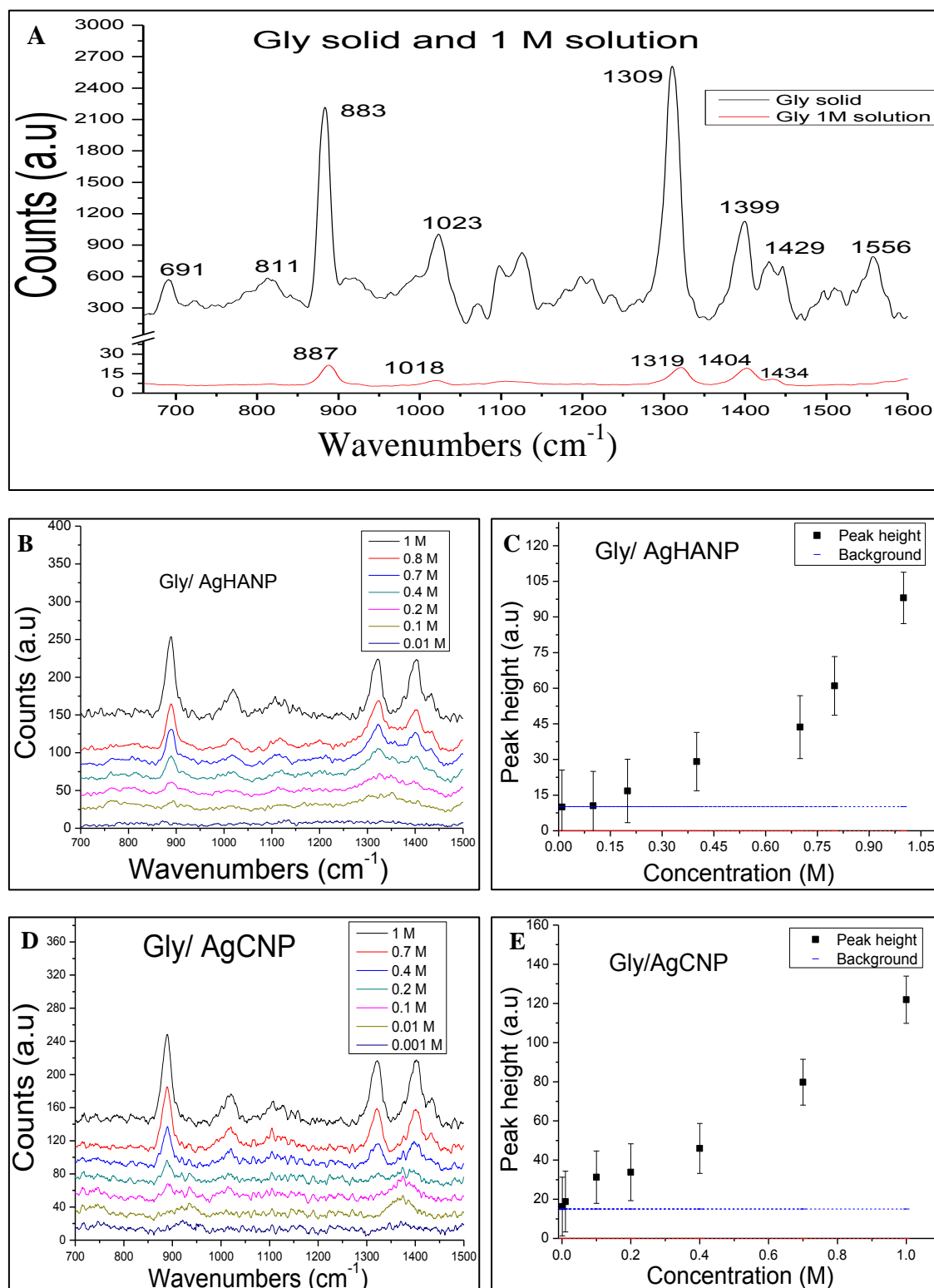


**Figure 25:** RS spectra of Gly solid and 1M solution are shown in A. B and D are SERS spectra of Gly with AgHANP and AgCNP respectively. C and E are graphs showing the change in Gly concentration against peak height for AgHANP and AgCNP respectively. The horizontal line in figs. C and E show the background counts.

RS bands [ $\text{cm}^{-1}$ ]		SERS bands for each type of nanoparticle [ $\text{cm}^{-1}$ ]			Band assignment
Spectrum of solid	Solution spectra	AgHANP	AgCNP	AuNP	
691					$-\text{COO}^-$ def.
883	887	888	888	896	C- $\text{COO}^-$ str.
1023	1018	1018	1020	1019	
1309	1319	1322	1321	1321	$\text{CH}_2$ wag.
1399	1404	1403	1400	1402	$-\text{COO}^-$ sym. str.
1429	1441	1432	1433	1436	

**Table 6-5:** Experimental Raman shifts and Raman band assignments for Gly [27],[102].

An aqueous solution of 1 M was prepared for Gly. Glycine is the simplest of the amino acids as it only has hydrogen as a side chain. The most intense bands at  $883 \text{ cm}^{-1}$  and  $1309 \text{ cm}^{-1}$  in spectrum of solid (fig. 25 A) are found at  $887 \text{ cm}^{-1}$  and  $1319 \text{ cm}^{-1}$  in the solution spectra (fig. 25 A) respectively. These are the markers of glycine. The Raman bands in the solution spectra have low intensity and are shifted in position compared to those in the spectrum of solid, suggesting chemical interactions with the solvent. This shift in bands was also reported by Zhu *et al* in [88]. It is noticed that the positions of the group  $\text{CH}_2$  in Gly/AgHANP (fig. 25 B) and Gly/AgCNP (fig. 25 D) is at  $1322 \text{ cm}^{-1}$  and  $1321 \text{ cm}^{-1}$  respectively are shifted from the position of the same band in the spectrum of solid which is at  $1309 \text{ cm}^{-1}$ , suggesting chemical enhancement of this mode. The low enhancement of the same alkane band for Gly/AgHANP and Gly/AgCNP also supports the fact that alkanes do not have ideal electronic orbitals to take part in charge transfer mechanisms probably due to less available electrons, as compared to alkenes and aromatics which do have [27]. The amine group, the  $\text{NH}_3^+$  deformation, could not be confidently identified in RS and SERS spectra, probably because it was oriented away from the metallic surface. In both the RS and SERS spectra the C=O band expected in the range  $1600\text{-}1620 \text{ cm}^{-1}$  is absent. This could be evidence that there has been deprotonation of the COOH bond to form  $-\text{COO}^-$ . Both the observation of  $-\text{COO}^-$  deformation band and the  $-\text{COO}^-$  symmetric stretching band and their shift in position are also reported by S. Stewart and P.M. Fredericks [27]. Their shift in position suggests chemical enhancement of these modes. We propose that the deprotonated carboxylate group (C- $\text{COO}^-$  stretching mode) and the  $\text{CH}_2$  were likely oriented on the metal surface with the protonated amine group facing away from the silver surface. The carboxylate group may have benefited considerably due to charge transfer mechanism. Concentration study was done with respect to the Raman band between  $850$  and  $950 \text{ cm}^{-1}$ . The detection limit for Gly/AgHANP was  $0.01 \text{ M}$  and that for Gly/AgCNP was  $0.001 \text{ M}$ .

## 6.2.5 L-lysine

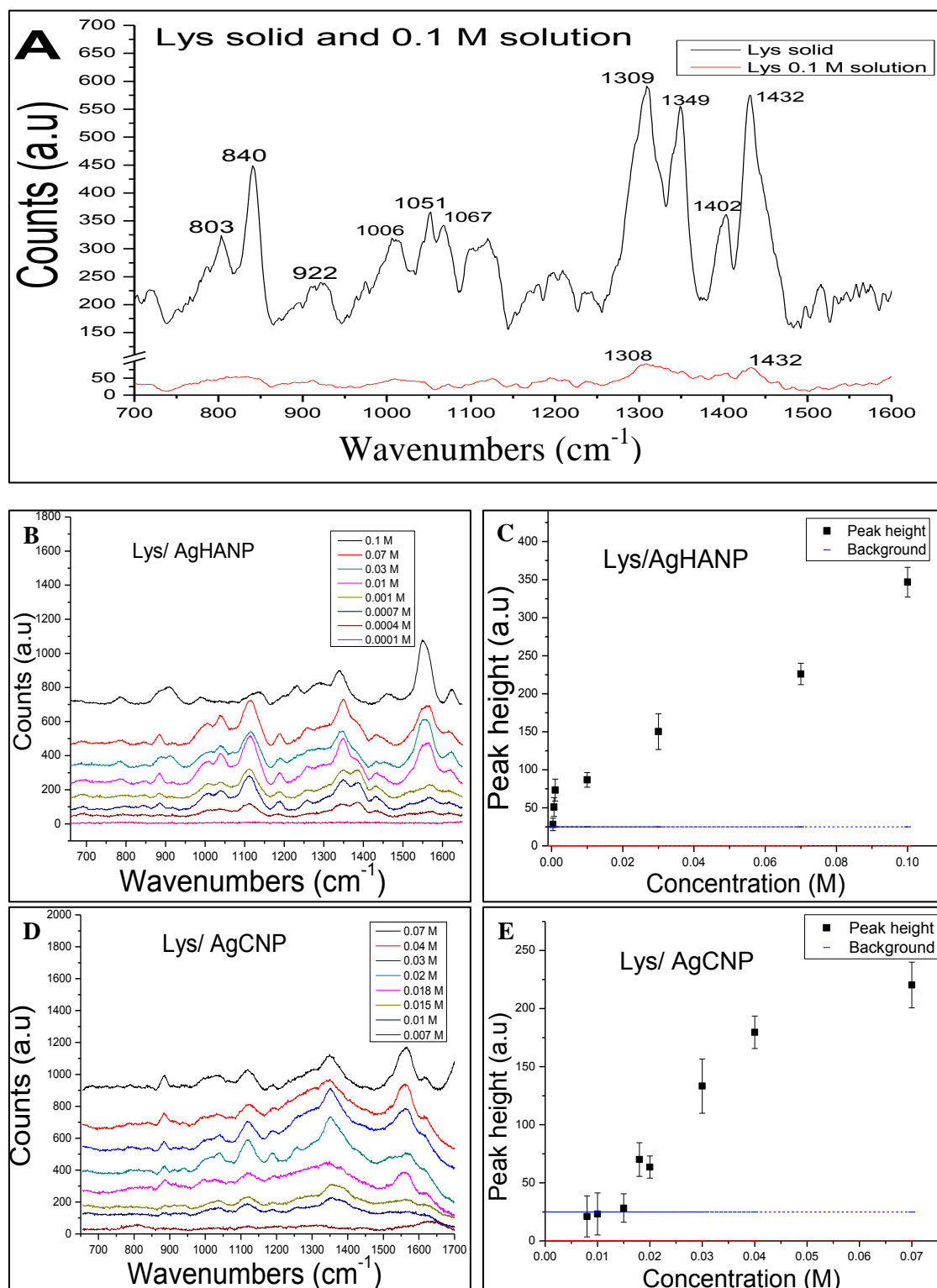


**Figure 26:** RS spectra of Lys solid and 0.1 M solution are shown in A. B and D are SERS spectra of Lys with AgHANP and AgCNP respectively. C and E are graphs showing the change in Lys concentration against peak height for AgHANP and AgCNP respectively. The horizontal line in figs. C and E show the background counts.

RS bands [ $\text{cm}^{-1}$ ]	SERS bands for each type of nanoparticle [ $\text{cm}^{-1}$ ]				Band assignment
	Spectrum of solid	Solution spectra	AgHANP	AgCNP	
840		782	884	809	$\text{C}_\gamma$ -twist; $\text{C}_\epsilon$ -wag.; $\text{C}_\beta$ -wag.
922		910	932	912	$\text{C}_\epsilon$ -wag.;
1006		988	1035	988	$\text{C}_\delta$ - $\text{C}_\epsilon$
1051		1067		1069	C-N str.; $\text{C}_\delta$ - $\text{C}_\epsilon$
1067				1099	C-N str. ; $\text{C}_\beta$ - $\text{C}_\gamma$
1120		1136	1118	1119	N-H wag.
		1233	1190	1197	N-H wag.
1309	1308	1290		1307	$\text{CH}_2$ wag.; $\text{COO}^-$ sym. str. ;
1349		1339	1348	1326	$\text{C}_\gamma$ -wag. ; $\text{C}_\epsilon$ -twist ; CH bend
1402		1358	1362	1392	$\text{COO}^-$ sym. str.; $\text{C}_\epsilon$ -rock;
1432	1432	1459		1431	$\text{CH}_2$ sciss. $\text{C}_\beta$ -bend
		1548	1565	1543	$\text{NH}_3^+$ asym. bend

**Table 6-6:** Experimental Raman shifts and Raman band assignments for Lys [27], [97], [103]–[105].

A concentration of 0.1 M was prepared for Lys solution. At neutral pH, Lys exists as  $\text{H}_3\text{N}^+\text{-HC}(\text{CH}_2)_4\text{-NH}_3^+\text{-COO}^-$  with two protonated amine groups. Lys has a very high solubility in water and its side chain resembles ammonia, making it basic. Most bands are absent in the spectra of the solution in fig. 26 A, consistent with findings by Zhu *et al.* [88]. In the measured SERS spectra with both AgHANP and AgCNP (figs. 26 B and D) none of the bands due to protonated amine groups were observed, suggesting that they could have been oriented away from the nanoparticle surface. Bands corresponding to the carboxylate groups are observed, together with those from the side chain methylene groups also dominating. This result was consistent with findings by S. Stewart and P. M. Fredericks in [27]. The proposed orientation is that the carboxylate group and the side chain methylene group were oriented close to the nanoparticle surface. Concentration study was done with respect to the Raman band between 1500 and 1600  $\text{cm}^{-1}$ . The detection limit for Lys/AgHANP was 0.000 1 M and for Lys/AgCNP it was 0.007 M.

## 6.2.6 L-aspartic acid

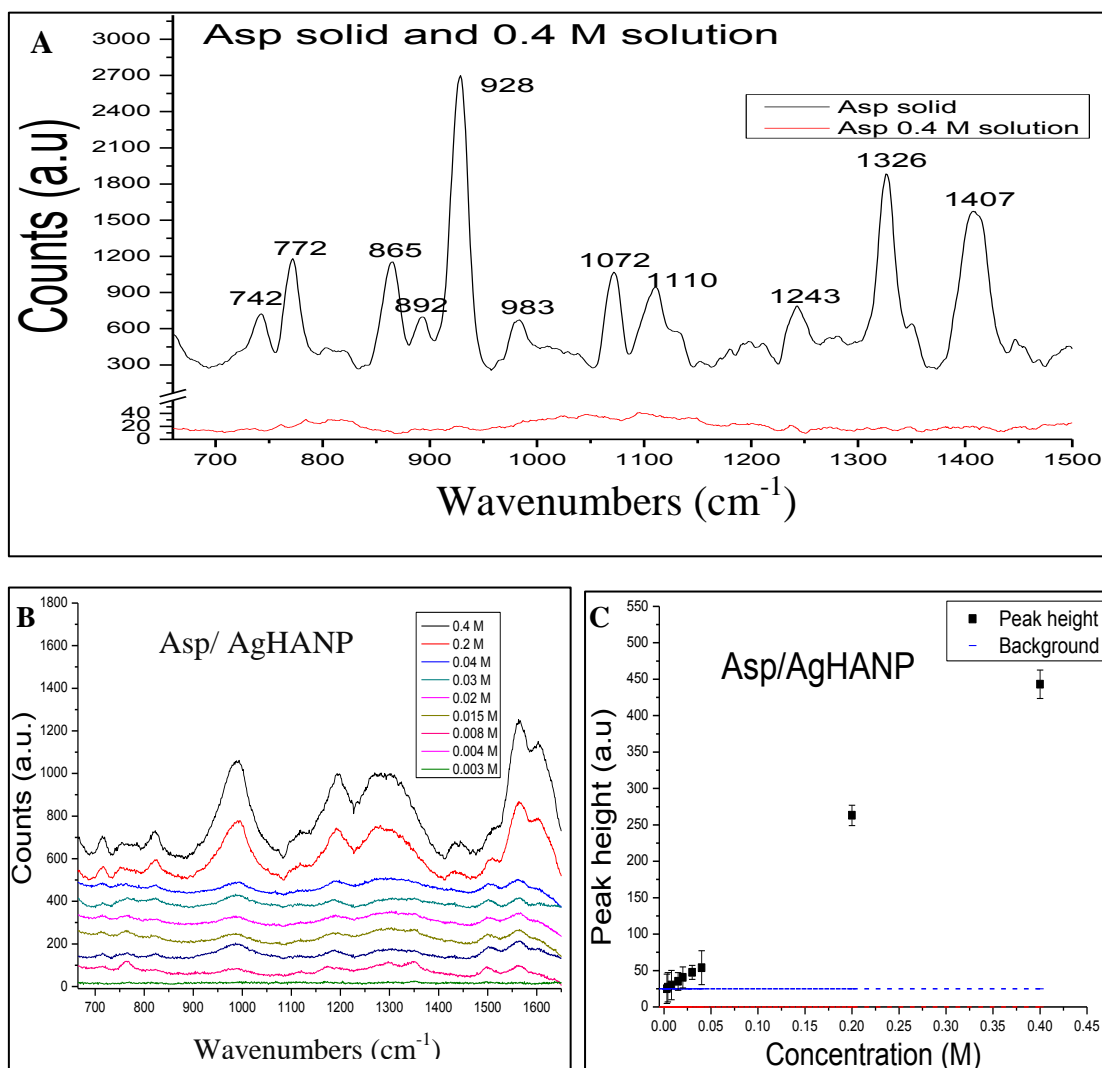


**Figure 27:** RS spectra of Asp solid and 0.4 M solution (with HCl as solvent) are shown in A. B is SERS spectra of Asp with AgHANP. C is a graph showing the change in Asp concentration against peak height for AgHANP. The horizontal line in fig. C shows the background counts.

RS bands [ $\text{cm}^{-1}$ ]		SERS bands for each type of nanoparticle [ $\text{cm}^{-1}$ ]		Band assignment
Spectrum of solid	AgHANP	AgCNP(aggregated AgCNP)	AuNP	
772	714	772		$\text{OCO}^-$ out-of-plane
865	822	840	815	C-C str.
928	988	932	919	OH out-of-plane bending; C-C
983		1024	990	
1072	1193	1068	1073	$\text{NH}_3^+$ wag.; C-N str.
1110	1283		1100	$\text{NH}_3^+$ wag.
1243	1444		1209	
1326		1386	1310	CH bend.
1407	1562	1386	1401	$\text{COO}^-$ ; $(\text{CH}_2)$ def.
		1541		
	1603	1614		$\text{NH}_2$ shear

**Table 6-7:** Experimental Raman shifts and Raman band assignments for Asp [88], [90].

A concentration of 50 mg/ml of Asp was dissolved in 0.5 M HCl with added heating to give 0.4 M of solution. HCl was used as a solvent due to the low solubility of Asp in water. Under acidic conditions, the amino group is protonated and the amino acid exists as  $\text{HOOC-CH}_2\text{-CH}(\text{NH}_3^+)\text{-COOH}$  [72], [90]. However, the  $\text{NH}_3^+$  band is not clearly observed when HCl is used as a solvent. For solid Asp, the strongest band observed was at  $928 \text{ cm}^{-1}$  in the spectrum of solid in fig. 27 A. However, in the solution spectra of fig. 27 A there are no identifiable bands. This band appears at  $988 \text{ cm}^{-1}$ , broad and shifted in Asp/AgHANP spectra in fig. 27 B. It is also noticeable that the spectrum of the solid Asp has sharp distinguishable peaks which are difficult to relate to those from aqueous samples. This is due to formation of new bonds which happens when the Asp sample interacts with water, HCl and the metal nanoparticles [72]. For Asp/AgCNP spectra, there were no bands which could be confidently identified. We propose that the carboxyl and the amine side chains are on the nanoparticle surface and taking part in charge transfer as they have the strongest bands. Concentration study was done with respect to the Raman band between  $870$  and  $1050 \text{ cm}^{-1}$ . The detection limit for Asp/AgHANP was 0.003 M. Raman bands for Asp with aggregated AgCNP are shown in table 5-7 but the spectrum is in section 6.3.

## 6.2.7 L-glutamic acid

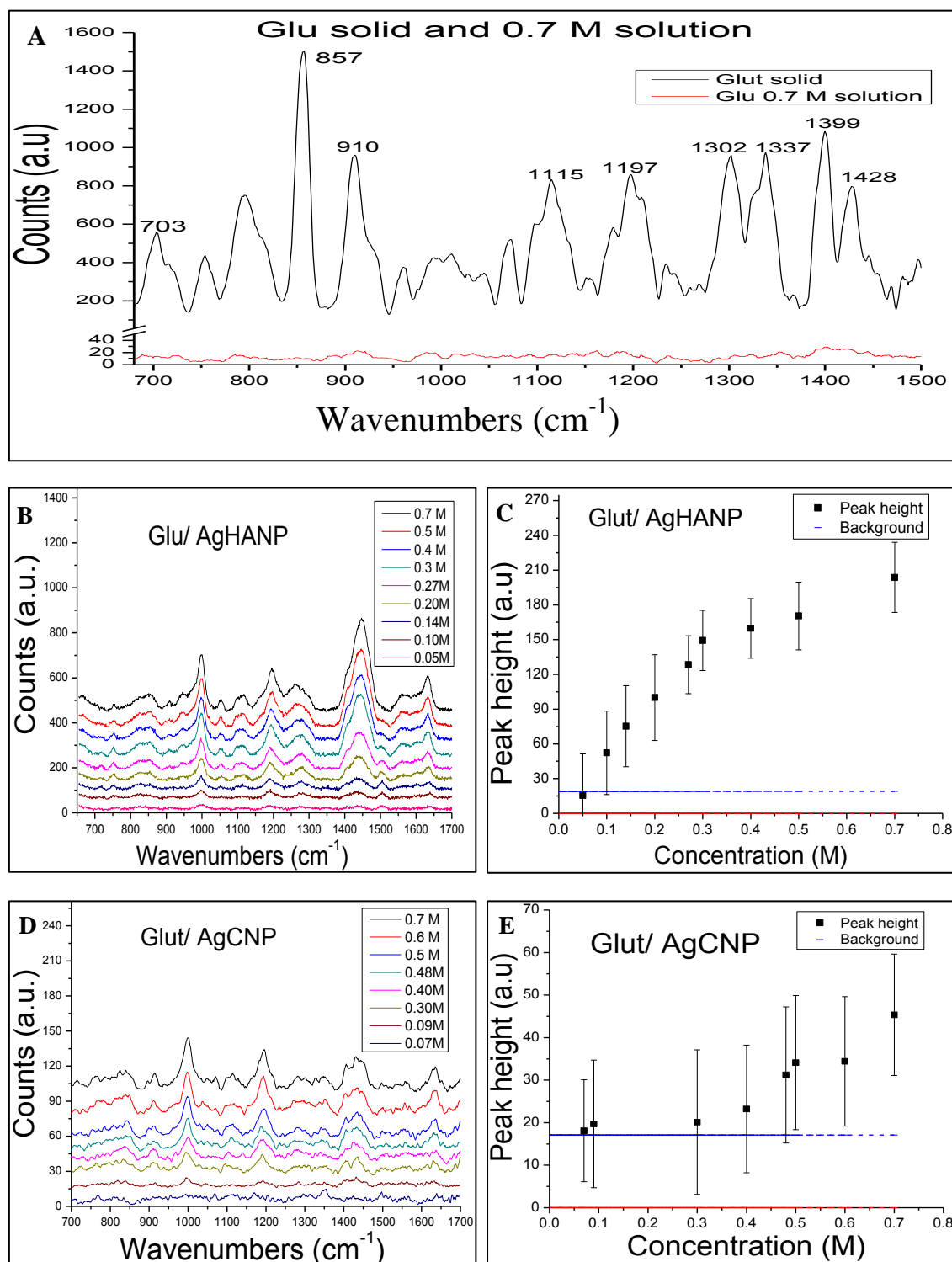


**Figure 28:** RS spectra of Glu solid and 0.7 M solution (with HCl as solvent) are shown in A. B and D are SERS spectra of Glu with AgHANP and AgCNP respectively. C and E are graphs showing the change in Glut concentration against peak height for AgHANP and AgCNP respectively. The horizontal line in figs. C and E show the background counts.

RS bands [ $\text{cm}^{-1}$ ]	SERS bands for each type of nanoparticle [ $\text{cm}^{-1}$ ]			Band assignment
	AgHANP	AgCNP	AuNP	
Spectrum of solid				
703		715	718	COO <sup>-</sup> def.
766	751	761	787	
857	854	839	845	COOH def.; C-C str.
910	908	915	908	C-C-N str. ; C-C str.
967	997	999	992	C-C str.
	1052			
		1070	1072	NH <sub>3</sub> <sup>+</sup> wag.; C-N str.
1115	1117	1114	1116	NH <sub>3</sub> <sup>+</sup> def.
1197	1195	1195	1197	CH <sub>2</sub> wag.
1302	1257	1281	1308	CH <sub>2</sub> wag.
1337		1346	1326	CH <sub>2</sub> sciss.
1399		1406	1403	COO <sup>-</sup> symm. str.
1428	1446	1431	1420	CH <sub>2</sub> sciss.; COO <sup>-</sup> symm. Str.
	1633	1635		

**Table 6-8:** Experimental Raman shifts and Raman band assignments for Glu [27], [88].

A concentration of 100 mg/ml of Glu was dissolved in 1M HCl with added heating to give 0.7 M of solution. Under acidic conditions, the amino group is protonated and the sample exists as HOOC-(CH<sub>2</sub>CH<sub>2</sub>)-CH(NH<sub>3</sub><sup>+</sup>)-COOH. The difference between Glu and Asp is the additional methyl group on the side chain. The band at 857  $\text{cm}^{-1}$  in the spectrum of the solid, Glu in fig. 28 A is the strongest for Glu acid and is attributed to COOH deformation vibration [88]. Spectra for Glu dissolved in HCl with AgHANP and AgCNP shows strong identifiable peaks. The amine band close to 1115  $\text{cm}^{-1}$  in all spectra for both figs. 28 B and D is present but weak in all SERS spectra suggesting that the band is possibly not oriented close to the nanoparticle surface. For this sample the side chain R-group seems to be close to the nanoparticle surface and experiencing chemical enhancement. Concentration study was done with respect to the Raman band near 1000  $\text{cm}^{-1}$ . The detection limit with Glu/AgHANP and Glu/AgCNP was 0.05 M and 0.07 M respectively.

### 6.3 SERS with aggregated nanoparticles

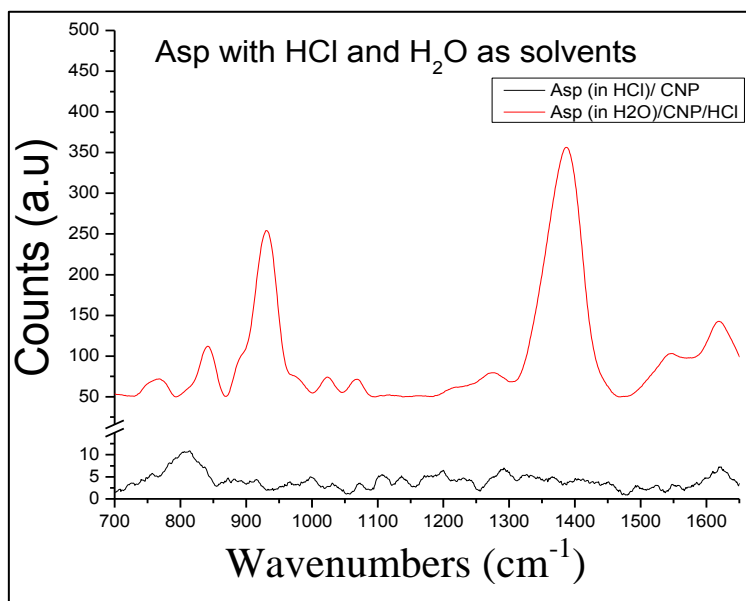
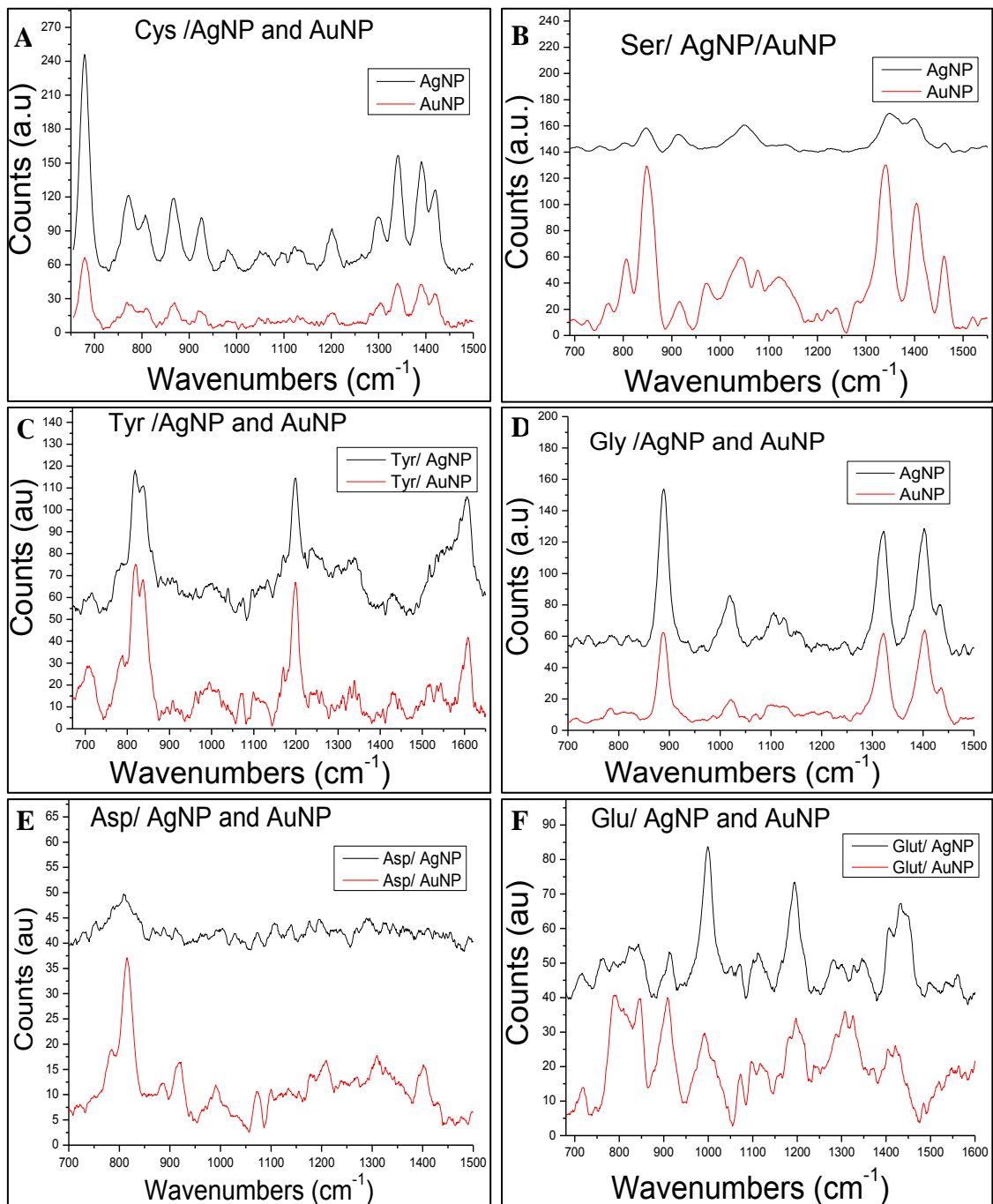


**Figure 29:** Spectra of Asp dissolved in HCl with AgCNP and Asp dissolved in water with AgCNP aggregated with HCl.

With water as solvent, 5 mg/ml Asp solution was made to give 0.04 M. The amount of Asp dissolved was according to the solubility of Asp in water. This was done because Asp dissolved in HCl did not work with AgCNP and some bands could not be confidently identified. Thus, water was then used as a solvent but now with aggregated AgCNP. For measurements, Asp solution was first put in a vial, followed by the rapid addition of the nanoparticles. HCl was added for it to induce aggregation and it was added last so as increase the chances of Asp molecules being trapped inside “hot spots” as the nanoparticles cluster.

Asp in water had a measured pH of 2.81 suggesting its state as  $\text{HOOC-CH}_2\text{-CH}(\text{NH}_3^+)\text{-COO}^-$  [72], [90]. Similar to the strongest band in spectrum of solid at  $928\text{cm}^{-1}$ , the same band is very strong for Asp/ AgCNP, at  $932\text{cm}^{-1}$ . This is due to the sample molecules being present within “hot-spots” and thus enhancing the Raman signal. In this case aggregation of nanoparticles indeed enhanced the Raman signal. The deprotonated  $\text{COO}^-$  band is indeed observed near  $1400\text{cm}^{-1}$ . Though broad and slightly shifted, it is the strongest band and considerably enhanced mainly due to charge transfer mechanism inside the induced “hot spots” created by aggregation. We can suggest that in this case the deprotonated carboxylate group was the closest to the nanoparticle surface and greatly benefited from the induced “hot spots”. However the  $\text{NH}_3^+$  band at  $1068\text{cm}^{-1}$  is present but very weak. According to our results it indeed shows that Asp existed in the suggested form. The results showed that pH does have an effect on the state of the amino acid. This result indeed showed increase in the Raman signal, confirming the formation of “junctions”/“hot spots” into which sample molecules were trapped. It is also important to note that aggregating agent may give different results based on the type of colloid being used, how it was prepared and the sample being analysed [81].

## 6.4 SERS with gold nanoparticles



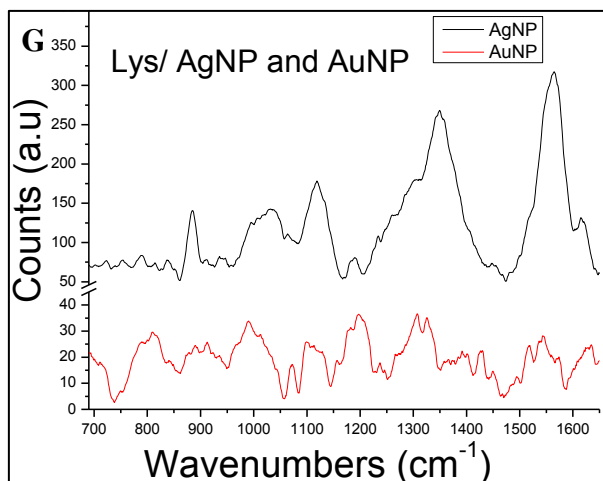


**Figure 30:** SERS spectra for amino acids with citrate reduced AgNP and AuNP. Spectrum A is 1M Cys, B is 0.5 M Ser, C is 0.6 M Tyr (with HCl as solvent), D is 1 M Gly, E is 0.4 M Asp (with HCl as solvent), F is 0.7 M Glu (with HCl as solvent), G is 0.1 M Lys.

In this section both types of nanoparticles, AgNP and AuNP, were citrate reduced, the only variable being the different metals used. Band assignments for the amino acids with AuNP are shown in the respective tables (tables 6-2 to 6-8) for each amino acid. Before SERS measurements, Raman spectra of the nanoparticles were measured to make sure no anomalous bands were present in the raw nanoparticles. SERS of these samples with AuNP was done so as to compare enhancement between nanoparticles made with different metals. Enhancement factors are calculated under section 6.5.

For samples such as Ser and Tyr, it can be noticed that with AuNP more bands appear which are similar to those in their respective spectrums of solid samples. For Cys, spectra with citrate reduced AuNP had similar features to that with citrate reduced AgNP. The strongest band being the C-S stretch at 678 cm<sup>-1</sup>. This suggested chemical interaction of this bond to the gold surface and its shifting indicates that attachment and charge transfer occurred towards the gold metal [94]. Other obviously enhanced bands for Cys include the COO<sup>-</sup> symmetric stretching band at 1390 cm<sup>-1</sup>, thus, the deprotonated carboxylate group chemically interacted with the gold surface. This interaction may have supported enhancement of the CH<sub>2</sub> twist which is at 1339 cm<sup>-1</sup> as the band would have benefited from the interaction of the lone electron pairs of the carboxylate group and the metal [94].

## 6.5 Enhancement factors and detection limit

To characterise the SERS effect we report the enhancement factor (EF) for the different samples measured with AgHANP, AgCNP and AuNP. The enhancement factor was calculated as a ratio of the SERS and the RS intensities, according to equation (18) below without taking into account the amino acid concentrations. From the data below, regardless of the amino acid concentration most of the amino acids gave higher EFs with AgHANP compared to the EFs given with AgCNP and AuNP. Between silver and gold nanoparticles, we expected higher EFs with gold nanoparticles since their absorption peak position of 524 nm was a close match to the wavelength of the excitation source, 532 nm, thus, causing near resonance excitation which greatly amplifies the Raman signal. However, only 2 amino acids, Ser and Tyr have high EFs with gold nanoparticles of  $6.6 \times 10^0$  and  $2.4 \times 10^1$  respectively. For those amino acids dissolved in water Lys gave the highest EF of  $5.4 \times 10^1$  with AgHANP. For all amino acid samples used in concentration study, Lys also gave the lowest detectable concentration when measured with AgHANP and AgCNP, of  $1 \times 10^{-4}$  M and  $7 \times 10^{-3}$  M respectively. This suggests that the detection limit, which we are defining as the lowest amino acid concentration that could be measured by the instrument, for all the amino acids, was a low  $1 \times 10^{-4}$  M of Lys with AgHANP. For the amino acids dissolved in HCl, Asp gave the highest EF of  $7.0 \times 10^1$ . The value indicated in the table for Asp with AgCNP is that of Asp dissolved in water and with aggregated AgCNP. The enhancement factor was a low  $4.7 \times 10^1$ , a value lower than that reported in literature which results from molecules trapped in between two or more clustered nanoparticles [30]. Possibly this was because of different measuring conditions and low solubility of Asp in water.

$$E.F. = \frac{I_{SERS}}{I_{RS}} \quad (19)$$

Amino acid	Group	Concentration	Raman band region/cm <sup>-1</sup>	Raman mode	Enhancement factor (EF)		
					AgHANP	AgCNP	AuNP
Ser	Alcohol	0.5 M	1300 - 1400	Unassigned	1.0x10 <sup>0</sup>	1.6x10 <sup>0</sup>	6.6x10 <sup>0</sup>
Cys	Sulphur	1.0 M	850 - 950	C-C str.	6.8x10 <sup>0</sup>		
			690 - 750	C-S asym. str.		2.0x10 <sup>0</sup>	1.0x10 <sup>0</sup>
Gly	Hydrophobic	1.0 M	850 - 950	C-COO str.	8.1x10 <sup>0</sup>	3.7x10 <sup>0</sup>	3.7x10 <sup>0</sup>
Glu	Acidic	0.7 M	970 - 1010	C-C str.	4.1x10 <sup>1</sup>	9.1x10 <sup>0</sup>	4.5x10 <sup>0</sup>
Tyr	Aromatic	0.6 M	1150 - 1250	Ring str. of para-substituted benzene	2.3x10 <sup>1</sup>	2.3x10 <sup>1</sup>	2.4x10 <sup>1</sup>
Lys	Basic	1.0 M	1550 - 1600	NH <sub>3</sub> <sup>+</sup> asym. bend	5.4x10 <sup>1</sup>	3.5x10 <sup>1</sup>	3.5x10 <sup>0</sup>
Asp	Acidic	0.4 M	950 - 1050	OH out-of-plane bending	7.0x10 <sup>1</sup>	4.7x10 <sup>1</sup>	4.4x10 <sup>0</sup>

**Table 6-9:** Enhancement factors for SERS of amino acids with AgHANP and with AgCNP.

These results are based on the conditions used in the study. It is important to realise that with SERS, changing measuring conditions such as laser power, measuring geometry, salt concentrations, temperature and nanoparticle size affects reproducibility of spectra. Also even if similar conditions are used, there are also factors which affect reproducibility of spectra which need to be considered, such as proximity and orientation of sample molecules on nanoparticle surface. These factors have the ability to cause slight variations in spectra. SERS is a very sensitive technique and to ensure reproducibility strict measuring protocols are to be followed.

## 6.6 Application of RS and SERS

### Raman spectroscopy of a natural protein source

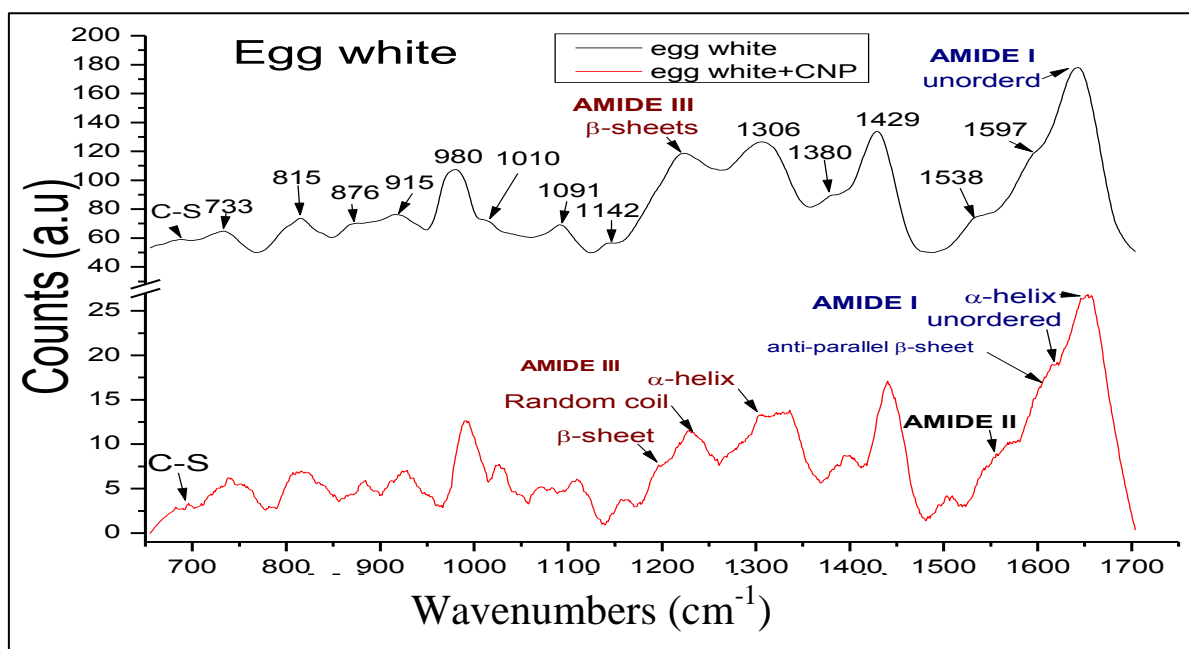


Figure 31: RS and SERS of egg white.

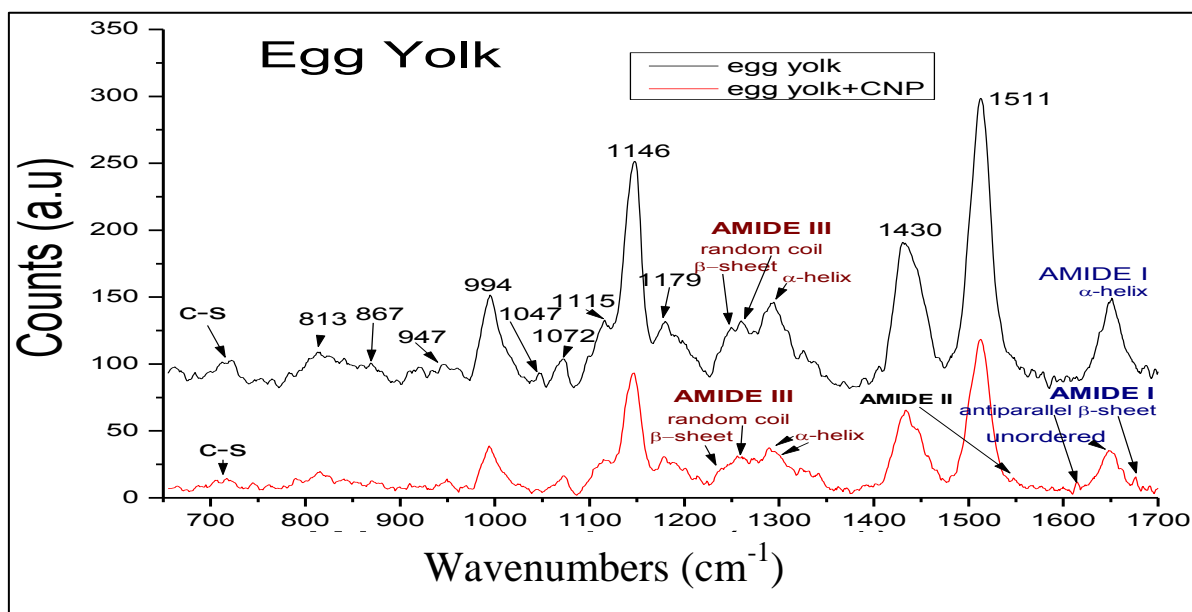


Figure 32: RS and SERS of egg yolk.

Egg white	Egg white + AgNP	Egg yolk	Yolk + AgNP	Band assignment	
688	683	723	715	C-S str. Cys	
733	750			Trp	
815	815	813	815	Tyr doublets	
876	884	867			
915	926			C-C vibration	
		947	949	C-C sym.str.	
980	994	994	993	Ring breathing (Phe)	
1010	1026			Phe	
		1047	1045	C-C str.	
		1072	1073	C-C; C-N str. (aliphatic)	
1091	1109			C-C sym. str.	
		1115	1116	C-C str.	
		1146	1146		
1142	1156			C-C str.	
		1179	1177		
1222	1227	1236	1235	$\beta$ -sheet	Amide III bands
	1252	1249	1255	Random coil	
	1300		1273	$\alpha$ -helix	
		1294	1289		
1306	1320			(CH <sub>2</sub> def; CH <sub>3</sub> def.	
1380	1394			COO <sup>-</sup> sym. str. aspartic and glutamic acids	
1429	1440	1430	1433	CH <sub>2</sub> bend.	
		1511	1511		
1538	1542			Trp	
	1550		1547		Amide II band
1597	1608			Phe/ Tyr	
	1615		1613	Antiparallel $\beta$ -sheet	Amide I band
1642	1646		1647	Unordered C=O str. peptic bonds of Amide I	
	1651-56	1651		$\alpha$ -helix	
			1676	Antiparallel $\beta$ -sheet	

**Table 6-10:** Experimental Raman shifts and Raman band assignments for chicken egg white and yolk [30], [106]–[109].

The egg was locally sourced and the egg white and yolk were used with no processing. The fingerprint region  $600 - 1800 \text{ cm}^{-1}$  consists of proteins, amide bands and amino acids present in the egg white and yolk. These spectra were measured to show that with the new Raman system we are indeed able to also measure real proteins from known substances and food stuffs. Both egg white and yolk contain similar proteins such as conalbumin, ovalbumin and lysozyme with egg yolk, however, also containing fatty acid esters / lipids [106], [110].

In their native structure proteins are stabilised by ionic bonds, hydrophobic interactions, hydrogen bonds and disulphide covalent bonds. Factors affecting protein environment include pH, salt concentration, temperature and type of solvent [30], [108]. By performing RS and SERS on egg white and yolk, we were able to see how bands were affected due to adsorption on the metallic surface. Amide bands were identified in different positions and shapes. These bands characterised the different protein conformations which are indicated in table 6-9. In the presence of AgCNP for both egg white and yolk, the shifting and appearance of new amide I bands shown in the SERS spectra may have been due pH changes which affected the H-bonds or protein-nanoparticle interactions, thus, consequently altering the native structure of proteins. The amide II band in both egg white and yolk is quite weak compared to other identified bands. The amide III band has matching conformations to those from amide I band. In amide I and III there is shifting of bands. This is caused by interaction of the proteins with the colloids.

Aromatic amino acids contributed greatly in the spectra. Examples are L-tyrosine (Tyr) and phenylalanine (Phe). The phenylalanine band close to  $1000 \text{ cm}^{-1}$  is one of the biomarkers of proteins and it usually stands out in proteins by having a high intensity and being insensitive to protein conformations. However, it displays low intensity in the measured spectra. The Tyr doublets at  $815 \text{ cm}^{-1}$  are weak but present, being caused by Fermi resonance of the in-plane breathing mode of the phenol ring and an overtone of the out-of-plane deformation mode [88], [108]. In egg white the Tyr doublets appear stronger in the presence of nanoparticles suggesting close proximity to the nanoparticle surface and the bonds experiencing chemical enhancement. Chemical enhancement is also ascribed to all other identified bands suggesting that they were directly attached to the nanoparticle surfaces. However, in egg yolk the Tyr doublets weaken and this indicates an effect in the structure of proteins.

The results obtained for measurements of egg white and yolk with nanoparticles do not support the concept of SERS since bands decreased in intensity instead of being enhanced. The SERS peak heights are not as good as those for the RS, instead they have low intensity contrary to what is expected in SERS signal enhancement. However, for egg white, more bands can be identified and distinguished in the SERS spectra. Though the SERS peaks had low intensity the spectra were reproducible and consistent. To our knowledge such results of decreased Raman signals have not been found in literature sources and the reason as to why there was decreased peak intensity is not known. However, from literature, SERS studies have been done on egg white and yolk using silver nanoparticles and Raman bands showed significant enhancement. In most studies, SERS or RS on egg is done using films of egg white and egg yolk. Philippidis and co-

workers performed SERS studies on egg white and natural amino acids in order to develop adaptable methods of investigating bio-organic materials [109]. In that study, there was increased peak intensity in the SERS spectra, however, a compact mobile Raman spectrometer was employed and thin films of egg white and natural amino acids were used, conditions different from those employed in our study.

## 7 Conclusion

### 7.1 Standard protocols of measurement on biomolecules (amino acids)

Finally, in this section we give the standard measuring protocols to be applied when investigating standard samples of proteins and amino acids using RS and SERS techniques based on the performance of our Raman setup and measuring conditions.

*Instrumentation:* It is important not to disrupt the instrumental setup in order to have the same measuring conditions on all samples being measured.

*Sample preparation and handling:* Gloves are to be used when preparing samples as well as use of clean plastic/metal spatulas for transferring solid samples. All samples to be analysed must be fresh in order to have strong signals. Some samples precipitate out over time, example is Cys, which will make them unusable for SERS measurement. Samples are to be contained in clean bottles or vials to avoid contamination. During RS or SERS measurement, a new micropipette tip is to be used for transferring any liquid, this avoids contamination. Once a small amount of chemical is transferred from the stock solution it cannot be returned into the stock solution to avoid contamination of the whole lot. Further instructions on handling chemicals may be consulted from chemical and health safety guides.

*Nanoparticles, storage and preparation:* It is essential for containers to be extremely clean for nanoparticles preparation. Contaminants during colloid preparation result in unwanted nucleation of foreign particles on the nanoparticles. This diminishes the quality of the nanoparticles, affecting their surface and consequently the foreign particles may also contribute their undesired Raman bands during measurements. All nanoparticles are very sensitive any foreign substance which makes its way into the colloid stock solution would lead to the whole batch being discarded and unfit for use. All nanoparticle ingredients are to be stored safely in a cupboard under room temperature and conditions. Gold (in the form of chloroauric acid) is easily oxidised if left open, thus the container should be tightly closed at all time. One simple way to check if the gold is still fresh is to put a small amount in a silver metal spatula in the lab. The surrounding spot where the gold is will start turning blue/ blue black as the metals react. Thus, a plastic spatula is appropriate for transferring chloroauric acid. During preparation of AuNP the prescribed synthesis methods are to be followed to produce the desired colloid. Colloids are to be stored in closed containers to avoid oxidation and in a dark place such as a cupboard or refrigerator. In the presence of light, nanoparticles are prone to photo-oxidation.

*Measurements (UV-Vis, TEM, RS, SERS):* Some nanoparticles require dilution with water for UV-Vis measurements to avoid detector saturation. Carbon coated copper grids for TEM are very small and care needs to be taken in storing and handling them to avoid other substance from sticking onto the grids, thus affecting their surface. When transferring colloids onto the grids, a generous amount must be transferred onto the grid. In this study the colloids were transferred with a dropper while the grids were on a tissue paper, afterward they were left open to dry under monitored room conditions

prior to TEM measurements. During RS or SERS measurements acquisition parameters are to be maintained according to the instrument being used. All RS and SERS measurements are to be done in a dark room, with no light. Light from other sources will also enter the detector, be registered and populate the RS or SERS spectra.

## 7.2 Summary

In this study SERS was carried out on a small selection of amino acids and assignments of vibrational bands were done based on the spectra acquired with reference to literature sources which have done RS and SERS studies with the same amino acids. Spectra of solids gave sharp distinguishable peaks due to the fact that in solid state there is no interaction of particles with any solvents which causes formation of new bonds which may result in broadened and shifted peaks. The majority of results correspond well with those from literature such as studies carried out on L-cysteine, glycine, L-lysine, L-serine, L-tyrosine and L-glutamic acid. Differences in our measured results in comparison with those from literature are found mainly due to different measuring conditions. For instance results by C. Jing and Y. Fang on Cys show that using a near infra-red laser excitation source there is significant enhancement of bands with gold nanoparticles and none with silver nanoparticles. In that study enhancement with silver was observed under aggregation of silver nanoparticles with chloride ions [94]. However, in this study both silver and gold showed significant enhancement during SERS with visible laser though the enhancement factors differed.

The detection limit was not the same for all amino acids. For most of the amino acids which include Cys, Gly, Lys, Asp and Glu, the lowest concentrations were measured with AgHANP. This is probably because from the absorption spectra there is narrow size distribution and more silver nanoparticles resonate close to the wavelength of the excitation source, thus, enhancing the RS signal. With AgCNP, there was a wide size distribution of nanoparticles and less of the nanoparticles resonate close to the laser line. This affects the enhancement factors. From our results, it was also observed that the lowest detectable amino acid concentrations are not actually very low compared to concentrations reported in literature. Though measuring conditions differ, some SERS studies have reported on measurements of concentrations as low as  $1 \times 10^{-4}$  M for amino acids such as Cys and Gly using colloidal silver [111]. However, these results were obtained using considerably smaller AgNP synthesized by the reduction of  $\text{Ag}^+$  using  $\text{NaBH}_4$ .

From the results of concentration study, peak intensity increases as amino acid concentration increases. However, for very high amino acid concentrations, not much increase in peak intensity would be expected because even though the amino acid molecules are increasing per given scattering volume, the concentration of nanoparticles will not be changing. Hence, in some cases peak intensities may start approaching a constant value as observed in Glut with AgHANP. Also, some data points may appear scattered as amino acid concentration increases and not show a 'smooth' trend because for that particular band being tracked, its orientation on the metallic surfaces changes with each new sample being measured as observed for Tyr with AgHANP and Glu with AgCNP.

In general, each amino acid had its own unique spectrum characteristic of its chemical structure. Some of the proteins had diagnostic bands which classified them into their respective groups based on the R-group side chain. However, there are some bands which are expected to be found in every amino acid spectra. Every amino acid has an amine and carboxyl side chain. Bands of these side chains were found in all the amino acid spectra presented in this report.

In section Appendix B, amino acids have been grouped according to their respective classes which are polar but uncharged (Cys, Tyr, Ser), acidic (Asp, Glu), basic (Lys) and hydrophobic (Gly) amino acids. The common bands in all spectra, which are the carboxylate and amine bands have been marked. Through an overall analysis of amino acid spectra measured in this study, there was a general observation made on how bands oriented on the nanoparticle surface. It was observed that bands would tend to orient via the carboxylate, amine or the R- group. The presence of the carboxyl group, in cases where it appears strong, suggests that it was oriented close/on to the metallic surface and experiencing chemical enhancement. In most cases the carboxyl group appeared broad and shifted. This is attributed to the charge transfer between the lone electron pairs of the oxygen atom and the metal itself, thus promoting chemical enhancement. Even in the protein source (egg white) used in this study the carboxyl group was also present. Nitrogen in the amine group also has a lone electron pair which also take part in charge transfer with the metallic nanostructure. Some amino acids which have strong bands, such as Tyr tend to orient via the functional group. The R-group of Tyr consists of  $\pi$  electrons which can also take part in charge transfer, thus, chemically enhancing RS signals. Cys has a sulphur group which has high affinity for metals and hence, it tends to bind strong strongly onto the nanoparticle.

Overall, these findings are in accordance with what has been reported on SERS of l-amino acids by authors such as Stewart and Fredericks [27] and Zhu *et al* [88]. They have also illustrated how the amino acids adsorb on metallic surfaces. For instance, Cys adsorbs via the thiol group as well as the carboxylate group. Findings by Podstawka *et al* on amino acids also showed similar patterns of adsorption via the carboxylate, amine and R-groups onto the silver surface for amino acids such as Cys and Gly [111]. Siddhanta and Narayana also stated that protein interaction with metal surfaces occurred through the carboxylate and the amino group [30]. This is in line with findings of this study that the carboxylate, the amino and the R-group do interact with the metal substrates.

As previously stated, some of the results presented may differ from those found in literature possibly due to different measuring conditions. However, it is important to note that these results are new and to our knowledge have not been published before in literature. These are results performed under the same conditions using different classes of amino acids and employing silver and gold nanoparticles, which are easy to synthesize. Investigation on RS and SERS was done using a single RS setup developed by our labs with the main purpose of advancing the SERS tool for bio-analytical purposes using our in-house developed instrument. This was the main aim of the project. Further on, protein sources found and used in day to day lives were measured using our instrument. Amino acids were identified in egg white and yolk. This further showed the ability of our instrument to measure real life proteins. Nanoparticles utilised for the SERS studies were successfully synthesised using standard recipes and

characterisation was done using TEM and UV-Vis techniques. Modification of the nanoparticles by aggregation indeed achieved high Raman signals due to the intimate interaction of sample molecules with the large plasmon resonances as well as charge transfer mechanism in the generated “hot spots”.

### 7.3 Future work and general comments

We seek to increase the level of sophistication of this research by optimising our Raman setup to enable detection of very low concentrations. We anticipate that by doing so we will obtain more information on protein and amino acid structure, which could help in better understanding them. For further studies in biofilms, the identification and characterization of standard proteins and eventually microorganisms found embedded in EPS and their growth dynamics based on produced metabolites are very important in fields ranging from the accurate and rapid diagnosis of bacterial infections to industrial processes and in industry. Apart from the utilised metals namely Ag and Au, other metals such as Cu may be employed, but taking into account that the plasmon resonance of Cu is not as strong as those of Ag and Au. Recent studies have suggested cost effective ways of fabrication Cu nanostructures using ultrafast laser pulses [112]. Studies on metallic substrates have also highlighted how graphene and graphene-metallic films enable SERS sensitivity and stability and how graphene plasmonics can be excited from mid-infrared to terahertz range with low loss in low frequency regions, at the same time also enabling single molecule detection [113]. In this study a label free<sup>11</sup> SERS method of detection of biomolecules was employed as it allowed direct acquiring of biomolecule spectra. However, the SERS label free method has its limitations as it is difficult to apply in cases of bulk proteins. Recent studies have highlighted developments in multiple protein identification, by employing extrinsic<sup>12</sup> SERS labelling techniques which allow indirect detection of biomolecules such as DNA/RNA.

---

<sup>11</sup> Direct method of detecting biomolecules without use of Raman dyes.

<sup>12</sup> Indirect method of detecting biomolecules by use of Raman dyes.

## Appendices

### A. Modified Polyfit Method for background subtraction written in Matlab:

```
% -----Clearing all commands-----

clc
clear

% -----Modified Polyfit Method-----

a = load('values.csv'); % load data into MATLAB
count=0;
while(count < 200) % do 200 or less iterations depending on the amount of fluorescence
    count = count+1;
    if count==1
        y=a(:,2); % the y column of raw data
    else
        temp = y2;
        y = y2; % initialising the variable y2 for the polynomial y values to be calculated
    end
    x=a(:,1); % the x column of the data
    p = polyfit(x,y,7); % generate polynomial coefficients
        % the degree of the polynomial is changed as
        % desired/necessary
    poly = polyval(p,x); % for each polynomial value calculated assign the corresponding
x value

    y2 = poly; % the calculated polynomial y values
    for i=1:size(x)
        if count==1
            if y2(i) - y(i) > 0; % if data point in generated curve has intensity value > its
respective
                % pixel value in nanoparticle spectrum then reassign
                y2(i)=y(i); % reassignment
            end
        else
            if y2(i) - y(i) > 0;
                y2(i)=temp(i);
            end
        end
    end
end
end

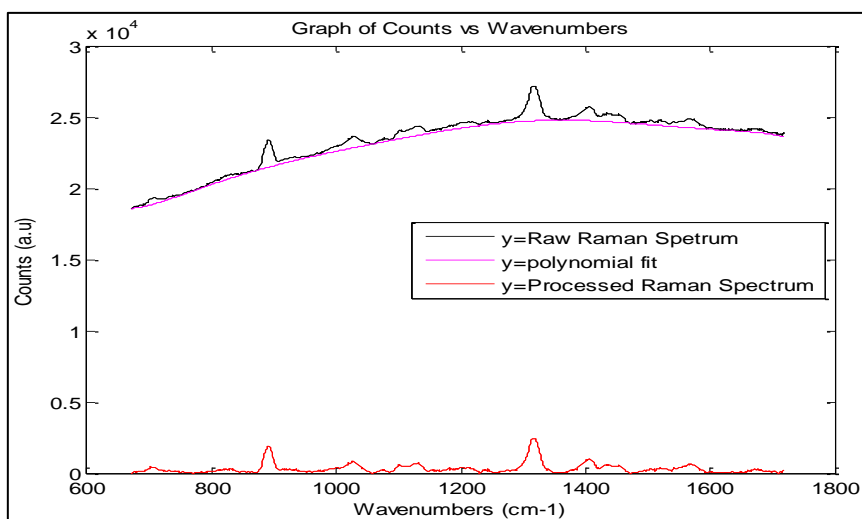
%-----plotting the final fit after background subtraction-----

x=a(:,1); % the x column of the data
```

```

y=a(:,2); % the original y column of the data
for e=1:(length(y2))
    final(e) = y(e)-y2(e); % subtrating original y-value from nth iterated y-value
end
plot(x,y,'k'); % plot original raw graph
hold on
plot(x,y2,'m') % plot polynomial
hold on
plot(x,final,'r') % plot final graph after background subtraction
title('Graph of Counts vs Wavenumbers')
xlabel('Wavenumbers (cm-1)') % x-axis label
ylabel('Counts (a.u)') % y-axis label
legend('y=Raw Raman Spetrum','y=polynomial fit','y=Processed Raman Spectrum','location','east')
%-----End-----

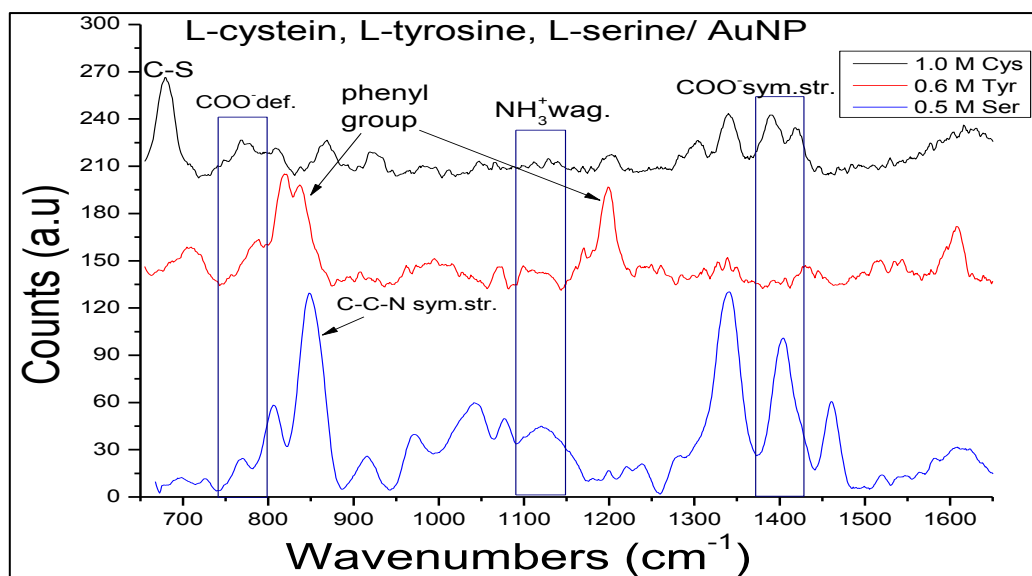
```



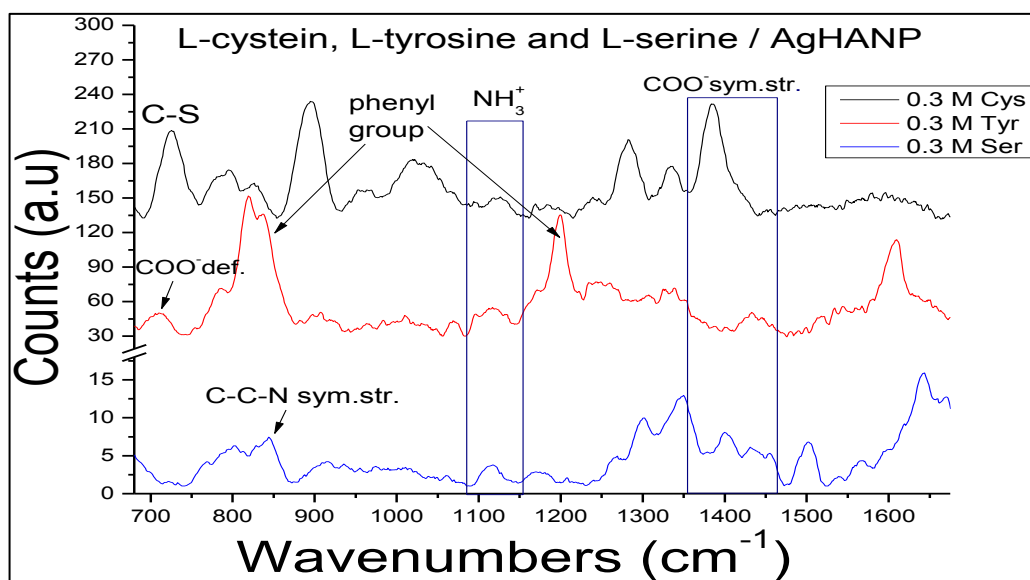
**Figure 33:** Example of graph, before and after background subtraction.

In this section the amino acids used in this study are presented and classified according to their respective classes. For particular type of nanoparticle some of the samples are of the same concentration while for another type of nanoparticles the sample concentrations are different. The important information being presented here are the common bands for side chains which appear in almost every amino acid according to the SERS spectra. These bands are the carboxylate and the amine side chains.

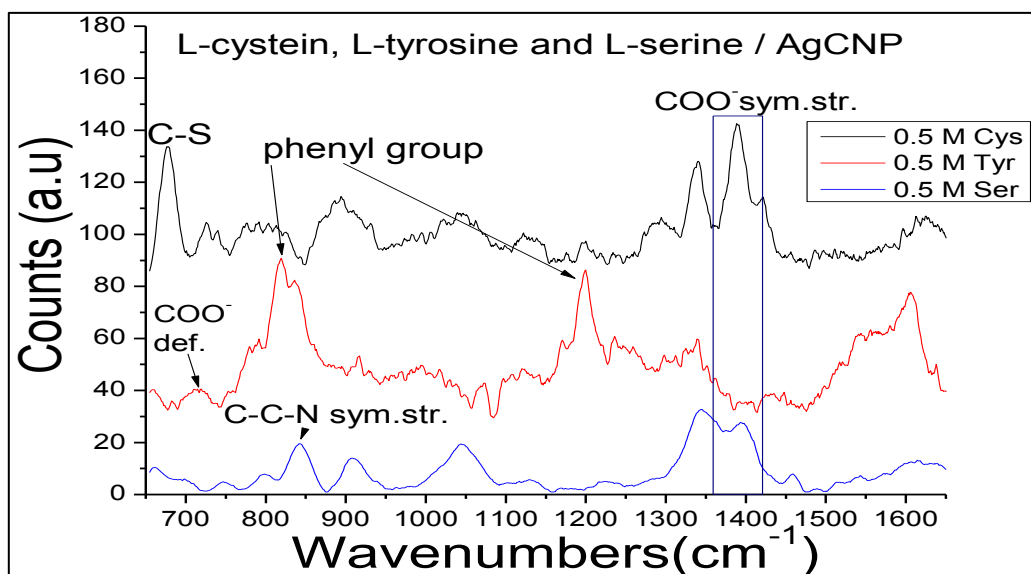
## B. Polar but uncharged amino acids



**Figure 34:** SERS spectra of polar but uncharged amino acids with AuNP. The samples have different concentrations and the spectra were only for showing the carboxylate, amine and R-groups in the amino acids.

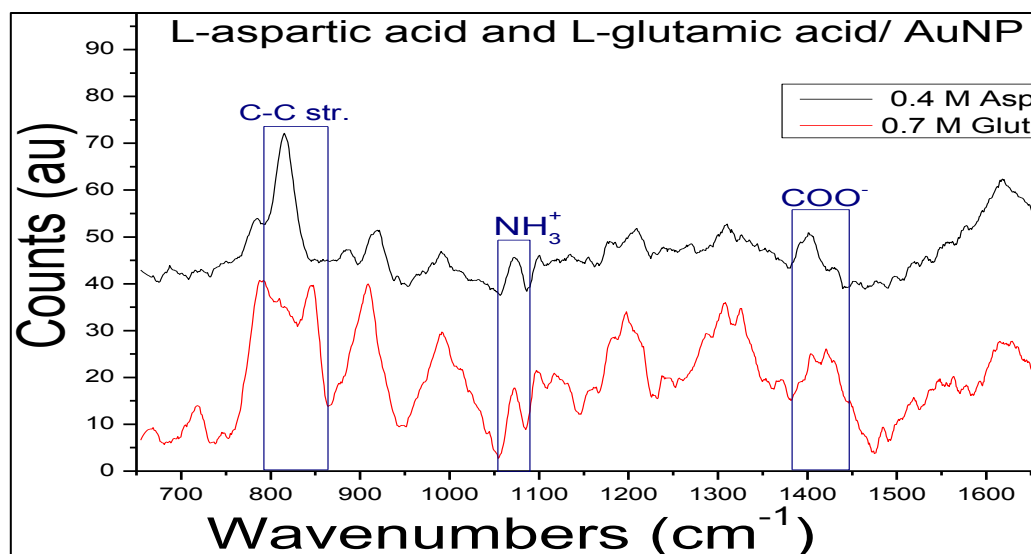


**Figure 35:** SERS spectra of polar but uncharged amino acids with AgHANP. The concentration is the same for all three samples, the carboxylate, amine and R-groups have been labelled.

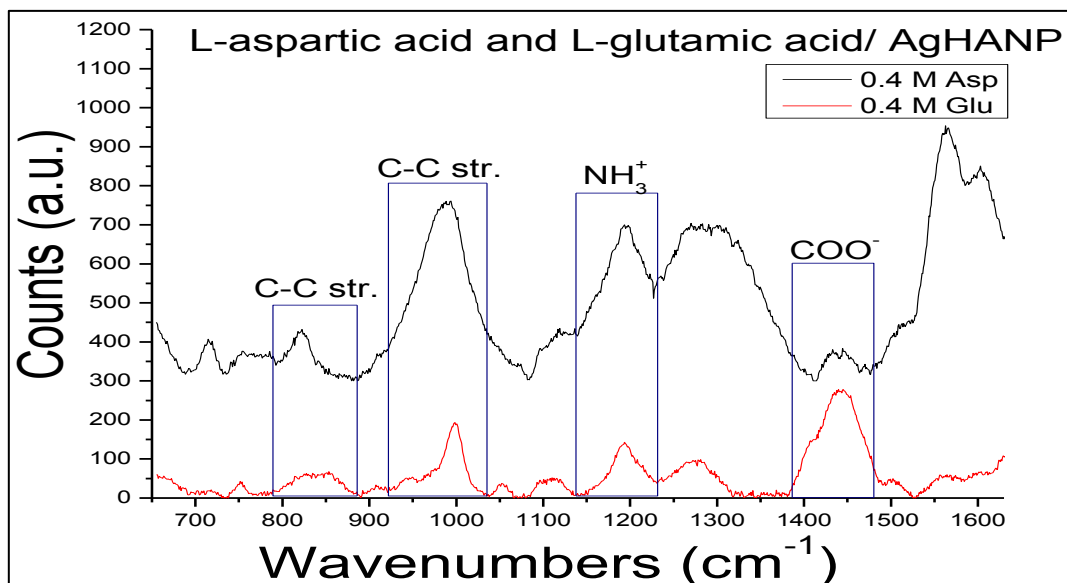


**Figure 36:** SERS spectra of polar but uncharged amino acids with AgCNP. The concentration is the same for all three samples, the carboxylate, amine and R-groups have been labelled.

### C. Acidic amino acids

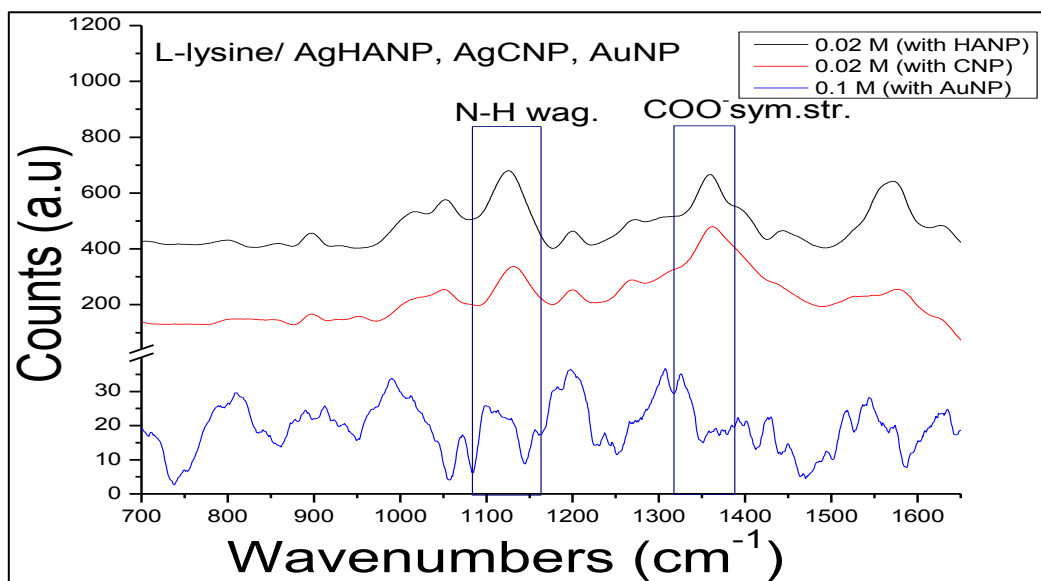


**Figure 37:** SERS spectra of acidic amino acids with AuNP. The carboxylate and amine groups have been labelled.

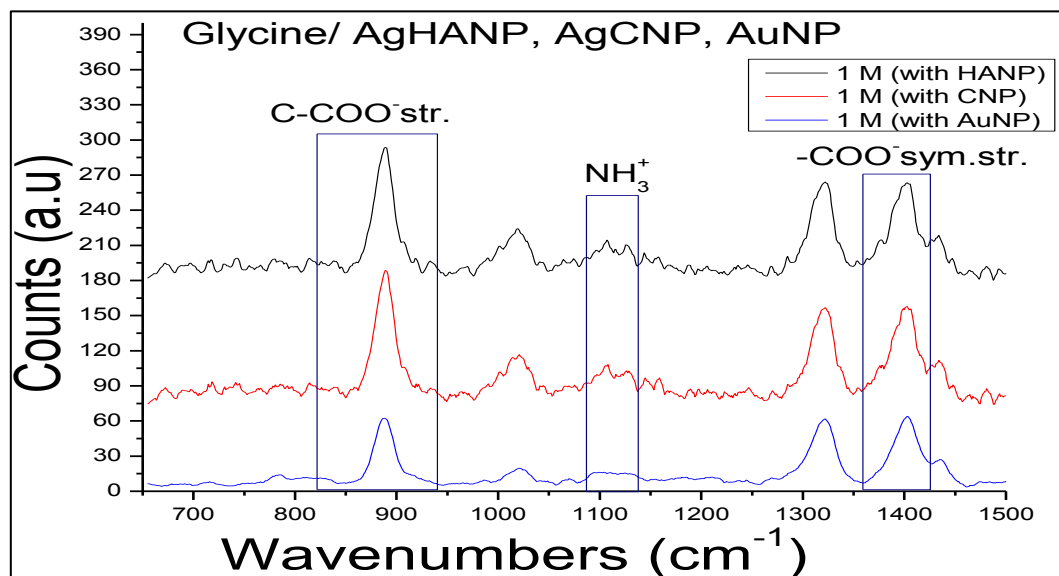


**Figure 38:** SERS spectra of acidic amino acids with AgHANP. The carboxylate and amine groups have been labelled. The samples are of the same concentration.

#### D. Basic amino acid(s)



**Figure 39:** SERS spectra of a basic amino acid with AgHANP, AgCNP and AuNP. All three spectra have been presented on one plot only to show the carboxylate, and amine groups which appear in the spectra.

**E. Hydrophobic amino acid(s)**

**Figure 40:** SERS spectra of a hydrophobic amino acid with AgHANP, AgCNP and AuNP. All three spectra have been presented on one plot only to show the carboxylate and amine groups which appear in the spectra.

## Bibliography

- [1] A. T. Henrici, "Studies of Freshwater Bacteria I. A Direct Microscopic Technique," *J. Bacteriol.*, vol. 25, no. 3, pp. 277–287, 1933.
- [2] N. P. Ivleva and M. Wagner, "Label-free in situ SERS imaging of biofilms," *J. Phys. Chem. B*, vol. 114, pp. 10184–10194, 2010.
- [3] G. O'Toole, H. B. Kaplan, and R. Kolter, "Biofilm Formation and microbial development," *Microbiology*, vol. 54, pp. 49–79, 2000.
- [4] D. Lopez, H. Vlamakis, and R. Kolter, "Biofilms," *Cold Spring Harb. Perspect. Biol.*, vol. 2, pp. 1–11, 2010.
- [5] I. W. Sutherland and I. W. Sutherland, "The biofilm matrix – an immobilized but dynamic microbial environment," *Microbiology*, vol. 9, no. 5, pp. 222–227, 2001.
- [6] G.-P. Sheng, H.-Q. Yu, and X.-Y. Li, "Extracellular polymeric substances (EPS) of microbial aggregates in biological wastewater treatment systems: A review," *Biotechnol. Adv.*, vol. 28, no. 6, pp. 882–894, 2010.
- [7] C. Laspidou, "A unified theory for extracellular polymeric substances, soluble microbial products, and active and inert biomass," *Water Res.*, vol. 36, no. 11, pp. 2711–2720, 2002.
- [8] I. Francolini and G. Donelli, "Prevention and control of biofilm-based medical-device-related infections," *Immunol. Med. Microbiol.*, vol. 59, pp. 227–238, 2010.
- [9] X. Bai, X. Ma, F. Xu, J. Li, H. Zhang, and X. Xiao, "The drinking water treatment process as a potential source of affecting the bacterial antibiotic resistance," *Sci. Total Environ.*, vol. 533, pp. 24–31, 2015.
- [10] R. B. Srivastava, "Recent research in microbial fouling and corrosion," *Indian Inst. Sci.*, vol. 79, pp. 485–495, 1999.
- [11] C. Staudt, H. Horn, D. C. Hempel, and T. R. Neu, "Volumetric Measurements of Bacterial Cells and Extracellular Polymeric Substance Glycoconjugates in Biofilms," *Biotechnol. Bioeng.*, vol. 88, no. 5, 2004.
- [12] O. Samek, S. Bernatová, R. Jan Ježek, M. Šiler, M. Šerý, V. Krzyžánek, K. Hrubanová, P. Zemánek, and V. Holá, "Identification of individual biofilm-forming bacterial cells using Raman tweezers," *Biomed. Opt.*, vol. 20, no. 5, 2015.
- [13] J. R. Ferraro, K. Nakamoto, and C. W. Brown, *Introductory Raman Spectroscopy*, Second. Elsevier Science (USA), 2003.
- [14] E. Smith and G. Dent, *Modern Raman Spectroscopy: A Practical Approach*. WILEY, 2005.
- [15] P. Naglic, "Raman spectroscopy for medical diagnostics," University of Ljubljana, 2012.
- [16] J. Javier, "An Introduction to Raman Spectroscopy: Introduction and Basic Principle," *Raman / Infrared Spectroscopy*, 2014. [Online]. Available: <http://www.spectroscopynow.com/details/education/sepspec1882education/An->

- Introduction-to-Raman-Spectroscopy-Introduction-and-Basic-Principles.html?&tzcheck=1&tzcheck=1.
- [17] X. Zhu, T. Xu, Q. Lin, and Y. Duan, "Technical Development of Raman Spectroscopy: From Instrumental to Advanced Combined Technologies," *Appl. Spectrosc. Rev.*, vol. 49, no. 1, pp. 64–82, 2014.
- [18] a. Rygula, K. Majzner, K. M. Marzec, a. Kaczor, M. Pilarczyk, and M. Baranska, "Raman spectroscopy of proteins: A review," *J. Raman Spectrosc.*, vol. 44, no. 8, pp. 1061–1076, 2013.
- [19] BWTEKInc, "Theory of Raman Scattering," *Raman Spectroscopy*, 2015. [Online]. Available: <http://bwtek.com/raman-theory-of-raman-scattering/>.
- [20] R. Aroca, *Surface-Enhanced Vibrational Spectroscopy*. John Wiley and Sons, Ltd, 2007.
- [21] J. S. Suh and M. Moskovits, "Surface-Enhanced Raman Spectroscopy of Amino Acids and Nucleotide Bases Adsorbed on Silver," *J. Am. Chem. Soc.*, vol. 108, no. 21, pp. 44711–4718, 1986.
- [22] R. L. McCreery, *Raman Spectroscopy for chemical analysis*. Columbus, Ohio: John Wiley and Sons, INC, 2000.
- [23] M. Moskovits and J. S. Suh, "Surface selection rules for surface-enhanced Raman spectroscopy: calculations and application to the surface-enhanced Raman spectrum of phthalazine on silver," *J. Phys. Chem.*, vol. 88, no. 2, pp. 5526–5530, 1984.
- [24] M. Fleischmann, P. J. Hendra, and a J. McQuillan, "Raman spectra of pyridine adsorbed at a silver electrode," *Chem. Phys. Lett.*, vol. 26, no. 2, pp. 163–166, 1974.
- [25] D. L. Jeanmaire and R. P. Van Duyne, "Surface raman spectroelectrochemistry," *Journal of Electroanalytical Chemistry and Interfacial Electrochemistry*, vol. 84, no. 1. pp. 1–20, 1977.
- [26] J. A. Creighton, C. G. Blatchford, and M. G. Albrecht, "Plasma Resonance Enhancement of Raman Scattering by Pyridine Adsorbed on Silver or Gold Sol Particles of Size Comparable to the Excitation Wavelength," *Mol. Chem. Phys.*, vol. 75, no. 0, pp. 790–798, 1979.
- [27] S. Stewart and P. . Fredericks, "Surface-enhanced Raman spectroscopy of amino acids adsorbed on an electrochemically prepared silver surface," *Spectrochim. Acta Part A Mol. Biomol. Spectrosc.*, vol. 55, no. 7–8, pp. 1641–1660, 1999.
- [28] P. C. Lee and D. Meisel, "Adsorption and surface-enhanced Raman of dyes on silver and gold sols," *J.Phys.Chem.*, vol. 86, no. 17, pp. 3391–3395, 1982.
- [29] Y. Xia and N. J. Halas, "Shape-Controlled Synthesis and Surface Plasmonic Properties of Metallic Nanostructures," *MRS Bull.*, vol. 30, no. 05, pp. 338–348, 2011.
- [30] S. Siddhanta and C. Narayana, "Surface Enhanced Raman Spectroscopy of Proteins : Implications for Drug Designing," *Nanomater. Nanotechnol.*, vol. 2, pp. 1–13, 2012.
- [31] S. Schlucker, *Surface Enhanced Raman Spectroscopy Application: Biophysical*

*and life Science Application*. WILEY-VCH Verlag GmbH, 2011.

- [32] S. Hatch and G. Schatz, "Synthesis and Analysis of Silver / Gold Nanoparticles," *Nanotechnology*, 2015. [Online]. Available: [https://nanohub.org/wiki/GeneralChemistry/File:Silvergold\\_module.pdf](https://nanohub.org/wiki/GeneralChemistry/File:Silvergold_module.pdf). [Accessed: 17-Sep-2015].
- [33] E. Petryayeva and U. J. Krull, "Localized surface plasmon resonance : Nanostructures , bioassays and biosensing — A review," *Anal. Chem.*, vol. 706, no. 1, pp. 8–24, 2011.
- [34] R. Stiuftuc, C. Iacovita, C. M. Lucaci, G. Stiuftuc, A. G. Dutu, C. Braescu, and N. Leopold, "SERS-active silver colloids prepared by reduction of silver nitrate with short-chain polyethylene glycol," *Nanoscale Res. Lett.*, vol. 8, no. 1, p. 47, 2013.
- [35] N. Leopold and B. Lendl, "A New Method for Fast Preparation of Highly Surface-Enhanced Raman Scattering (SERS) Active Silver Colloids at Room Temperature by Reduction of Silver Nitrate with Hydroxylamine Hydrochloride," *J. Phys. Chem. B*, vol. 107, no. 24, pp. 5723–5727, 2003.
- [36] E. C. Le Ru and P. G. Etchegoin, "Rigorous justification of the enhancement factor in Surface Enhanced Raman Spectroscopy," *Chem. Phys. Lett.*, vol. 423, no. 1–3, pp. 63–66, 2006.
- [37] K. Shameli, M. Bin Ahmad, S. D. Jazayeri, S. Sedaghat, P. Shabanzadeh, H. Jahangirian, M. Mahdavi, and Y. Abdollahi, "Synthesis and characterization of polyethylene glycol mediated silver nanoparticles by the green method," *Int. J. Mol. Sci.*, vol. 13, no. 6, pp. 6639–6650, 2012.
- [38] R. J. Chimentao, I. Kirm, F. Medina, X. Rodriguez, Y. Cesteros, P. Salagre, J. E. Sueiras, and J. L. G. Fierro, "Sensitivity of styrene oxidation reaction to the catalyst structure of silver nanoparticles," *Appl. Surf. Sci.*, vol. 252, pp. 793–800, 2005.
- [39] T. Pal, "Gelatin-A Compound for All Reasons," *Chem. Educ.*, vol. 71, no. 8, pp. 679–681, 1994.
- [40] Y. Zhang, K. Zhang, and H. Ma, "Electrochemical DNA biosensor based on silver nanoparticles/poly(3-(3-pyridyl) acrylic acid)/carbon nanotubes modified electrode," *Anal. Biochem.*, vol. 387, no. 1, pp. 13–19, 2009.
- [41] J. Zheng, Y. Ding, B. Tian, Z. L. Wang, and X. Zhuang, "Luminescent and Raman Active Silver Nanoparticles with Polycrystalline," *Am. Chem. Soc.*, vol. 130, no. 32, pp. 10472–10473, 2008.
- [42] M. Zargar, A. H. Hamid, F. Abu Bakar, M. Nor Shamsudin, K. Shameli, F. Jahanshiri, and F. Farahani, "Green Synthesis and Antibacterial Effect of Silver Nanoparticles Using Vitex Negundo L.," *Molecules*, vol. 16, pp. 6667–6676, 2011.
- [43] Y. Sa, L. Jung, and Y. M. Jung, "Avidin induced silver aggregation for SERS-based bioassay," *Bull. Korean Chem. Soc.*, vol. 33, no. 11, pp. 3681–3685, 2012.
- [44] M. V. Cañamares, J. V. Garcia-Ramos, S. Sanchez-Cortes, M. Castillejo, and M. Oujja, "Comparative SERS effectiveness of silver nanoparticles prepared by

- different methods: A study of the enhancement factor and the interfacial properties,” *J. Colloid Interface Sci.*, vol. 326, no. 1, pp. 103–109, 2008.
- [45] E. M. Egorova, *Biological Effects of Silver Nanoparticles*. NOVA Science Publishers, 2010.
- [46] R. Behra, L. Sigg, M. J. D. Clift, F. Herzog, M. Minghetti, B. Johnston, A. Petrifink, and B. Rothen-rutishauser, “Bioavailability of silver nanoparticles and ions : from a chemical and biochemical perspective,” *J. R. Soc. Interface*, vol. 10, no. 87, pp. 1–15, 2013.
- [47] A. H. Pakiari and Z. Jamshidi, “Interaction of amino acids with gold and silver clusters.,” *J. Phys. Chem. A*, vol. 111, no. 20, pp. 4391–4396, 2007.
- [48] L. Braydich-Stolle, H. Saber, J. J. Schlager†, and M. Hofmann, “In Vitro Cytotoxicity of Nanoparticles in Mammalian Germline Stem Cells,” *Toxicol. Sci.*, vol. 42, no. 2, pp. 157–162, 2005.
- [49] Cytodiagnosics Inc, “Silver Nanoparticle Properties,” 2015. [Online]. Available: <http://www.cytodiagnosics.com/store/pc/Silver-Nanoparticle-Properties-d11.htm>. [Accessed: 15-May-2015].
- [50] E. Podstawka, Y. Ozaki, and L. M. Proniewicz, “Surface-Enhanced Raman Scattering of Amino Acids and Their Homopeptides Monolayers Deposited onto Colloidal gold Surface,” *Appl. Spectrosc.*, vol. 59, no. 1, 2005.
- [51] J. L. Hammond, N. Bhalla, S. D. Rafiee, and P. Estrela, “Localized Surface Plasmon Resonance as a Biosensing Platform for Developing Countries,” *Biosensors*, vol. 4, pp. 172–188, 2014.
- [52] M. A. El-sayed and P. K. Jain, “Plasmonic coupling in noble metal nanostructures,” *Chem. Phys. Lett.*, vol. 487, pp. 153–164, 2010.
- [53] J. M. Pitarke, V. M. Silkin, E. V Chulkov, and P. M. Echenique, “Theory of surface plasmons and surface-plasmon polaritons,” *Physics (College. Park. Md.)*, vol. 70, pp. 1–87, 2007.
- [54] A. J. Haes and R. P. Van Duyne, “Nanoscale optical biosensors based on localized surface plasmon resonance spectroscopy,” *Plasmonics*, vol. 5221, no. 1, pp. 47–58, 2003.
- [55] S. Kruszewski and M. Cyrankiewicz, “Aggregated silver sols as SERS substrates,” *Acoust. Biomed. Eng.*, vol. 121, no. 1 A, pp. 68–74, 2012.
- [56] X. Chen, C. Jiang, and S. Yu, “Nanostructured materials for applications in surface-enhanced Raman scattering,” *CrystEngComm*, vol. 16, pp. 9959–9973, 2014.
- [57] M. K. Hossain and Y. Ozaki, “Surface-enhanced Raman scattering: Facts and inline trends,” *Raman Spectrosc.*, vol. 97, no. 2, pp. 192–201, 2009.
- [58] E. C. Le Ru, M. Meyer, and P. G. Etchegoin, “Surface Enhanced Raman Scattering Enhancement Factors: A Comprehensive Study,” *J. Phys. Chem. C*, vol. 111, no. 37, pp. 13794–13803, 2007.
- [59] E. C. Le Ru and P. G. Etchegoin, *Principles of Surface Enhanced Raman Spectroscopy*. Elsevier, 2009.

- [60] P. Alonso-González, P. Albella, M. Schnell, J. Chen, F. Huth, a. García-Etxarri, F. Casanova, F. Golmar, L. Arzubiaga, L. E. Hueso, J. Aizpurua, and R. Hillenbrand, "Resolving the electromagnetic mechanism of surface-enhanced light scattering at single hot spots," *Nat. Commun.*, vol. 3, p. 684, 2012.
- [61] R. W. Taylor, T. Lee, O. A. Scherman, R. Esteban, J. Aizpurua, F. M. Huang, J. J. Baumberg, S. Mahajan, and T. E. T. Al, "Precise Subnanometer Plasmonic Junctions for SERS within Gold Nanoparticle Assemblies Using Cucurbit [n] uril ' Glue ,'" *Am. Chem. Soc.*, vol. 5, no. 5, pp. 3878–3887, 2011.
- [62] Y. Wang, D. Li, P. Li, W. Wang, W. Ren, S. Dong, and E. Wang, "Surface Enhanced Raman Scattering of Brilliant Green on Ag Nanoparticles and Applications in Living Cells as Optical Probes," *J. Phys. Chem. C*, vol. 111, no. 45, pp. 16833–16839, 2007.
- [63] E. J. Liang and W. Kiefert, "Chemical Effect of SERS with Near-Infrared Excitation," *J. Raman Spectrosc.*, vol. 27, pp. 879–885, 1996.
- [64] Ipcc, "Working Group I Contribution to the IPCC Fifth Assessment Report - Summary for Policymakers," *Clim. Chang. 2013 Phys. Sci. Basis*, vol. 53, no. September 2013, pp. 1–36, 2013.
- [65] T. A. El-Brolosy, T. Abdallah, M. B. Mohamed, S. Abdallah, K. Easawi, S. Negm, and H. Talaat, "Shape and size dependence of the surface plasmon resonance of gold nanoparticles studied by Photoacoustic technique," *Eur. Phys. J. Spec. Top.*, vol. 153, no. 1, pp. 361–364, 2008.
- [66] A. L. Jenkins, R. a. Larsen, and T. B. Williams, "Characterization of amino acids using Raman spectroscopy," *Spectrochim. Acta - Part A Mol. Biomol. Spectrosc.*, vol. 61, no. 7, pp. 1585–1594, 2005.
- [67] P. V. Sengbusch, "Amino acids." [Online]. Available: [https://s10.lite.msu.edu/res/msu/botonl/b\\_online/e16/16j.htm](https://s10.lite.msu.edu/res/msu/botonl/b_online/e16/16j.htm). [Accessed: 15-Mar-2015].
- [68] A. V. Vutturi, "Solubility of phenols in alkalies." [Online]. Available: <http://www.adichemistry.com/qb/organic/acids/1-phenol-solubility.html>. [Accessed: 20-Mar-2015].
- [69] Bettelheim, Brown, Campbell, and Farrell, "Alcohols, Ethers, and Thiols," *Spectroscopy*. [Online]. Available: [https://www.google.com/url?sa=t&rct=j&q=&esrc=s&source=web&cd=7&cad=rja&uact=8&ved=0CEkQFjAGahUKEwjU5vTniejHAhVHPPhQKHYc2BP0&url=https://course1.winona.edu/rreuter/Chem\\_210\\_F09/Ch14Alcohols,EthersandThiols.ppt&usg=AFQjCNHAKsbw5z6Hd-0iQgVyUYC1c-u-N](https://www.google.com/url?sa=t&rct=j&q=&esrc=s&source=web&cd=7&cad=rja&uact=8&ved=0CEkQFjAGahUKEwjU5vTniejHAhVHPPhQKHYc2BP0&url=https://course1.winona.edu/rreuter/Chem_210_F09/Ch14Alcohols,EthersandThiols.ppt&usg=AFQjCNHAKsbw5z6Hd-0iQgVyUYC1c-u-N). [Accessed: 20-Aug-2015].
- [70] PearsonNCS, "tutor Vista.com," 2015. [Online]. Available: <http://chemistry.tutorvista.com/biochemistry/tyrosine.html>. [Accessed: 01-Aug-2015].
- [71] N. Taniguchi, "Amino Acids and Proteins," in *Medical Biochemistry*, 3rd ed., M. A. D. J. W. Baynes, Ed. China: Elsevier, 2010, pp. 5–21.
- [72] J. L. Castro, M. A. Montañez, J. C. Otero, and J. I. Marcos, "SERS and Vibrational Spectra of Aspartic Acid," *Mol. Struct.*, vol. 349, pp. 113–116, 1995.

- [73] S. L. Seager and M. R. Slabaugh, "Amines and amides," *Contemp. Org. Synth.*, vol. 1, no. 6, p. 475, 1994.
- [74] A. Barth and C. Zscherp, "What vibrations tell us about proteins.," *Q. Rev. Biophys.*, vol. 35, no. 4, pp. 369–430, 2002.
- [75] W. R. Premasiri, D. T. Moir, M. S. Klempner, N. Krieger, G. Zones, and L. D. Ziegler, "Characterization of the Surface Enhanced Raman Scattering (SERS) of Bacteria," *J. Phys. Chem. B*, vol. 109, pp. 312–320, 2005.
- [76] ScientificHoriba, "Synapse CCD and EMCCD Cameras," 2015. [Online]. Available: <http://www.horiba.com/scientific/products/optical-spectroscopy/detectors/scientific-cameras-for-spectroscopy-cdd-ingaas-emccd/ccds/details/synapse-ccd-and-emccd-cameras-216/>. [Accessed: 11-May-2014].
- [77] YvonIncHORIBA Jobin, "SYNAPSE CCD Detection System User Manual," 2006. [Online]. Available: [https://www.nanocenter.umd.edu/equipment/nanoopticslab/manuals/optics-02/Synapse CCD Manual.pdf](https://www.nanocenter.umd.edu/equipment/nanoopticslab/manuals/optics-02/Synapse%20CCD%20Manual.pdf). [Accessed: 12-Jun-2015].
- [78] B. Bleiensteiner, "Dispersive Raman Instruments Application Scientist HORIBA Scientific," *Raman Spectrosc.*, 2009.
- [79] I. R. Lewis and H. G. M. Edwards, *Handbook of Raman spectroscopy: From the Research Laboratory to the Process Line.*, Illustrate. New York: Taylor & Francis, 2001.
- [80] Joint Committee for Guides in Metrology (JCGM), "Evaluation of measurement data: Guide to the expression of uncertainty in measurement," 2008. [Online]. Available: <http://www.bipm.org/en/publications/guides/gum.html> [http://www.bipm.org/utis/common/documents/jcgm/JCGM\\_100\\_2008\\_E.pdf](http://www.bipm.org/utis/common/documents/jcgm/JCGM_100_2008_E.pdf). [Accessed: 27-Oct-2015].
- [81] N. R. Yaffe and E. W. Blanch, "Effects and anomalies that can occur in SERS spectra of biological molecules when using a wide range of aggregating agents for hydroxylamine-reduced and citrate-reduced silver colloids," *Vib. Spectrosc.*, vol. 48, no. 2, pp. 196–201, 2008.
- [82] C. A. Lieber and A. Mahadevan-Jansen, "Automated Method for Subtraction of Fluorescence from Biological Raman Spectra," *Appl. Spectrosc.*, vol. 57, no. 11, pp. 1363–1367, 2003.
- [83] K. C. Grabar, R. G. Freeman, M. B. Hommer, and M. J. Natan, "Preparation and Characterization of Au Colloid Monolayers," *Anal. Chem.*, vol. 67, no. 4, pp. 735–743, 1995.
- [84] W. Haiss, N. T. K. Thanh, J. Aveyard, and D. G. Fernig, "Determination of Size and Concentration of Gold Nanoparticles from UV - Vis Spectra," *Anal. Chem.*, vol. 79, no. 13, pp. 4215–4221, 2007.
- [85] A. Sileikaite, I. Prosycevas, J. Puiso, A. Juraitis, and A. Guobiene, "Analysis of Silver Nanoparticles Produced by Chemical Reduction of Silver Salt Solution," *Mater. Sci.*, vol. 12, no. 4, pp. 287–291, 2006.
- [86] F. Benetti, M. Fedel, L. Minati, G. Speranza, and C. Migliaresi, "Gold

- nanoparticles: Role of size and surface chemistry on blood protein adsorption,” *J. Nanoparticle Res.*, vol. 15, no. 6, pp. 2–10, 2013.
- [87] A. M. Atta, H. a. Al-Lohedan, and A. O. Ezzat, “Synthesis of silver nanoparticles by green method stabilized to synthetic human stomach fluid,” *Molecules*, vol. 19, no. 5, pp. 6737–6753, 2014.
- [88] G. Zhu, X. Zhu, Q. Fan, and X. Wan, “Raman spectra of amino acids and their aqueous solutions,” *Spectrochim. Acta - Part A Mol. Biomol. Spectrosc.*, vol. 78, no. 3, pp. 1187–1195, 2011.
- [89] A. P. Stevenson, D. Blanco Bea, S. Civit, S. Antoranz Contera, A. Iglesias Cerveto, and S. Trigueros, “Three strategies to stabilise nearly monodispersed silver nanoparticles in aqueous solution,” *Nanoscale Res. Lett.*, vol. 7, no. 1, p. 151, 2012.
- [90] J. F. Arenas, J. L. Castro, J. C. Otero, and J. I. Marcos, “Study of interaction between aspartic acid and silver by surface-enhanced Raman scattering on H<sub>2</sub>O and D<sub>2</sub>O sols,” *Biopolym. - Biospectroscopy Sect.*, vol. 62, no. 5, pp. 241–248, 2001.
- [91] T. Shoeib, K. W. M. Siu, and A. C. Hopkinson, “Silver ion binding energies of amino acids: Use of theory to assess the validity of experimental silver ion basicities obtained from the kinetic method,” *J. Phys. Chem. A*, vol. 106, no. 25, pp. 6121–6128, 2002.
- [92] A. Ravindran, N. Chandrasekaran, and A. Mukherjee, “Studies on Differential Behavior of Silver Nanoparticles Towards Thiol Containing Amino Acids,” *Curr. Nanosci.*, vol. 8, no. 1, pp. 141–149, 2012.
- [93] A. H. B. Dourado, R. Queiroz, M. L. a. Temperini, and P. T. a. Sumodjo, “Investigation of the electrochemical behavior of l-cysteine in acidic media,” *Journal of Electroanalytical Chemistry*, 2015. [Online]. Available: , <http://dx.doi.org/10.1016/j.jelechem.2015.09.004>.
- [94] C. Jing and Y. Fang, “Experimental (SERS) and theoretical (DFT) studies on the adsorption behaviors of l-cysteine on gold/silver nanoparticles,” *Chem. Phys.*, vol. 332, no. 1, pp. 27–32, 2007.
- [95] T. Watanabe and H. Maeda, “Adsorption-controlled redox activity. Surface-enhanced Raman investigation of cystine versus cysteine on silver electrodes,” *J. Phys. Chem.*, vol. 93, no. 7, p. 3258, 1989.
- [96] J. Clark, “Electronegativity,” 2013. [Online]. Available: <http://www.chemguide.co.uk/atoms/bonding/electroneg.html>. [Accessed: 18-Jun-2015].
- [97] J. De Gelder, K. De Gussen, P. Vandenabeele, and L. Moens, “Reference database of Raman spectra of biological molecules,” *Raman Spectrosc.*, vol. 38, pp. 1133–1147, 2007.
- [98] A. Culka, J. Jehlička, and H. G. M. Edwards, “Acquisition of Raman spectra of amino acids using portable instruments: Outdoor measurements and comparison,” *Spectrochim. Acta - Part A Mol. Biomol. Spectrosc.*, vol. 77, no. 5, pp. 978–983, 2010.

- [99] A. Gunzler, H and Williams, *Handbook of Analytical Technique: Infrared and Raman Spectroscopy*. WILEY-VCH Verlag GmbH, 2001.
- [100] R. P. Rava and T. G. Spiro, "Selective enhancement of tyrosine and tryptophan resonance Raman spectra via ultraviolet laser excitation," *Phys. Chem. Chem. Phys.*, vol. 89, pp. 1856–1861, 1985.
- [101] J. Moger, P. Gribbon, a Sewing, and C. P. Winlove, "Feasibility study using surface-enhanced Raman spectroscopy for the quantitative detection of tyrosine and serine phosphorylation.," *Biochim. Biophys. Acta*, vol. 1770, no. 6, pp. 912–918, 2007.
- [102] T. M. Herne, A. M. Ahern, and R. L. Garrell, "Surface-enhanced Raman spectroscopy of peptides: preferential N-terminal adsorption on colloidal silver," *J. Am. Chem. Soc.*, vol. 113, p. 846, 1991.
- [103] J. T. Edsall, J. W. Otvos, and A. Rich, "Raman spectra of amino acids and related compounds," *J. Am. Chem. Soc.*, vol. 72, pp. 474–477, 1950.
- [104] C. H. Chuang and Y. T. Chen, "Raman scattering of L-tryptophan enhanced by surface plasmon of silver nanoparticles: vibrational assignment and structural determination," *J. Raman Spectrosc.*, vol. 40, pp. 150–156, 2009.
- [105] N. Derbel, B. Hernandez, F. Pfluger, J. Liquier, F. Geinguenaud, N. Jaidane, Z. B. Lakhdar, M. Ghomi, and G. Guiffo-Soh, "Vibrational Analysis of Amino Acids and Short Peptides in Hydrated Media. I. L-glycine and L-leucine," *J. Phys. Chem. B*, vol. 111, no. 43, pp. 1470–1477, 2007.
- [106] Y. Yuan, L. Ling, X. Wang, M. Wang, R. Gu, and J. Yao, "Micro-Raman and fluorescence spectroscopy for the assessment of the effects of the exposure to light on films of egg white and egg yolk," *J. Raman Spectrosc.*, vol. 38, no. June, pp. 1280–1287, 2007.
- [107] A. Nevin, I. Osticioli, D. Anglos, A. Burnstock, S. Cather, and E. Castellucci, "Raman Spectra of Proteinaceous Materials Used in Paintings : A Multivariate Analytical Approach for Classification and Identification," *Anal. Chem.*, vol. 79, no. 16, pp. 6143–6151, 2007.
- [108] C. David, "Raman Spectroscopy for proteins," *Raman Spectroscopy*, 2012. [Online]. Available: [http://www.horiba.com/fileadmin/uploads/Scientific/Documents/Raman/HORIBA\\_webinar\\_proteins.pdf](http://www.horiba.com/fileadmin/uploads/Scientific/Documents/Raman/HORIBA_webinar_proteins.pdf). [Accessed: 10-Jul-2015].
- [109] A. Philippidis, Z. E. Papliaka, and D. Anglos, "Surface Enhanced Raman and 2D-Fluorescence spectroscopy for the investigation of amino acids and egg proteins," *Microchem. J.*, vol. 126, pp. 230–236, 2016.
- [110] G. Chiavari and K. Words, "Analytical Pyrolysis as Diagnostic Tool in the Investigation of Works of Art," *Chromatography*, vol. 58, no. 9, pp. 543–554, 2003.
- [111] E. Podstawka, Y. Ozaki, and L. M. Proniewicz, "Part I: Surface-enhanced Raman spectroscopy investigation of amino acids and their homodipeptides adsorbed on colloidal silver," *Appl. Spectrosc.*, vol. 58, no. 5, pp. 570–580, 2004.
- [112] S. Hamad, G. K. Podagatlapalli, M. A. Mohiddon, and V. R. Soma, "Cost

- effective nanostructured copper substrates prepared with ultrafast laser pulses for explosives detection using surface enhanced Raman scattering,” *Appl. Phys. Lett.*, vol. 104, no. 26, p. 263104, 2014.
- [113] Y. Zhao and Y. Zhu, “Graphene-based hybrid films for plasmonic sensing,” *R. Soc. Chem.*, vol. 7, pp. 14561–14576, 2015.